

Role of Rheology in Morphology Development and Advanced Processing of Thermoplastic Polymer Materials: A Review

Ritima Banerjee and Suprakas Sinha Ray*



Cite This: *ACS Omega* 2023, 8, 27969–28001



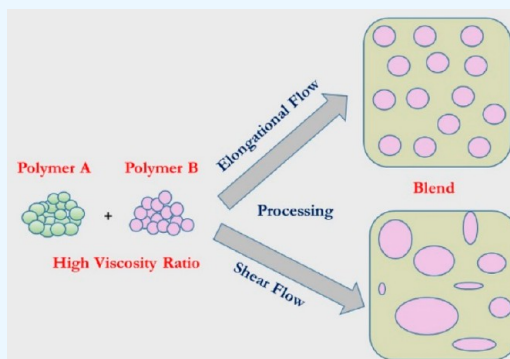
Read Online

ACCESS |

Metrics & More

Article Recommendations

ABSTRACT: This review presents fundamental knowledge and recent advances pertaining to research on the role of rheology in polymer processing, highlights the knowledge gap between the function of rheology in various processing operations and the importance of rheology in the development, characterization, and assessment of the morphologies of polymeric materials, and offers ideas for enhancing the processabilities of polymeric materials in advanced processing operations. Rheology plays a crucial role in the morphological evolution of polymer blends and composites, influencing the type of morphology in the case of blends and the quality of dispersion in the cases of both blends and composites. The rheological characteristics of multiphase polymeric materials provide valuable information on the morphologies of these materials, thereby rendering rheology an important tool for morphological assessment. Although rheology extensively affects the processabilities of polymeric materials in all processing operations, this review focuses on the roles of rheology in film blowing, electrospinning, centrifugal jet spinning, and the three-dimensional printing of polymeric materials, which are advanced processing operations that have gained significant research interest. This review offers a comprehensive overview of the fundamentals of morphology development and the aforementioned processing techniques; moreover, it covers all vital aspects related to the tailoring of the rheological characteristics of polymeric materials for achieving superior morphologies and high processabilities of these materials in advanced processing operations. Thus, this article provides a direction for future advancements in polymer processing. Furthermore, the superiority of elongational flow over shear flow in enhancing the quality of dispersion in multiphase polymeric materials and the role of extensional rheology in the advanced processing operations of these materials, which have rarely been discussed in previous reviews, have been critically analyzed in this review. In summary, this article offers new insights into the use of rheology in material and product development during advanced polymer-processing operations.



1. INTRODUCTION

Polymer processing has significantly advanced from the basic operations of mixing and molding to advanced manufacturing techniques such as film blowing, foaming, three-dimensional (3D) printing, and electrospinning. Rheology plays a crucial role in all polymer-processing operations. The morphological characteristics of polymer blends, composites, and nanocomposites are considerably influenced by the rheological characteristics of the polymer(s) under the applied processing conditions. Morphological characteristics, along with the rheological characteristics of the resulting multiphase polymeric materials, affect the processabilities and product qualities of subsequent advanced processing operations, including foaming and blown film extrusion. Thus, in the advanced processing of multiphase polymeric materials, rheology performs a dual function. It not only directly influences the ease of processing and quality of the achieved product but also indirectly plays a vital role in the development of the morphological characteristics of the materials being processed. In addition to its role in processability and product quality,

rheology provides valuable information about the morphologies of polymeric materials. Although the function of rheology in various processing operations has been reported by several research groups, reviews that highlight the importance of rheology in the development and characterization of the morphologies of polymeric materials and assessment of the processabilities of polymeric materials in advanced processing techniques are limited. The present review aims at bridging this knowledge gap. First, fundamental knowledge related to the role of rheology in the development and assessment of the morphologies of polymeric materials is discussed, and a comprehensive and critical understanding of the crucial role of

Received: May 12, 2023

Accepted: July 10, 2023

Published: July 25, 2023



rheology in the processabilities of polymeric materials in advanced processing techniques is provided. Notably, the processing techniques discussed herein, namely film blowing, electrospinning, centrifugal jet spinning, and 3D printing, have recently gained significant importance in academic and industrial research. Although foaming is an advanced processing operation that is widely used in industry and research, it has not been reviewed in this article as we have systematically discussed the role of rheology in foaming in our previous studies.^{1,2} This review mainly includes the following topics. (a) Role of extensional rheology in the development of the morphological characteristics of multiphase polymeric systems: at equal elongation and shear rates, the mixing and dispersion efficacies achieved in extensional flow are ten times those attained in shear flow.³ Thus, extensional rheology not only plays an important role in processing operations involving stretching, such as foaming,⁴ film blowing,⁵ and thermoforming,⁶ but may also be effectively utilized in melt processing to achieve high qualities of dispersion and to process shear-sensitive polymers without degradation.⁷ (b) Rheology as a tool for morphological assessment: rheological characterization can provide vital information on the morphological characteristics of polymeric materials and can help predict the morphologies of these materials before their morphological characterization.^{8,9} (c) Function of rheology in the processabilities of polymeric materials: a comprehensive understanding of the rheological characteristics of polymeric materials can assist in the selection of appropriate materials and/or grades and processing conditions for achieving superior processabilities of polymeric materials in various processing operations.¹

This review provides a critical overview of the role of rheology in morphology developments and processabilities of polymeric materials in advanced processing techniques and is expected to offer a path for future developments in polymer processing.

2. FUNDAMENTALS OF POLYMER MELT RHEOLOGY

2.1. Viscosity and Viscoelasticity. The viscosity of Newtonian and non-Newtonian fluids is commonly described by the “power-law”, given by eqs 1 and 2:

$$\eta = K\dot{\gamma}^{n-1} \quad (1)$$

$$\sigma = K\dot{\gamma}^n \quad (2)$$

where η is the viscosity, $\dot{\gamma}$ is the shear rate, σ is the shear stress, and K and n are constants. For Newtonian fluids, $n = 1$ and K becomes equal to η . For pseudoplastic or shear-thinning fluids, $n < 1$, while for dilatant or shear-thickening fluids, $n > 1$.¹⁰

As observed in Figure 1(a), the viscosity versus shear rate plot of a polymer melt comprises three distinct regions. At low shear rates, flow is Newtonian. The viscosity at low shear rates is known as the zero shear viscosity. At intermediate shear rates, flow is pseudoplastic, whereas at higher shear rates, flow is again Newtonian.

The shear rheological behavior of polymer melts can be understood from the spatial orientation of the macromolecules. When at rest, the spatial orientation of the polymer molecules is completely random. This random orientation remains undisturbed at low shear rates, which explains the first Newtonian region. As the shear rate increases, the macromolecules start getting oriented in the direction of the application of shear. A polymer system comprises molecules

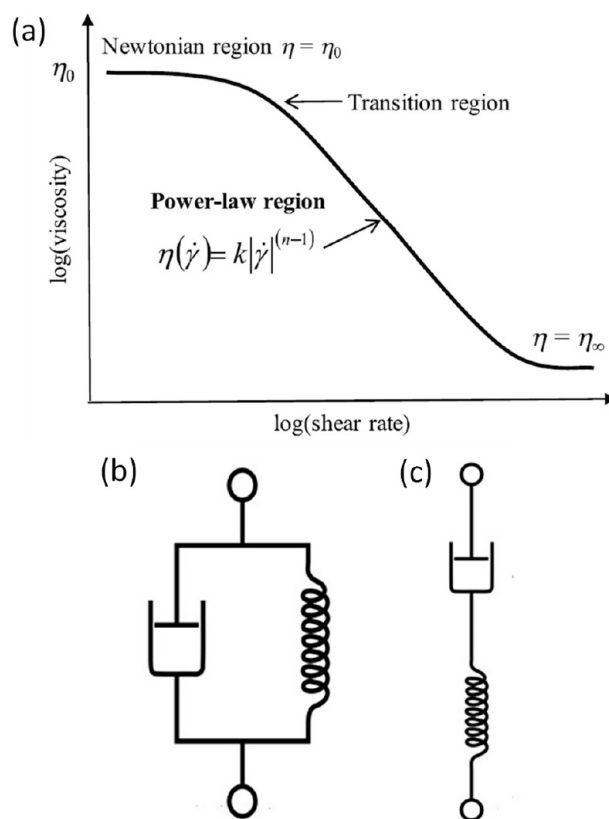


Figure 1. (a) Polymer viscosity versus shear rate response. Reproduced with permission from ref 13. Copyright 2018 Springer. (b) Voigt model and (c) Maxwell model. Reproduced and modified from ref 14. Copyright 2020 The Authors.

of different chain lengths. The higher molecular weight molecules need more energy to get oriented in the direction of shear, unlike the lower molecular weight molecules, which get oriented at relatively lower shear rates. Thus, with an increased rate of shear, more and more molecules get oriented in the direction of the application of shear, which leads to reduced resistance to flow or lowering of viscosity with increased shear rate. This explains the pseudoplasticity of polymer melts in the intermediate shear region. When the shear rate has increased sufficiently, all molecules are oriented, and a further increase in shear rate does not result in increased orientation. Thus, the viscosity does not reduce with an increase in the shear rate in the high shear rate region. This explains the second Newtonian region.¹¹ Melt processing of polymers is carried out at shear rates corresponding to the shear thinning region to achieve improved flow without causing degradation at excessively high shear rates.

Polymeric materials exhibit both viscosity and elasticity. In the case of cross-linked rubbers, flow is not possible. However, viscosity is manifested as a delayed response to a change in stress. The viscoelasticity of a cross-linked rubber can be qualitatively represented by a Voigt model [Figure 1(B)(a)], which comprises a spring in parallel with a dashpot. The spring is a linear elastic element, and the dashpot is a linear viscous element. This assembly will always return to the rest length of the spring when no force is acting on it. When a constant stress s is applied to this assembly, the dashpot starts moving at a rate of s/η , which is reduced asymptotically to zero as the stress is gradually transferred to the spring. The stress on the viscous

element is the external stress minus the stress in the elastic element. The rate of flow at any instant $d\varepsilon_R/dt$ is the rate of flow of the viscous element and is given by eq 3:

$$\frac{d\varepsilon_R}{dt} = \frac{s - \varepsilon_R E}{\eta} \quad (3)$$

Integration of eq 3 yields eq 4:

$$\varepsilon_R = \frac{s}{E} [1 - e^{-(E/\eta)t}] = \varepsilon_\infty (1 - e^{-t/\lambda}) \quad (4)$$

where $\varepsilon_\infty = s/E$ is the deformation at infinite time and $\lambda = \eta/E$ is a time constant. Eq 4 is the equation for the flow curve for a Voigt unit. This equation indicates a retarded elastic deformation. As the time constant approaches zero, the behavior becomes purely elastic.

The rheological behavior of an elastic liquid, such as a polymer melt, can be qualitatively represented by a Maxwell model [Figure 1(B)(b)], which comprises a spring and a dashpot in series. Unlike the Voigt model, this assembly does not have a unique reference length and deforms indefinitely under the influence of an external force. This behavior is similar to that of an un-cross-linked polymer above its glass transition temperature (T_g)/melting point. The rate of flow in such an assembly is given by eq 5:

$$\frac{d\varepsilon}{dt} = \frac{1}{E} \frac{ds}{dt} + s/\eta \quad (5)$$

If a Maxwell unit is given a certain strain and is held constant, the entire deformation will occur initially in the spring. But with time, the flow will occur in the dashpot, and the stress will dissipate gradually. Since strain is constant, $d\varepsilon/dt = 0$ and the residual stress after time t is obtained by integrating eq 5, which gives

$$s = s_0 e^{-t/\lambda} \quad (6)$$

where s_0 is the original stress and $\lambda = \eta/E$ is the relaxation time, which is the time required for the stress to decrease to $1/e$ of its original value. This is the equation for the relaxation curve of a Maxwell unit. A Voigt unit does not exhibit any relaxation mechanism under constant strain.

When a Maxwell unit is subjected to constant stress, $ds/dt = 0$, and the strain after time t may be obtained by integrating eq 5, which gives

$$\varepsilon = \varepsilon_0 + v_0 t \quad (7)$$

where $\varepsilon_0 = s/E$ and $v_0 = s/(E\lambda)$ is the creep rate. This is the equation for the flow curve.^{10,12}

Understanding the cause of polymeric materials' elasticity necessitates an insight into the molecular structure of polymers. A polymer molecule may be visualized as a long chain with many joints capable of rotation, thus imparting flexibility to the molecule. The enhanced flexibility of these macromolecules is responsible for several molecular configurations. A molecule will continuously change its configuration at temperatures above T_g due to Brownian motion. However, we can use statistical averages to describe the state of many macromolecules. For example, at a given temperature, there will be a unique value of the average end-to-end distance R of the molecules of a polymer melt that is at equilibrium. Deformation of the melt will change the average end-to-end distance. But once the deformation is stopped, Brownian motion will restore the average value of R to its equilibrium value. This explains the elasticity of polymeric materials.¹⁰

The simplest category of viscoelastic behavior is linear viscoelasticity. This behavior is observed when the deformation is so small that the polymer molecules are disturbed from the equilibrium configuration and entanglement to a negligible extent.¹⁰ The linear viscoelastic properties of polymer melts are determined using small amplitude oscillatory shear. In this experiment, a thin test specimen is sheared, such that the shear strain is a function of time and is given by eq 8:

$$\gamma(t) = \gamma_0 \sin(\omega t) \quad (8)$$

where γ_0 is the strain amplitude and ω is the frequency. The shear rate as a function of time can be determined by differentiation of eq 8:

$$\dot{\gamma}(t) = \gamma_0 \omega \cos(\omega t) = \dot{\gamma}_0 \cos(\omega t) \quad (9)$$

where $\dot{\gamma}_0$ is the shear rate amplitude. If γ_0 is adequately small, the stress can be determined using the Boltzmann superposition principle and is given by eq 10:

$$\sigma(t) = \sigma_0 \sin(\omega t + \delta) \quad (10)$$

where σ_0 is the stress amplitude and δ is a phase shift known as the mechanical loss angle.

The results of an oscillatory shear experiment can be presented by plotting the amplitude ratio $G_d (= \sigma_0/\gamma_0)$ and the phase shift as functions of ω . However, these quantities are not directly related to the material functions used to describe viscoelasticity. This problem has been overcome by using a trigonometric identity for writing eq 10 as

$$\sigma(t) = \gamma_0 [G'(\omega) \sin(\omega t) + G''(\omega) \cos(\omega t)] \quad (11)$$

where $G'(\omega)$ and $G''(\omega)$ are the storage modulus and loss modulus, respectively. These can be calculated using eqs 12 and 13:

$$G' = G_d \cos(\delta) \quad (12)$$

$$G'' = G_d \sin(\delta) \quad (13)$$

In a purely elastic solid, because there is no viscous dissipation and hence no phase shift, $G'' = 0$. In a purely viscous liquid, there is no energy storage and $G' = 0$. Thus, $G'(\omega)$ is a measure of elasticity and hence energy storage. $G''(\omega)$, on the other hand, is a measure of viscosity and hence energy loss.¹⁰

It is at times convenient to consider $G'(\omega)$ and $G''(\omega)$ as the real and imaginary components, respectively, of a complex modulus $G^*(\omega)$, given by eq 14:

$$G^*(\omega) \equiv G'(\omega) + iG''(\omega) \quad (14)$$

G_d is the magnitude of G^* and is given by eq 15:

$$G_d = \frac{\sigma_0}{\gamma_0} = |G^*| = \sqrt{(G')^2 + (G'')^2} \quad (15)$$

Alternatively, the results of small amplitude shear tests may be represented using two functions $\eta'(\omega)$ and $\eta''(\omega)$, both having the unit of viscosity:¹⁰

$$\sigma(t) = \dot{\gamma}_0 [\eta'(\omega) \cos(\omega t) + \eta''(\omega) \sin(\omega t)] \quad (16)$$

where η' and η'' are given by eqs 17 and 18, respectively:

$$\eta' = (\sigma_0/\dot{\gamma}_0) \sin \delta = G''/\omega \quad (17)$$

$$\eta'' = (\sigma_0/\dot{\gamma}_0) \cos \delta = G'/\omega \quad (18)$$

The complex viscosity η^* is given by

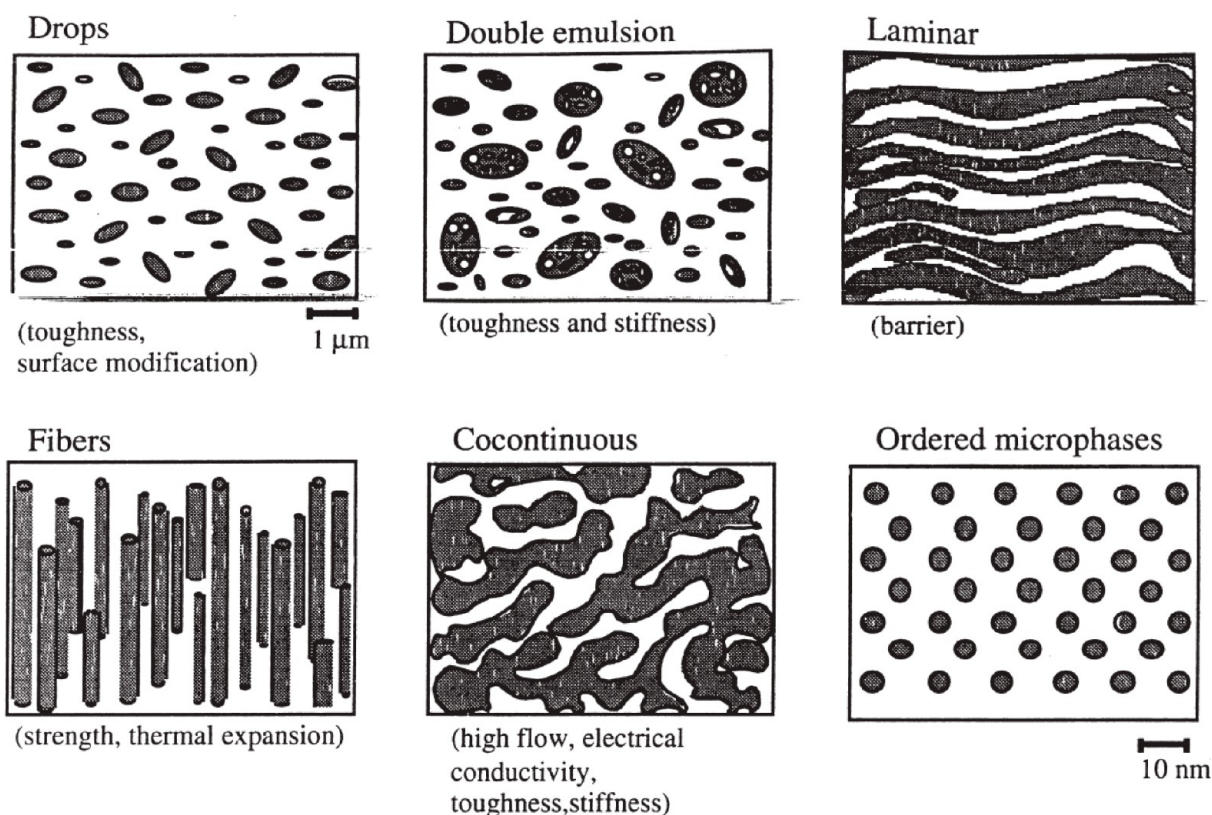


Figure 2. Schematic of the useful morphologies that can be produced by polymer–polymer melt blending. “Toughness and surface modification”, “strength and thermal expansion”, “high flow, electrical conductivity, toughness, and stiffness”, and “Co-continuous” appear as “toughness, surface modification”, “strength, thermal expansion”, “high flow, electrical conductivity, toughness, and stiffness”, and “Cocontinuous”, respectively. Reproduced with permission from ref 23. Copyright 2000 Wiley.

$$\eta^*(\omega) \equiv \eta'(\omega) - i\eta''(\omega) \quad (19)$$

$$|\eta^*| = \sigma_0/\dot{\gamma}_0 = \sqrt{(\eta')^2 + (\eta'')^2} \quad (20)$$

In an oscillatory shear test, the high-frequency region corresponds to the short range, whereas the low-frequency region corresponds to the long-time range. The frequency sweep test offers insight into the internal structure of materials. For example, a neat thermoplastic exhibits $G'' > G'$ in the lower frequency region (predominance of liquidlike behavior), a crossover point corresponding to $G' = G''$ and $G' > G''$ in the higher frequency region. The crossover frequency is equal to the reciprocal of the relaxation time.¹⁵ In contrast, a clay nanocomposite of the same polymer with a higher clay loading exhibits predominance of G' over the entire frequency range with no crossover point because of pseudosolid-like behavior brought about by prevented relaxation.^{16,17}

2.2. Extensional Viscosity and Strain Hardening.

Extensional flow may be defined as a deformation involving stretching along streamlines. The simplest extensional flow is a uniaxial extension, which is an axisymmetric flow involving stretching along the direction of the axis of symmetry. Another axisymmetric extensional flow is the biaxial extension, which involves compression in the direction of the axis of symmetry and stretching in the radial direction. In addition, there are many nonaxisymmetric extensional flows, such as “planar” extension.¹¹

For very small or slow deformations, linear viscoelasticity is unifying since it provides relationships between material functions that are measured using various kinds of

deformation. For example, according to this theory, the shear stress growth coefficient $\eta^+(t)$ is independent of the shear rate. Also, it specifies the relationship between $\eta^+(t)$ and the tensile stress growth function $\eta_E^+(t)$, which is measured at the beginning of a simple steady extension:

$$\eta_E^+(t) = 3\eta^+(t) \quad (21)$$

Large deformations and deformations applied at a high rate do not have any unifying theory. The response of a polymer melt to such a deformation depends on the extent, rate, and kinetics of the deformation. However, even at large strain rates, the initial part of the $\eta_E^+(t)$ curve should obey eq 21 since the total strain is less at small t values. For Newtonian flow, both shear and extensional viscosity are constant and independent of time and strain rate. They are related by the Trouton equation:¹⁸

$$\eta_E = 3\eta \quad (22)$$

Thus, shear flow properties and linear viscoelasticity are often used to gain a holistic understanding of the rheological properties of polymers at small strains. However, there are certain situations when two polymers have identical shear flow properties but have different processabilities in processing operations involving extension, such as foaming and film blowing.¹⁹ For example, Meissner²⁰ observed that in the film blowing of three grades of LDPE, two of the grades had identical performance but the third could not be drawn down to the same extent as the others. The zero-shear viscosities of the three grades were very similar. However, the extensional stress growth behavior of the three grades was significantly different, with the grade exhibiting the highest extensional

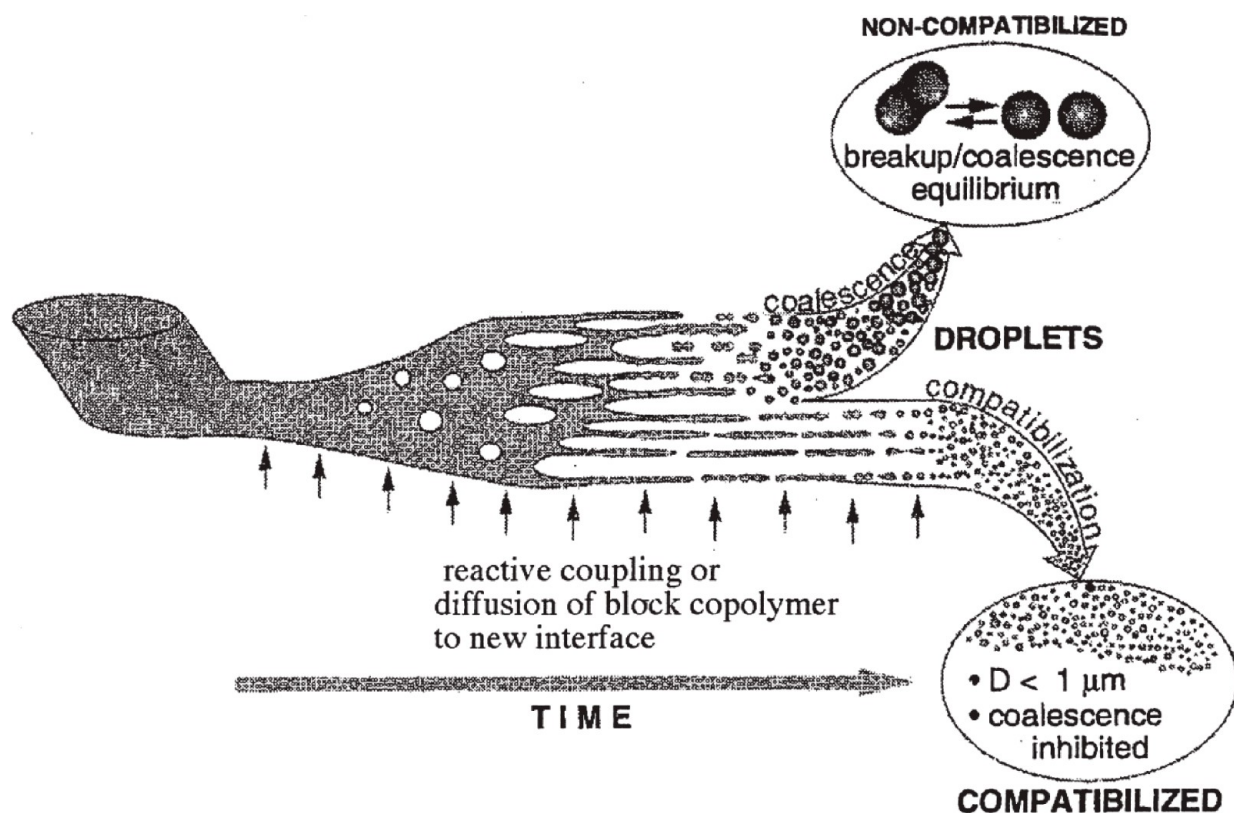


Figure 3. Schematic of the morphology development of polymer blends during melt blending. Reproduced with permission from ref 23. Copyright 2000 Wiley.

stress also being the one which could not be drawn down as the others. The grades were ascribed to differences in the extent of long-chain branching. The presence of long chain branches in polymer molecules gives rise to strain hardening, in which the stress increases more rapidly in comparison with the prediction of the linear theory. Strain hardening can be measured in terms of the strain hardening ratio (SHR), defined by Ruinaard²¹ as the ratio between the maximum value of elongational viscosity of the rheological melt extension (RME) curve (at time t_{\max}) and $3\eta_0^+(t)$ of the dynamic mechanical spectrometry (DMS) frequency sweep curve at time t_{\max} . Details of the RME method of determining elongational viscosity can be found in reference.²² Thus, subtle changes in molecular architecture, which may not affect the shear flow properties of a polymer, might significantly alter its extensional rheological properties.

Thus, it may be summarized that the high molecular weight and complexities in the molecular structure are responsible for the complex rheological behavior of polymeric materials. The influence of rheology on morphology development and processability in advanced processing operations have been discussed in the subsequent sections.

3. ROLE OF RHEOLOGY IN THE DEVELOPMENT OF THE MORPHOLOGIES OF POLYMERIC MATERIALS

3.1. Polymer Blends. **3.1.1. Fundamentals of the Morphology Developments of Polymer Blends.** Majority of immiscible polymer blends are produced in extruders. Melt blending can generate a broad spectrum of morphologies ranging from droplet/matrix to fibrillar, lamellar, and cocontinuous (Figure 2). Control over morphology is essential for achieving polymer blends with the required properties.

During melt blending, the softening polymer experiences high shear stress in the mixing equipment, which results in sheets of the dispersed phase. Scott and Macosko^{24,25} proved the formation of these sheets by quenching the samples in a batch mixer followed by selectively dissolving the polymer matrix in an appropriate solvent. In their opinion, the dispersed sheets or ribbons lose their stabilities under the influences of flow and interfacial tension. Moreover, holes are created in the ribbons. Sizes and concentrations of these holes increase until a fragile lace structure is produced, which breaks into particles with irregular shapes. These particles further disintegrate into almost spherical particles. This mechanism rapidly generates small dispersed-phase particles with sizes similar to those of the particles achieved via prolonged mixing. Prolonged mixing essentially reduces the size distributions of the largest particles.

Sheeting mechanism is followed during melt processing in single-screw extruders,²⁶ twin-screw extruders (TSEs),²⁷ and small cup and rotor mixers.²⁷ The dispersed-phase particles are stretched into sheets and ribbons, which further break into cylinders.²⁷ These cylindrical particles disintegrate into droplets due to Rayleigh-type instabilities. Knowledge of the dimensions of the developed cylindrical particles is critical to accurately predict the size distributions of the corresponding droplets. Morphological characteristics of polymer blends are substantially influenced by the quenching time. Thus, to appropriately assess polymer mixing, the polymer blends should be quickly quenched within a minute of their formation. Otherwise, the change in morphology during quenching must be considered, and this may not be relevant to mixing. Compared to the cases of large mixers, where the stress levels vary, the shear stress levels in small mixers are uniform. Both higher and lower stress levels are required for the effective

mixing of polymers during the production of polymer blends. At higher stress levels, particles with extended shapes are generated by the stretching of the dispersed phase. These particles experience instabilities and rupture at lower stress levels. In a small mixer, the dispersed phase is subjected to only one stress level, and thus, particles with highly extended shapes are obtained. Similar dispersions are produced in TSEs and internal mixers at comparable maximum shear rates. At comparable shear rates, similar dispersions of reactive blends are created in all mixers. However, small mixers exhibit inferior performances in forming a dispersion with superior quality during the processing of high-viscosity uncompatibilized blends. In these cases, the processing conditions must be altered for effective mixing. Additionally, Sundararaj et al.^{28,29} demonstrated that sheets were produced by the shearing of large molten droplets at adequately high shear rates. They reported that micrometer thick sheets were formed from millimeter-sized pellets under the action of shear in the parallel disc geometry. Extensional flow was not necessary for the creation of sheets. Disintegration of the pellets occurred in three ways: (i) stretching of the pellets into cylinders having droplets at the ends; (ii) extension of sheets that produced fingers at the edges; and (iii) stretching of the pellets into thin sheets that ruptured because of the creation of holes. A schematic of the breaking of these pellets was formulated using the Deborah number and the ratio of the first normal stress difference of the continuous phase to the restoring stress of the dispersed phase (droplet). The restoring stress of the droplet was the summation of the surface stress induced by interfacial tension and the first normal stress difference of the droplet. Numerous jointly acting stress levels were needed for the disintegration of the dispersed particles. The dispersed particles were affinely stretched in the higher-stress region. This was followed by their relaxation and breakage in the lower-stress region. Interfacial reaction stabilized the dispersed particles, and when the reaction produced a viscous, elastic shell surrounding the large, dispersed domains, ease of particle disintegration decreased. In these cases, stable sheets were generated by stretching, and subsequent hole formation did not take place.³⁰

Figure 3 shows a schematic of the evolution of the morphologies of polymer blends from sheets to fibers to droplets during the melt blending of polymers.

Morphological characteristics of immiscible polymer blends are significantly governed by rheology, which is discussed in the next section.

3.1.1.1. Role of Rheology. The classical method of predicting the final sizes of dispersed particles in immiscible polymer blends is based on the fundamental process of breakup of isolated particles in a flow-field of the continuous phase. This process is influenced by the capillary number (Ca) (represented by eq 23):

$$Ca = \frac{\tau R}{\sigma} = \frac{\eta_m \dot{\gamma} R}{\sigma} \quad (23)$$

where τ is the shear stress, η_m is the viscosity of the continuous phase, $\dot{\gamma}$ is the shear rate, σ is the interfacial tension, and R is the particle radius. When Ca exceeds a critical value, Ca_{crit} , τ overrules the interfacial stress, and the particle is stretched until it ruptures. The diameter of the produced droplet (B_{min}) is given by eq 24:

$$B_{min} = \frac{2Ca_{crit}\sigma}{\eta_m \dot{\gamma}} \quad (24)$$

In the case of the rupture of Newtonian droplets in stationary flow, Ca_{crit} is affected by the type of flow and the viscosity ratio λ (represented by eq 25).³¹

$$\lambda = \frac{\eta_d}{\eta_m} \quad (25)$$

where η_d is the viscosity of the dispersed phase.

These findings are valid only for isolated particles. Nevertheless, during melt blending, several particles are very close to each other. This can lead to their coalescence, thereby increasing the sizes of the dispersed particles. Furthermore, the Ca_{crit} values obtained in the above-mentioned study indicate the conditions for droplet stability in stationary flow. However, during the melt blending of polymers, the dispersed phase undergoes nonstationary deformation. When the Ca values are sufficiently high, the dispersed particles are elongated into long threads, which eventually disintegrate into a series of droplets.^{32,33} Elongation reduces the diameter of the stretching droplet, thereby lowering the local Ca until Ca_{crit} for the breakup of the elongated thread is reached ($Ca_{crit} = 1$).³³ Then, the elongated thread disintegrates according to the Raleigh mechanism, forming a line of droplets with diameters approximately twice the thickness of the thread undergoing rupture.³⁴

Hence, the final sizes of the dispersed particles are regulated by the total deformations of the original particles. Thread diameter (B_{thread}) is dependent on the total amount of strain exerted ($\gamma = \dot{\gamma}t$) and is presented by eq 26:

$$\frac{B_{thread}}{2R_0} = (1 + \gamma^2)^{-1/4} \quad (26)$$

where R_0 is the original particle radius based on the assumption of affine deformation. This affine deformation is feasible under the action of shear only if $Ca/Ca_{crit} > 2$.³⁵ In the case of extensional flow, affine deformation is possible only if $Ca/Ca_{crit} > 5$.³³ Nevertheless, in most polymer-processing equipment, the shear flow overrules because sustaining elongation for an extended period of time is difficult.

Rupture of the thread based on the Raleigh mechanism occurs only if the residence time of the thread exceeds the time needed for the disintegration of the thread. The breakup time t_b can be calculated using eq 27, which is based on Tomotika's theory:³⁶

$$t_b = \frac{\eta_m B_{thread}}{\sigma \Omega_m} \ln \left(\frac{0.81 B_{thread}}{2\alpha_0} \right) \quad (27)$$

where α_0 is the amplitude of the initial disturbance, generally in the range of 10^{-7} – 10^{-9} m,^{36,37} and Ω_m is a function of λ .³⁸ However, as eq 27 is only applicable to Newtonian fluids at rest, it is valid for the melt blending of polymers. Stretching stabilizes the liquid thread against breakup, thereby forming thinner threads.³⁷ Droplet coalescence increases the average particle size, rendering the predictions of eqs 24 and 26 invalid. Coalescence takes place only when the concentration of the dispersed phase is sufficiently high and when the particle radius is not higher than the critical radius.³³

The above-mentioned theories are only applicable to dispersed particles and threads and are not valid to their initial formations. In the early stages of the melt blending of

polymers, a rapid change, involving the creation of striated structures, in morphology takes place.^{25,26,29,39–41} According to Plochocki,³⁹ this change occurs by an “abrasion” mechanism. Macosko et al.^{25,29,41} suggested a “sheeting” mechanism, in which molten pellets are stretched into ribbons or “sheets”. Sundararaj et al.²⁸ presented the various conditions of the development of “sheets” or threads. According to them, the production of sheets and threads was governed by the ratio of normal stresses and the Deborah number. They proposed that sheets were readily generated in shear flow, and threads were exclusively produced at low shear rates ($<5 \text{ s}^{-1}$). Sheets were not converted into threads because interfacial forces were usually inadequate to significantly alter the shapes of the sheets.^{29,32}

Shear flow decreases the sheet thickness until the sheet is ruptured by interfacial disturbances. The reduction in the sheet thickness can be calculated as described hereinafter.⁴² A sphere with the initial radius R_0 will be converted into a ribbon (“sheet”) under a shear-flow field. The width of the ribbon will be R_0 , whereas the thickness B_{sheet} will be considerably less; nevertheless, both the ribbon and sheet will have equal volumes. B_{sheet} is represented by eq 28 when $\gamma \gg 1$.³⁴

$$\frac{B_{\text{sheet}}}{R_0} = \frac{2}{3}(1 + \gamma^2)^{-1/2} \quad (28)$$

The dependence of B_{sheet} on total deformation is depicted in Figure 4. B_{sheet} significantly and rapidly decreases with deformation than in the case of B_{thread} .

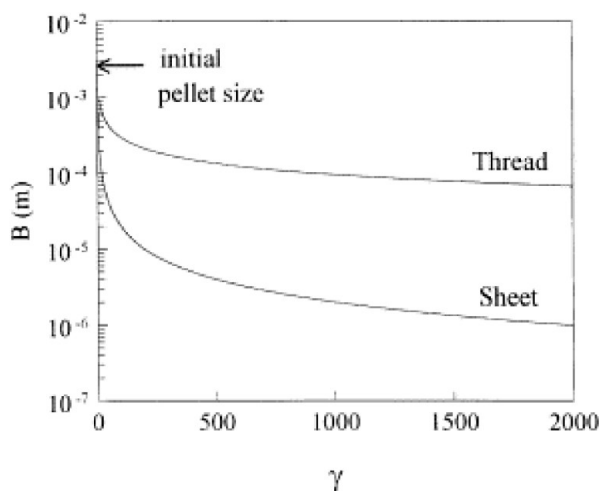


Figure 4. Diameter of the thread and thickness of the sheet in the case of affine deformation of a pellet with a 3 mm thickness into a thread (eq 26) or a sheet (eq 28), respectively. Reproduced with permission from 34. Copyright 1999 Elsevier Science Ltd.

At a certain thickness, the rupture of the sheet starts by the creation of holes. This breakage may be caused by the interfacial instabilities developed in the laminar structures in the course of flow⁴³ or contamination of the blend.⁴¹ Sizes of the holes increase because of interfacial forces, and eventually coalescence takes place, generating a network of filaments. Threads and droplets are produced by the rupture of this network²⁶ depending on the processing conditions. The final sizes of the dispersed particles are of the same order of magnitude as the final sheet thickness. Hence, eq 28 can be used to predict the final sizes of the dispersed particles. The

sizes of the particles typically obtained after melt blending of the polymers are actually predicted to be 0.1–1 mm by eq 28 (Figure 4). Therefore, a “sheeting” mechanism can elucidate the rapid decrease in the sizes of particles during the melt blending of polymers.^{25,26,29,39–41} Thus, shear flow is efficient for achieving dispersion as it reduces the striation thickness by rupturing the sheets into dispersed particles. The decrease in the sizes of particles by the elongation of threads followed by their disintegration into droplets is considerably less effective in this regard.

When the concentrations of the dispersed particles exceed 1%, the particles collide and the particle size increases because of coalescence. The final particle size is controlled by the equilibrium between droplet coalescence and formation because of the breakage of fibers.²⁷ Coalescence may be minimized using compatibilizers. The mechanism of compatibilization is beyond the scope of this review.

In their studies on the production of polyethylene (PE)/ polystyrene (PS) blends, Willemsse et al.³⁴ reported the prevalence of the “sheeting mechanism” in both single-screw extrusion and static mixing. The particle size rapidly decreased, in accordance with the theoretical prediction. After breakup, further significant lowering of particle size was not observed. The type of morphology was governed by the stabilities of the fibers generated after the rupture of sheets. Fibrillar morphology was achieved when Ca exceeded one. Lower values of Ca resulted in the formation of droplet-matrix morphology. The final particle size was independent of Ca. The development of fibrillar morphology is enhanced under an elongational flow field, as discussed in the next section.

The most efficient mixing in the production of a cocontinuous structure via shear is accomplished when the viscosities and volume fractions of the two blend components are equal. Equal volume fractions maximize the opportunity for achieving connectivity between these components. However, in the majority of blends, the viscosities of these phases are not equal. The phase possessing lower viscosity has the tendency to remain continuous as this leads to minimum energy dissipation during flow. This tendency can be overcome if the volume fraction of the phase having higher viscosity is enhanced to the same extent as the difference between the viscosities of the phases. Consequently, cocontinuity of phases with different viscosities can be achieved.

The composition corresponding to phase inversion can be determined via several equations. Eq 29 represents the relationship between the phase inversion composition and the volume fractions and viscosities of components:^{44,45}

$$\frac{\varphi_{1,PI}}{\varphi_{2,PI}} \times \frac{\eta_2}{\eta_1} \cong 1 \quad (29)$$

where η_i and $\varphi_{i,PI}$ are the viscosity and volume fraction, respectively, of the component i at phase inversion. As $\lambda = \eta_1/\eta_2$ and $\varphi_{1,PI} = 1 - \varphi_{2,PI}$, eq 29 can be written as

$$\varphi_{2,PI} = \frac{1}{1 + \lambda} \quad (30)$$

λ should be calculated using the viscosities at the shear stress employed during melt blending.^{46–48} As polymer blends are frequently produced in torque rheometers or similar processing devices, Avgeropoulos et al.^{49,50} utilized the torque ratio τ_1/τ_2 as an alternative to λ .

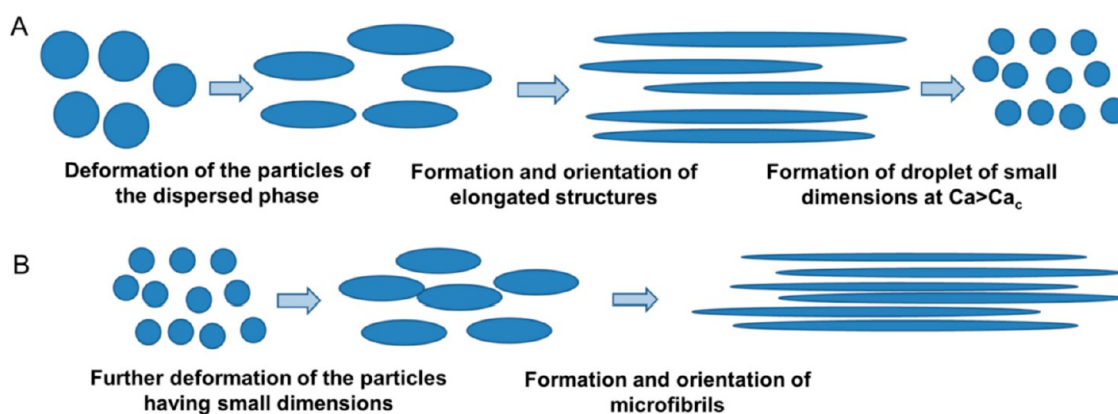


Figure 5. Schematic of the possible mechanism of the droplet-to-fibril transition in immiscible blends subjected to elongational flow: (A) deformation of the original particles of the dispersed phase and (B) formation of microfibrillar structures. Reproduced from ref 82. Copyright 2020 The Authors.

The basic equation was applicable to blends when λ was near unity.^{51–54} Nevertheless, significant deviations occurred when λ was not close to unity.^{47,55,56} Thus, the equation was modified by several research groups to obtain a better match between the theoretical predictions and experimental observations. For example, in their investigations on the polypropylene (PP)/ethylene-propylene rubber (EPR) and PS/styrene-butadiene rubber (SBR) blends produced in an internal mixer, Ho et al.⁵⁷ used an exponent and a prefactor and obtained eq 31:

$$\frac{\varphi_{1,PI}}{\varphi_{2,PI}} = 1.22(\tau_1/\tau_2)^{0.29} \quad (31)$$

Kitayama et al.⁵⁸ reported that an appropriate match between the theoretical and experimental observations of uncompatibilized polyamide 6 (PA6)/styrene-acrylonitrile (SAN) copolymer blends was achieved when the coefficient in eq 31 was altered:

$$\frac{\varphi_{1,PI}}{\varphi_{2,PI}} = 0.887(\tau_1/\tau_2)^{0.29} \quad (32)$$

where 1 = PA6 and 2 = SAN. Everaert et al.⁵⁹ observed that eq 33 was applicable to the PP/(PS/poly(2,6-dimethyl-1,4-phenylene oxide (PPO))) blend system:

$$\frac{\varphi_{1,PI}}{\varphi_{2,PI}} = (\eta_1/\eta_2)^{0.3} \quad (33)$$

where 1 = PP and 2 represent different compositions of miscible PS/PPO blends.

Utracki⁴⁷ employed an approach involving intrinsic viscosity ($[\eta]$) and the maximum packing volume fraction φ_{max} . He considered the viscosity-concentration behavior and speculated that blend viscosities were equal when the polymer 2 was added to the polymer 1 and vice versa at the phase inversion composition. Furthermore, he employed a relation suggested by Krieger and Dougherty for monodispersed hard spheres and proposed eq 34, which was simplified to eq 35 for $0.1 < \lambda < 10$.

$$\lambda = \left[\frac{(\varphi_{max} - \varphi_{2,PI})}{(\varphi_{max} - \varphi_{1,PI})} \right]^{[\eta]\varphi_{max}} \quad (34)$$

$$\varphi_{2,PI} = \frac{(1 - \log \lambda / [\eta])}{2} \quad (35)$$

where $[\eta]$ was regarded as 1.9 for spherical domains and $\varphi_{max} = 0.84$.

Interfacial viscosity or interfacial tension effects can also be considered using other equations for $[\eta]$.⁴⁷ The validity of the equation was determined by comparing literature data acquired under numerous mixing conditions using different λ determination methods.³⁰ The results were in better agreement with the experimental data than those predicted by eq 30, specifically when the λ values were not close to unity.^{47,51,56}

Thus, the morphological characteristics of immiscible blends are significantly regulated by the rheological properties of the blend components. Rheology governs both the kind of blend morphology and the dispersed particle size. Ca and λ are of considerable importance in the evolution of the morphologies of blends. Elongational flow also facilitates morphology development of blends. The role of extensional rheology in the morphology development of blends is explained in the subsequent section.

3.1.1.1. Role of Extensional Rheology. Shear flow exhibits lower energy efficiencies in both dispersive and distributive mixings when compared with those of elongational flow.^{60–62} Moreover, melt droplets of high- λ -blends are more efficiently broken under an extensional flow field than under a shear flow field.^{63–66} According to Luciani and Utracki,⁶⁷ the higher efficacy of elongational flow field in causing improved dispersion in blends is more significant when λ is 3.8 or higher. In recent years, substantial research, such as the use of extensional mixing elements (EMEs) in single-screw^{60,68,69} and TSEs,^{70,71} has been performed on the development of processing equipment that imparts elongational flow. The unique nonscrew devices called vane extruders (VEs), comprising several vane plasticizing and conveying units^{72,73} and eccentric rotor extruders (EREs), are regulated by elongational flow.^{74,75} Extensional flow fields are usually generated in converging channels. Yang et al.⁷⁶ designed a triangle-arrayed triple-screw extruder (TTSE) possessing three mesh zones and a convergence-divergence central zone, which were responsible for the creation of a complicated flow field. The melt in the central zone experienced high axial flow velocity. The axial pressure gradient caused the fluid to flow out. Furthermore, some of the melt in the central region was forced into the mesh zones by the screw tips. Thus, the

material in the TTSE alternatively experienced shear and extensional flow fields. The researchers processed polyamide-66 (PA66)/PPO blends with high λ values in the TTSE and compared the morphological characteristics and mechanical properties of the acquired blends with those of the TSE-processed blends with the same composition. The blends processed in the TTSE possessed smaller dispersed particles, leading to better mechanical properties of the blends. The superior morphologies of the blends processed in the TTSE were ascribed to the extensional flow field. Therefore, the researchers demonstrated that the extensional flow was more effective than the shear flow in the blending of polymers with high λ values.

Carson et al.^{77,78} introduced a static EME into a TSE and examined the PP/PS blends with λ values in the range of 0.3–10 processed in this TSE; results revealed that the generation of elongational flow improved the dispersion of particles over the entire viscosity range when compared with the case of the shear flow field of a standard TSE. Thus, the researchers demonstrated that elongational flow enhanced the dispersion of particles during the blending of polymers with different λ .

Extensional flow is effective for the development of fibrillar morphology.^{79–81} He et al.⁸⁰ produced a supertough polylactic acid (PLA)/thermoplastic poly(ester)urethane (TPU) blend with 25 wt % TPU using a continuous elongational flow field in an ERE. The blend comprised *in situ*-generated aligned TPU nanofibers and favorable interfacial adhesion.

Figure 5 depicts a schematic of a plausible mechanism that explains the droplet-to-fibril transition occurring in immiscible blends when they are subjected to extensional flow. Under an elongational flow field, the polymer molecules of the matrix phase exhibit the tendency to orient and align themselves in the direction of flow. The particles of the dispersed phase also deform, creating elongated structures aligned in the direction of stretching (Figure 5A). When Ca_{crit} is reached, these elongated structures disintegrate, forming small droplets. These droplets are further deformed in extensional flow, eventually generating microfibrils aligned in the direction of flow (Figure 5B).⁸²

In their studies on low-density PE (LDPE)/PA6 blends, Mistretta et al.⁸³ observed that the blend samples prepared under an elongational flow field without a compatibilizer exhibited superior mechanical properties comparable to those of the samples achieved using a compatibilizer (ethylene-glycidyl methacrylate) under a shear flow field. The excellent mechanical properties of the samples acquired under the elongational flow field were attributed to the orientations of molecules during extensional flow.

Hedegaard et al.⁸⁴ analyzed the role of extensional rheology in the development of a cocontinuous morphology. They produced cocontinuous blends of PE and PLA. The extensional and shear rheological properties of PE and PLA were independently varied by tuning the long-chain branching. Branching significantly enhanced the zero-shear and extensional viscosities; however, it did not change the shear viscosity at the shear rates usually employed during mixing. Use of a branched polymer facilitated the percolation of the other blend component into a continuous structure with less material. When a linear/linear blend was replaced by a branched/branched blend, the range of compositions affording cocontinuity broadened from 39–59 to 25–76 vol %. This was ascribed to the ability of a strain-hardening polymeric matrix to promote elongation and thus percolation of the

minor phase. Particle size reduced in the presence of a small amount of strain hardening as this facilitated the creation of narrow structures and stabilized the acquired morphology. After being annealed, all blends demonstrated a rate of morphological coarsening inversely proportional to the zero-shear rate viscosity, indicating that the coarsening of the blend morphology was controlled by shear rheology instead of extensional rheology.

Thus, it may be concluded that during the melt blending of polymers, extensional flow facilitates the achievement of superior dispersion, specifically when the λ values of the polymers being blended are high. Furthermore, extensional rheology plays a vital role in the construction of fibrillar morphology and may influence the development of cocontinuity. More research needs to be conducted on the role of extensional rheology in the establishment of cocontinuity.

3.2. Polymer Composites and Nanocomposites.

3.2.1. Basics of Morphology Development. During the processing of discontinuous fiber-reinforced composites, shear induces the alignment of fibers in the flow direction. In contrast, stretching leads to the alignment of fibers in the direction of stretch. In injection molding, the skin, which is the layer in contact with the mold walls, contains fibers aligned in the flow direction because of shear. Below the skin, the polymer melt with suspended fibers continues to be sheared, which aligns the fibers along the lines of shear. At the core, that is, the center of the melt, the shear rate is low, and the flow is predominantly elongational, leading to fiber alignment in the transverse direction. Hence, in an injection-molded discontinuous fiber-reinforced composite, the fibers in the center of the product are aligned transverse to the direction of flow, whereas those near the edges of the product are aligned parallel to the direction of flow.^{85,86}

During the injection molding of fiber-reinforced composites, the injection speed substantially influences the alignments of fibers. Slower speed results in higher alignments of fibers in the flow direction. This is due to the fact that during slower mold filling, thicker solid layers are generated in the proximity of the cold mold surface, leading to a sharper velocity gradient in the direction of layer thickness. This consequently results in a predominant shear flow, which enhances fiber alignment in the direction of flow.^{86,87}

A major cause of concern in the injection molding of fiber-reinforced thermoplastics is extensive fiber attrition during molding, which may lower the number-average fiber length from 12 mm to a value as low as 1 mm.⁸⁸ Gupta et al.⁸⁹ and von Turkovich et al.⁹⁰ have demonstrated that fiber breakage occurs throughout the plasticating unit. The extent of fiber breakage depends on various factors such as screw design, shear rate, melt viscosity, and fiber volume fraction.⁹¹

The factors causing fiber attrition include fiber–fiber interactions, fiber–machine interactions, and the rheological characteristics of the matrix.⁹⁰ The first two factors rely on the collisions of fibers with neighboring objects and are often minor factors.⁹² Because of their rotation during downstream flow under the influence of shear, the fibers undergo a significant number of collisions with an increase in their volume fraction, resulting in more considerable attrition.^{93,94} Fiber–fiber interactions take place at relatively high fiber contents. With an increase in the aspect ratios of fibers, the extent of interactions occurring at a specific fiber content increases.⁹⁵ Abrasion of the processing equipment during the processing of fiber-reinforced thermoplastics is indicative of

Table 1. Classification of Fiber Suspensions

	crowding factor	category	type of fiber contact
$nL^3 \ll 1$	$N_c < 1$	dilute	rare collision
$nL^3 > 1$ or $nL^2d > 1$	$1 < N_c < 60$	semidilute	frequent collision
$nL2d > 1$	$N_c > 60$	semiconcentrated	continuous contact

fiber–machine interactions and their roles in fiber attrition.⁹⁶ Melt rheology substantially affects fiber breakage during composite processing. Fibers experience stresses because of shear and extension. During shear flow, the rotating fibers are subjected to deforming forces. Fiber attrition occurs when the critical shear stress is reached, leading to buckling of the fibers.^{97–99} The critical shear stress is influenced by the elastic moduli and aspect ratios of the fibers. During pure elongational flow, typically, the fibers do not break.¹⁰⁰ Nevertheless, in most processing equipment, both shear and elongational flows take place. The role of rheology in fiber attrition is discussed in the next section.

During the extrusion of fiber-reinforced composites, the application of convergent dies results in a high extent of fiber orientation in the direction of flow. Moreover, the use of a breaker plate between the extruder screw and convergent die further enhances the extent of fiber orientation as the breaker plate increases the shear flow. The highest extent of fiber alignment is obtained when the breaker plate is positioned at the entry point to the convergence zone.¹⁰¹

Similar to the case of injection molding, fiber attrition is a major problem encountered during the extrusion of fiber-reinforced thermoplastics. The mechanisms of fiber attrition are common for both processing techniques. The shapes of the polymer granules being fed into the extruder affect the amount of fiber breakage because of the occurrence of the fiber–polymer interaction during the crushing of the fibers by the solid polymer particles. Bigg¹⁰² has demonstrated that breakage is more prominent with pellets than with powder when processing is performed in a single-screw extruder. Additionally, a higher extent of breakage occurs in a TSE than that in a single-screw extruder. This can be attributed to the higher shear forces experienced by the fibers in the melting zone of the TSE. The fiber length in this zone is approximately 50% of the initial fiber length.⁹⁰ Lunt and Shortall^{103,104} have reported that fiber breakage in the melting zone mainly occurs in the thin film between the solid bed and barrel wall. Furthermore, fiber length is influenced by the fiber content and viscosity of the melt. Similar to the case of injection molding, fiber–polymer interaction is the predominant cause of fiber attrition.^{105,106}

Melt processing of polymer nanocomposites is governed by the thermodynamic interaction between polymer molecules and nanoparticles. In the cases of clays, the migration of the polymer molecules into clay galleries is also important.^{107,108} The dispersion quality achieved during melt blending is regulated by the enthalpic interaction between the polymer molecules and nanoparticles and by the processing conditions. Favorable enthalpic interactions are crucial for realizing nanolevel dispersion, and in the absence of these interactions, microcomposites are formed. Optimum processing conditions are of equal importance.¹⁰⁹ Paul et al.^{110,111} have reported that during the production of polymer/clay nanocomposites, intercalation/exfoliation is regulated by shear, resulting in the separation/peeling of the platelets of clay tactoids by the combination of mechanical and chemical forces. This theory is

different from the conventional theory,^{108,112} according to which upon entering the clay galleries, the macromolecules enhance the d -spacing between platelets, thereby overcoming the van der Waals forces between them, causing the separation of platelets. The mechanism of peeling and function of shear in the generation of polymer/clay nanocomposites have also been investigated by other researchers.^{113,114} The roles of both high shear rate and longer residence time in the achievement of high delamination have been reported by Treece et al.¹¹⁶ and Zhu et al.¹¹⁷

3.2.1.1. Role of Rheology. The properties of short-fiber composites are significantly governed by the fiber orientation distribution acquired during processing, which is consequently influenced by the flow behavior of the fiber suspension. Thus, understanding the flow behavior of the fiber suspension with respect to the fiber orientation is necessary for the optimization of mold design and processing conditions to maximize the composites performance.^{118,119}

Similar to polymer melts and solutions, fiber suspensions exhibit characteristics, including the Weissenberg effect, shear thinning, and viscoelasticity, of non-Newtonian fluids.^{120–122}

Generally, with an increase in filler content, the viscosities of the composites increase. However, different types of relationships between these two quantities have been reported in the literature. These relationships depend on several factors such as filler type and concentration.^{123–126} Moreover, this increase in the viscosities of the composites is affected by the shear rate or angular velocity.^{127–135} At low shear rates, the increase in viscosity is substantially high. It can be hypothesized that an increase in shear rate increases the alignments of fibers in the flow direction. Consequently, the contributions of fibers to the viscosities of the composites are reduced. At high fiber contents, flow restrictions and even yielding behaviors are noticed in the low-shear rate region. This has been attributed to significant fiber–fiber interactions.^{123,132–135}

Rheological characteristics of fiber suspensions are influenced by fiber properties, fiber interactions, suspending fluid properties, and the imposed flow field.¹²⁰ The fiber interactions rely on not only the volume fraction (V_ϕ) of the fiber but also the aspect ratio (L/d , where L is the length of the fiber and d is the diameter of the fiber) of the fiber.¹³⁶ According to Kerekes and Schell,^{137,138} the crowding factor N_c is presented by eq 36:

$$N_c = \frac{2}{3} V_\phi \left(\frac{L}{d} \right)^2 \quad (36)$$

Different parameters, for example, nL^3 and nL^2d , where n is the number of fibers per unit volume of suspension, have been used to classify fiber suspensions. For suspensions with rodlike particles, V_ϕ is represented by eq 37:

$$V_\phi = n\pi d^2 \frac{L}{4} \approx nd^2L \quad (37)$$

Fiber suspensions are classified into three categories: dilute, semidilute, and semiconcentrated (Table 1):^{136,137}

In a dilute suspension, each fiber can freely rotate without hindrance from the neighboring fibers. In a semidilute suspension, the average separation between two adjacent fibers is larger than the fiber diameter and less than the fiber length. Although hydrodynamic interactions between fibers become more prominent in semidilute suspensions, they do not cause significant fiber–fiber interactions. In a semi-concentrated suspension, the average separation between two adjacent fibers is lower than the fiber diameter. This prevents the independent rotation of the fiber, except around its axis of symmetry. Any motion of a fiber must involve the motions of all neighboring fibers.¹³⁶

Jeffery¹³⁹ examined dilute particle dynamics. He investigated the movement of an elliptical particle in shear flow without considering inertia. His analytical solutions can be employed to describe the particle alignment, and his calculations reveal that the particle undergoes rotation around the vorticity axis in an orbit called Jeffery's orbit. The orbits of blunt-ended particles, such as rigid rods and fibers, are similar.¹⁴⁰ According to Jeffery's theory, the fiber orientation (Φ , θ) in spherical coordinates is presented by coupled differential equations, and the solutions of these equations afford eqs 38 and 39:

$$\tan \varnothing = A_r \tan \left(\frac{Gt}{A_r + A_r^{-1}} \right) \quad (38)$$

$$\tan \theta = \frac{CA_r}{\sqrt{(A_r^2 \cos^2 \varnothing + \sin^2 \varnothing)}} \quad (39)$$

where A_r is the fiber aspect ratio, G is the shear rate, t is the local time in the orbit, and C is a constant of integration called the orbit constant. C can take any positive value. When $C = 0$, the fiber is aligned along the z -axis and spinning in the vorticity direction, exhibiting a “log-rolling” motion. When $C \rightarrow \infty$, the fiber is rotating in the xy -plane, tumbling in the plane of shear. Particularly, a single fiber with a large A_r spends most of the time aligned in the direction of flow and quickly flips every half-period. When the shear stress reaches a steady state, a pseudoequilibrium orientation of the fiber is attained, which may gradually change after a short time span.¹⁴⁰

Folgacs and Mason^{97,141} conducted experiments and determined the average rotations of fibers in linear shear flow. They examined both the dilute and semidilute suspensions. They observed that the Jeffery's theory provided a suitable approximation for determining the fiber rotation even in the semidilute suspension.

At low fiber concentrations, interfiber interaction is rare, and the flow behavior is influenced by long-range hydrodynamics.¹²⁰ With an increase in the fiber concentration, the fiber–fiber interaction can severely affect the fiber motion.^{142,143} Comparison of the results predicted by simulation studies performed using the Jeffery's equation and actual measurement results of fiber orientation in an injection-molded part indicated that the Jeffery's equation overestimated the extent of orientation and shear strain at which the steady state was attained. Therefore, Folgar and Tucker¹⁴⁴ modified the Jeffery's equation to include a term that explained the inhibition of full alignment of the fiber. This term considers the fiber–fiber interaction. The Folgar–Tucker model improved the predictions of the steady-state fiber orientation. Nevertheless, the estimation of the strain at which this orientation was reached was not improved. Consequently, Huynh¹⁴⁵ introduced the strain reduction factor, explaining

that as the fibers moved in clusters, they experienced less strain when compared with the case of the bulk. Other models used in fiber suspension rheology for predicting the fiber orientation are Kamal and Mutel's model,¹⁴⁶ the reduced strain closure (RSC) model,¹⁴⁷ and the anisotropic rotary diffusion (ARD) model.¹⁴⁸ On the basis of the ARD–RSC model,¹⁴⁸ Tseng et al.^{149,150} developed an improved ARD model combined with the retarding principal model (iARD–RPR model) for estimating the core–shell orientations of fibers in both short- and long-fiber-reinforced composites. In a separate study,¹⁵¹ the researchers utilized the iARD–RPR model for injection molding simulations to predict the orientations of fibers in both short- and long-fiber-reinforced composites of two different kinds of fibers (glass and carbon). Under the extreme conditions of high fiber concentration and long fiber length, the predicted orientation pattern comprised a thick core and narrow shell. The estimated orientation was in accordance with the experimental observations. Thus, the researchers demonstrated the ability of the iARD–RPR model to predict anisotropic fiber orientation in fiber-reinforced thermoplastics.

Several studies have been conducted on the simulation of the suspensions of flexible fibers. Yamamoto and Matsuoka¹⁵² have described flexible fibers as chains of rigid spheres linked with springs, exhibiting the potential to mimic the resistances to twisting and bending. Chain connectivity is sustained by constraints; thus, they presented equations that must be solved along with the equations of motion. Ross and Klingenberg⁹⁸ have defined flexible fibers as inextensible chains of rigid prolate spheroids, linked by ball-and-socket joints. This model can be representative of large aspect-ratio fibers with fewer bodies, eliminating the need for iterative constraints for maintaining fiber connectivity. This facilitates the simulation of concentrated suspensions by simplifying the computations. Schmid et al.¹⁵³ have described flexible fibers as chains of spherocylinders linked by ball-and-socket joints, which interact via short-range repulsive and frictional forces. They have demonstrated that the fiber equilibrium shape, flexibility, and interfiber friction must be considered in the prediction of the suspension microstructure and flocculation behavior. Switzer III and Klingenberg¹²⁰ have investigated the relationships between fiber properties, fiber–fiber interactions, and the resultant rheological characteristics using the model proposed by Schmid et al.¹⁵³ They have indicated that the rheological characteristics are governed by the fiber suspension properties including equilibrium shape, flexibility, aspect ratio, friction, concentration of the fiber, and suspending fluid features. The fibers have been defined as chains of interconnected rods undergoing shear flow and exhibiting fiber–fiber interactions. However, hydrodynamic interactions have not been considered. Lindstrom and Uesaka^{154–156} have conducted further studies using the model proposed by Schmidt et al. with several additions to include the influences of particle inertia, noncreeping fiber–fluid interactions, hydrodynamic interactions between fibers, and self-interactions of the suspension microstructure and flocculation behavior. They also introduced artificial dampening of the joints between fiber segments. The new model demonstrated high numerical stability.

As predicted by hydrodynamic theories, the viscosity of a suspension is presented by eq 40:

$$\mu_r = 1 + \alpha_0 V_\phi \quad (40)$$

where μ_r is the relative viscosity, V_ϕ is the volume fraction of the suspended particles, and α_0 is a dimensionless factor that

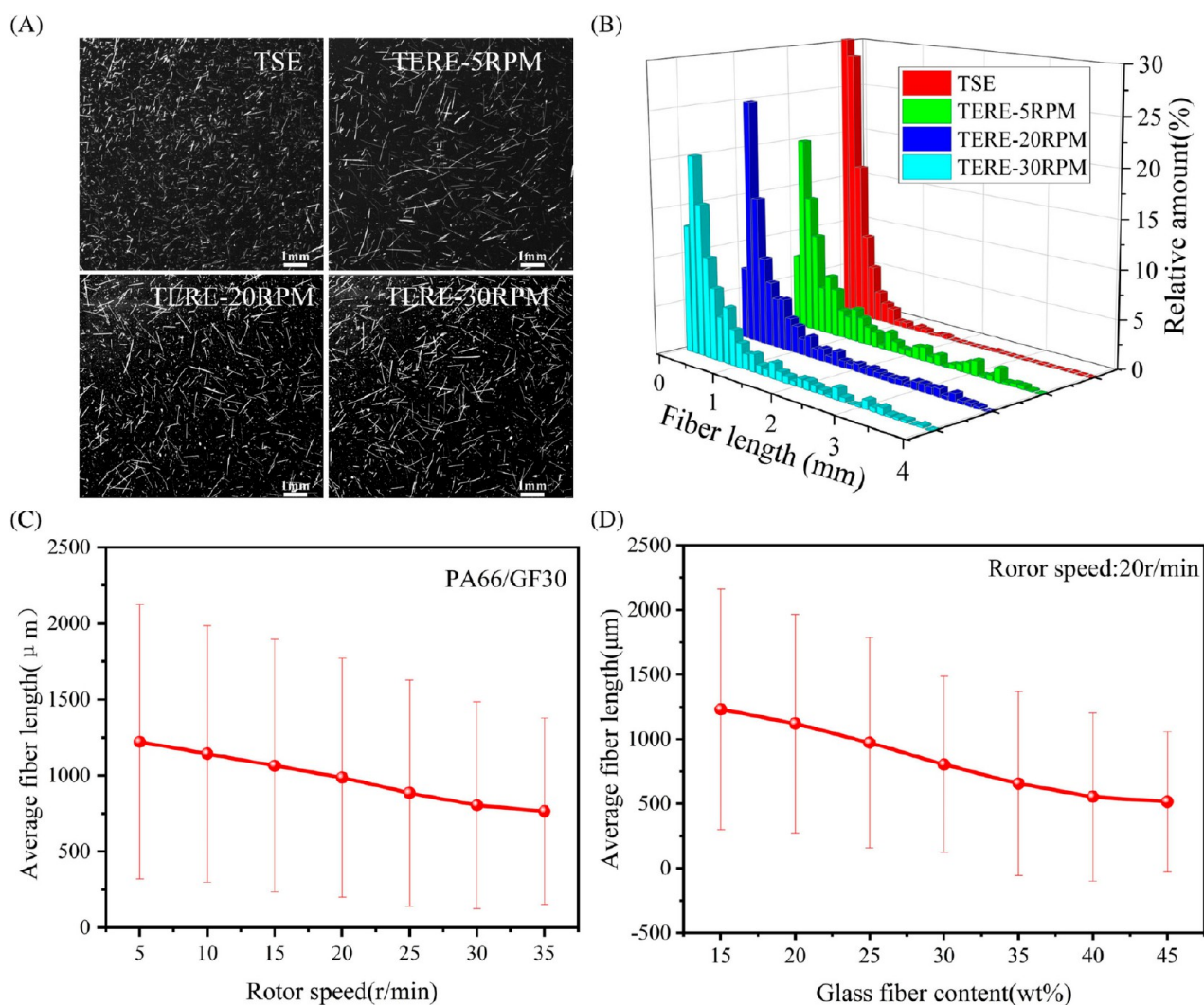


Figure 6. Fiber length distributions of PA66/GF30 prepared in the (A) TSE and (B) TERE at the rotor speeds of 5, 20, and 30 r/min. Reproduced with permission.¹⁶⁶ Copyright 2021 Wiley.

depends on the shapes, dimensions, and alignments of the suspended particles.¹³⁶ According to Burger,¹⁵⁷ α_0 for cylindrical rods is represented by eq 41:

$$\alpha_0 = \left[\frac{\left(\frac{L}{d}\right)^2}{6\left(\ln \frac{2L}{d} - 1.80\right)} \right] \sin^4 \theta \sin^2 \varphi \quad (41)$$

where L/d is the aspect ratio of the rod and θ , φ are the spherical coordinates. Burger has neglected wall effects, Brownian motion, slip, particle interactions, and the effects of thickness and ends of cylindrical rods. Experimental studies of Nawab and Mason¹⁵⁸ indicate that the actual results are approximately three times those predicted by Burger. According to them, fiber curvature has a significant effect on viscosity. Kitano et al.¹⁵⁹ have reported an empirical relationship between the relative viscosities and volume fractions of several fillers, for instance, glass and carbon fibers. They have observed that the use of different materials would result in different suspension viscosities. Goto et al.^{121,160} have experimentally determined the relationship between the flexibilities of fibers and viscosity of the suspension. They

have demonstrated that the fibers with high flexibilities exhibited higher viscosities than those of the stiffer fibers.

Suspensions of flexible fibers demonstrate the tendencies to exhibit flocculation. During the manufacture of fiber-reinforced composites, a homogeneous dispersion of fibers is required to produce a uniform product. Flexible fibers tend to agglomerate in a process called flocculation, generating spatially heterogeneous structures called fiber flocs.¹³⁶

Flocculation occurs only if the fibers interact and is caused by fiber–fiber interactions. Factors that affect flocculation include aspect ratio, shape, and volume fraction of the fiber and shear rate and nature of the fluid flow. In many fiber suspensions, the major mechanisms of flocculation are associated with mechanical and elastic effects.^{161,162} Mechanical surface linkages form at the points of contact of irregularly shaped fibers, resulting in entanglements. Additionally, fibers may be fibrillated, and the fibrils may become mechanically entwined. Elastic fiber interlocking takes place when flexible fibers develop an elastic network. The viscous forces experienced by the flowing fiber suspensions may induce the elastic deformation of fibers. As the fibers attempt to relax, they become constrained in elastically strained configurations because of their interaction with other fibers. The fiber

surfaces experience frictional forces proportional to the normal force between fibers, and the normal force depends on fiber flexibility.¹³⁶

Numerous research groups^{110,111,113–117} have highlighted the importance of shear in enhancing the quality of dispersion of nanoparticles in a polymer matrix. Kalra et al.¹⁶³ conducted studies on the influence of shear flow on the quality of dispersion of a polymer nanocomposite in which the nanoparticle–nanoparticle interaction was higher than the nanoparticle–polymer interaction. Thus, for the investigated systems, the final state was always an agglomerated particle cluster. Shear flow substantially affected the kinetics of nanoparticle aggregation and aggregation time scale which increased by up to 2 orders of magnitude due to the influence of shear flow. Shear flow influenced the quality of dispersion in two ways: it affected the diffusion coefficients of the nanoparticles, and it caused rupture-like deformation of the nanoparticles. For better understanding, the researchers varied various factors such as the shear rate and lengths of the polymer chains. The effect of shear flow on nanoparticle diffusion was strongly dependent on the polymer chain length, which affected the aggregation time scale. Therefore, the researchers demonstrated the influence of shear on particle agglomeration kinetics of polymer nanocomposites.

Thus, the flow behaviors of polymer/fiber suspensions under the influence of shear significantly affect the quality of dispersion and orientations, attrition, and flocculation of fibers, thereby influencing the development of the morphologies of discontinuous fiber-reinforced polymer composites. In the cases of polymer nanocomposites, the quality of dispersion is regulated by the shear and elongational flows. Elongational flow facilitates morphology development of fiber-reinforced polymer composites. The impacts of extensional rheology on the morphology developments of polymer composites and nanocomposites are reviewed in the subsequent section.

3.2.1.1.1. Role of Extensional Rheology. Production of discontinuous fiber-reinforced polymer composites under an extensional flow field leads to lower attrition of fibers as compared to that in the case of fiber processing under a shear flow field. The lower fiber attrition is achieved without compromising the quality of dispersion and distributions of fibers.¹⁶⁴

Kugler et al.¹⁶⁵ analyzed the influence of extensional rheology on the orientations of fibers in discontinuous fiber-reinforced polymer composites. They utilized a particle-based mechanistic model for evaluating the alignments of fibers under both shear and extensional flows. The mechanistic model was validated using the experimental data acquired for long-fiber-reinforced composites. The predictions of the model matched the experimental results. Using the mechanistic model, the researchers discovered that in the cases of short fibers, the fiber orientation achieved in extensional flow was independent of the fiber length, fiber volume content, and rate of elongation. Nevertheless, the fiber orientation was slightly dependent on the viscosity of the polymer matrix. On the basis of these results, the researchers developed a novel flow-dependent macroscopic model for estimating the fiber orientation, which considered the effects of both elongational and shear flows. The model was objective and exhibited better performance than those of several fiber orientation models. Thus, the researchers demonstrated the influence of extensional flow on the orientation of fibers in fiber-reinforced composites.

Guo et al.¹⁶⁶ compared the morphological characteristics and other properties of short-glass fiber-reinforced PA66 prepared under the elongational flow field generated in a twin-ERE (TERE) with those of short-glass fiber-reinforced PA66 synthesized under the shear flow field in a conventional TSE. They noticed that the composites produced in the TERE exhibited less fiber attrition and better quality of fiber dispersion than those of the composites produced in the TSE (Figure 6), which resulted in better mechanical properties of the composites fabricated in the TERE. The average lengths of the dispersed fibers in the composites prepared in the TERE were 3.2 times those of the composites synthesized in the TSE. Wu et al.¹⁶⁷ performed similar studies on short-glass fiber-reinforced PA6 composites. Their results were similar to those reported for the short-glass fiber-reinforced PA66 composites. In their case, the average fiber length obtained in the case of the TERE was 2.7 times that acquired in the case of the TSE. The lowering of fiber attrition because of the replacement of a shear flow field with an extensional flow field has also been reported by Guo et al.¹⁶⁸ in their studies on various polymer/fiber systems. Thus, compared to a shear flow field, an extensional flow field results in a better quality of dispersion and lower attrition of fibers in discontinuous fiber-reinforced polymer composites.

Enhancement of the quality of dispersion using an extensional flow field instead of a shear flow field has also been reported in studies on polymer nanocomposites. Wu et al.¹⁶⁹ conducted investigations on the natural rubber/carbon black nanocomposites prepared in a biaxial ERE (BERE) based on elongational rheology. Compared with the processing of composites in an internal mixer, which is based on shear rheology, the BERE processing requires a shorter mixing time and lower unit energy and leads to superior quality of dispersion and better mechanical properties of composites. Furthermore, natural rubber, which is shear-sensitive, underwent less degradation in BERE than that in the internal mixer, resulting in higher molecular weight (MW) retention. Therefore, the researchers have demonstrated that a polymer nanocomposite produced by melt processing under an elongational flow field exhibits superior mechanical properties because of not only superior dispersion qualities of the nanoparticles but also lower degradation of shear-sensitive polymers. Researchers have reported the superior efficacy of elongational flow field in the mixing of other nanofillers, such as nanoclay^{170–173} and carbon nanotubes,^{170,174} in various polymers.

3.3. Nanocomposites of Blends. Blending an immiscible blend with filler results in a ternary composition with a complex microstructure. The filler particles may be dispersed in both blend components or selectively in one of the components. Furthermore, its interfacial adhesion with the two blend components will be different. Though not much work has been done on the role of rheology in the evolution of the morphology of these ternary polymeric materials, the limited available literature brings forth important findings.

Feng et al.¹⁷⁵ studied the influence of the viscosity ratio of poly(methyl methacrylate)(PMMA)/PP on the equilibrium location of carbon black (CB) particles. A ternary composition having a PP:PMMA volume ratio of 2.75 and 10 wt % CB content was prepared by melt processing all components in an internal mixer. The viscosity ratio of the blend components was varied using different PMMA grades. They observed that when the viscosity of PMMA was much higher than PP, the

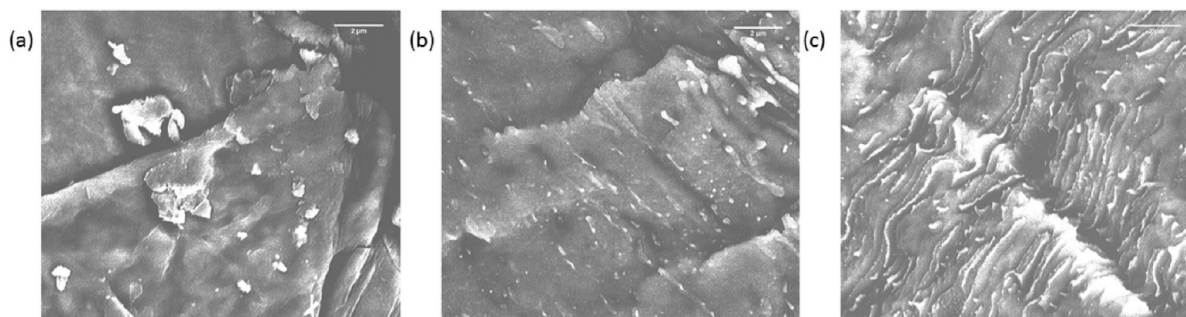


Figure 7. SEM images of different SEBS/PS blends at 20,000 magnification: (a) SEBS/10PS, (b) SEBS/30PS, and (c) SEBS/50PS cryo-fractured along the direction of extrusion. Reproduced from ref 187. Copyright 2018 The Authors.

particles of CB were selectively localized in PP, though they should have been confined in the PMMA as per the prediction based on the wetting parameter. This was ascribed to the difficulty in the diffusion of the CB particles into the higher viscosity PMMA phase. When the viscosity of PMMA was lowered, the CB particles were found to be present at the interface between the PP and the PMMA phases. At still lower viscosities of PMMA, when the viscosity ratio was close to 1, the filler particles were selectively localized in PMMA. Thus the morphology of the ternary composition was profoundly influenced by the viscosity ratio of the blend components. Similar results were reported by Yuan et al.,¹⁷⁶ in their studies on multiwalled CNT (MWNT)-filled LDPE/poly(vinylidene fluoride) blends when the CNTs were found to be localized in the significantly lower viscosity LDPE phase.

Rafeie et al.¹⁷⁷ conducted studies on linear low-density polyethylene (LLDPE)/PVDF/graphene nanoplatelet (GnP) composites having a 50/50 ratio of blend components, prepared by the melt mixing in an internal mixer. The GNPs were found to be selectively localized in the PVDF phase of a cocontinuous blend morphology. In an earlier work¹⁷⁸ on blends of the same grades of LLDPE and PVDF prepared, similarly, the researchers observed that the 50/50 blend possessed a droplet/matrix morphology. The cocontinuous morphology of the GnP-filled blends was ascribed to the increase in viscosity ratio of the PVDF to the LLDPE due to the selective localization of the GNPs in the PVDF phase. Thus, the researchers demonstrated that the selective localization of filler particles may also influence the blend morphology nanofiller reinforced blends due to its influence on the rheological properties of the system, as also reported by other research groups.^{179,180}

Cho et al.¹⁷⁹ conducted studies on PP/PS/Cloisite 20A nanocomposites prepared by melt mixing all components in a TSE. On the basis of morphological studies on samples drawn out of the TSE from various locations, the researchers proposed a mechanism for the evolution of the morphology of the ternary compositions. Initially, large PS domains were present in the PP matrix, and the clay particles, either aggregated or intercalated, were localized selectively either at the interface to lower the interfacial tension of the system or in the PS domains due to their higher compatibility with PS than with PP. The PS domains deformed under shear and were disintegrated into smaller droplets. Since the clay particles in the PS domains served as defects and hence as points of stress concentration, this breakup occurred at a lower capillary number compared with the immiscible blends in the absence of nanoclay. The nanoclay thus lowered the interfacial tension

of the PP/PS blend and facilitated the disintegration of the large PS domains. This process continued until the clay particles enveloped the interface adequately to prevent the occurrence of coalescence. The researchers thus proposed that nanoclay facilitates the development of a droplet/matrix blend morphology by enabling the breakup of large domains at a lower capillary number.

Aghjeh et al.¹⁸¹ conducted studies on PLA/ethylene vinyl acetate (EVA) blends and their nanocomposites with Cloisite 30B, prepared by melt mixing in a TSE. PLA-rich blends in which PLA formed the matrix had a coarser morphology than EVA-rich blends. This was attributed to the lower viscosity of PLA in comparison with EVA. The clay was found to be selectively localized in the PLA phase, with some portions present at the interface. The selective localization of clay in PLA was ascribed to the greater affinity of Cloisite 30B for PLA compared to EVA. SEM studies on the blend with 75 wt % PLA content and its nanocomposite revealed that nanoclay significantly reduced the dispersed particle size and polydispersity. This was ascribed to the compatibilization effect of clay and the influence of clay on the rheological properties of the system. The selective localization of clay in the PLA phase enhanced the viscosity of the PLA phase. It altered the viscosity ratio of the blend components, facilitating the evolution of a finer morphology with lower coalescence of the dispersed droplets. The researchers thus clearly demonstrated the role of rheology in the evolution of the morphology of ternary compositions.

It may be summarized that the viscosity ratio of the blend components profoundly influences the location of filler particles in nanocomposites of blends. Selective localization of the filler particles in one of the phases alters the viscosity ratio of the blend components, which in turn impacts the blend morphology.

3.4. Rheology as a Tool for the Evaluation of Morphology. The morphological and rheological characteristics of a polymeric material are closely associated, and consequently, rheology can be used as a tool for estimating the morphologies of polymer blends and nanocomposites.^{1,2} In his investigations on melt dynamic rheology of blends, Maani⁸ reported that for a certain composition, compatibilized blends demonstrated finer morphologies and higher complex viscosities and storage moduli when compared with those of uncompatibilized blends, which exhibited coarser morphologies. Li et al.^{182–184} used dynamic rheology to assess the interfacial rigidity of blends having a stable morphology and a rigid interface. A higher storage modulus value was taken as indicative of greater interfacial rigidity and hence higher

morphological stability of the blend. During their study on the foaming behaviors of styrene–ethylene–butylene–styrene (SEBS)/PS blends, Banerjee et al.¹⁸⁵ described that for a specific composition, a decrease in screw speed and an increase in the residence time during melt processing resulted in a finer blend morphology. These blends exhibited higher storage moduli (G') and complex viscosities (η^*) than those of the blends with coarser morphologies. They examined the rheological and morphological characteristics of the SEBS/PS blends with various compositions.^{186,187} Scanning electron microscopy (SEM) studies (Figure 7) revealed that blends with higher PS contents (30 and 50 wt %), denoted as SEBS/30PS and SEBS/50 PS, respectively, demonstrated fibrillar morphologies, contrary to the case of the blend containing 10 wt.% PS (SEBS/10PS). The fibrils were oriented in the flow direction. Shear viscosities of these blends were lower than the expected values. This was ascribed to additional slippage of the SEBS chains caused by the oriented lower-viscosity PS fibrils, which further corroborated the formation of a fibrillar morphology. In the weighted relaxation spectrum (Figure 8),

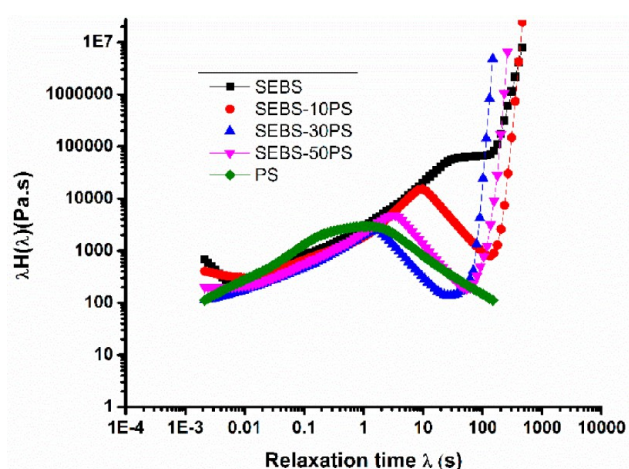


Figure 8. Weighted relaxation spectra of SEBS, PS, and the SEBS/PS blends. Reproduced from ref 187. Copyright 2018 The Authors.

neat SEBS and the SEBS/PS blends exhibited two modes of relaxation as compared to the case of neat PS, which demonstrated a single mode of relaxation. The two modes of relaxation were assigned to the thermoplastic and elastomeric phases, and the slower relaxation mode was ascribed to the elastomeric phase. The researchers concluded that the slow relaxation of the elastomeric phase led to a notable time-dependent shrinkage of neat SEBS and the blends in the cases of secondary processing methods.¹⁸⁷ This inference was supported by the findings of foaming studies.

Other researchers^{188–190} have also employed relaxation spectrum to gain insights into the morphologies of polymer blends. Souza and Demarquette¹⁸⁸ performed studies on PP/high-density PE (HDPE) blends. They observed that compatibilization resulted in finer morphologies of the blends and increased the form relaxation times of the dispersed particles. The enhancement in the form relaxation time was associated with the increased cohesive force between the dispersed particles and matrix. In their investigations on poly(methyl methacrylate) (PMMA)/PS blends, Gramespacher and Meissner¹⁸⁹ reported that the weighted relaxation time spectra of these blends exhibited an additional peak. This

additional peak was related to the interfacial tension between the components of the blend. According to Vinckier et al.,¹⁹⁰ the additional relaxation corresponded to the mechanical response of the interface between PMMA and PS.

Both melt and solid dynamic rheologies have been used to achieve an understanding of the microstructures of polymer nanocomposites. Bhattacharya et al.¹⁹¹ conducted studies on high-melt-strength PP/clay nanocomposites. They reported that the percolation threshold (concentration of nanoclay that corresponds to maximum delamination) could be determined from the sudden changes in the slopes of the terminal regions of melt dynamic rheology plots. In their investigations on polymer/clay nanocomposites, Sinha Ray et al.^{16,17} have attributed the lack of crossover frequency in the melt dynamic rheology plot to pseudosolid-like behaviors of the nanocomposites caused by the inhibited relaxation. Yu et al.¹⁹² have described the relationship between relaxations and variations in the microstructure of the macromolecule. Researchers have employed the glass transition temperature determined from the $\tan \delta$ peak of the dynamic mechanical analysis (DMA) plot for estimating the chain confinement arising from the addition of the nanofiller. A positive shift in the peak indicates the lowering of segmental mobility by intercalation in the clay galleries. Lowering of the height of the $\tan \delta$ peak suggests increased interfacial interaction with the nanofiller.^{193,194}

Although shear rheology is relatively less significant in evaluating the microstructures of macromolecules, it has also been employed for understanding flow behaviors in terms of the morphological characteristics of polymer blends and nanocomposites. In their investigations on PP/nylon 6 blends, Afshari et al.¹⁹⁵ have represented a correlation between the deviation of viscosity from the value predicted by the additive rule of mixtures and the alteration in morphology due to compatibilization. Additionally, the interaction between blend components has been correlated with shear viscosity by other researchers.^{196–198} A nanocomposite possessing a percolating network of finely dispersed nanoparticles exhibits high shear viscosity at low shear rates and a high shear thinning behavior at high shear rates, which is attributed to the shear-induced alignments of nanoparticles.¹⁹⁹ A similar behavior of complex viscosity is noticed in dynamic rheological studies. These nanocomposites are characterized by pseudosolid-like behaviors at low frequencies.⁴

Thus, even prior to morphological analysis, we can use rheology to gain an understanding of the quality of dispersion, interfacial interactions, and relaxation behaviors of multiphase polymeric materials.

4. RHEOLOGY IN ADVANCED POLYMER-PROCESSING OPERATIONS

4.1. Blown Film Extrusion. **4.1.1. Fundamentals of Blown Film Extrusion.** In blown film extrusion, also known as film blowing, an annular die is employed to extrude a molten polymer tube. The tube is inflated into a thin cylindrical bubble by blowing air via the die head. The bubble is cooled and vertically pulled via collapsible guides and nip rolls, where it is flattened. The layflat film is pulled downward over a deflection pulley via drive rolls and is taken up by the winder while maintaining a uniform takeoff speed.^{5,200} A typical blown film extrusion line is depicted in Figure 9.

In film blowing, the blow-up ratio (BUR), draw-down ratio (DDR), take-up ratio (TUR), and inhomogeneity index (r) are presented by eqs 42, 43, 44, and 45, respectively:

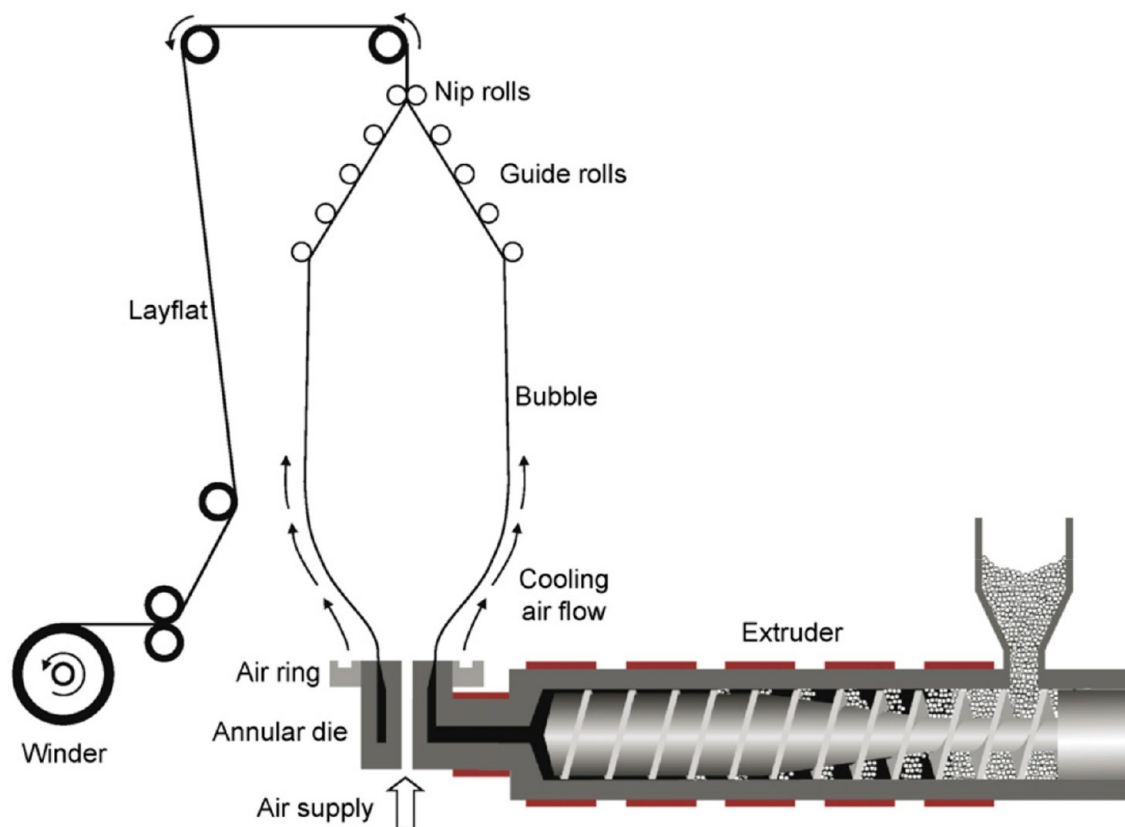


Figure 9. Extrusion blown film line. Reproduced with permission from ref 200. Copyright 2008 Elsevier Science Ltd.

$$\text{BUR} = \frac{\text{bubble diameter}}{\text{die diameter}} \quad (42)$$

$$\text{DDR} = \frac{\text{die gap}}{\text{film thickness} \times \text{BUR}} \quad (43)$$

$$\text{TUR} = \frac{v}{v_0} \quad (44)$$

$$r = \frac{S}{h_{\text{av}}} \quad (45)$$

where v is the velocity of the take-up roll, v_0 is the melt velocity at the die exit, h_{av} is the average film thickness, and S is the standard deviation. Lower r values indicate the presence of highly homogeneous films.^{5,201}

4.1.2. Rheology in Blown Film Extrusion. Being a stretching process, film blowing is substantially influenced by extensional rheology. Researchers have demonstrated the importance of extensional rheology in the blown film extrusion of various polymeric materials. Polyethylene terephthalate (PET), a polymer acknowledged for its packaging applications, has a linear molecular structure, which is responsible for its inferior melt strength and strain hardening behavior. This renders PET unsuitable for blown film extrusion. Härth and Dörnhöfer²⁰¹ investigated the enhancement of the extensional rheological characteristics and, hence, the film blowability of PET caused by the introduction of long-chain branches into PET. Long-chain branches were grafted onto commercial PET molecules via reactive extrusion. Studies were performed using two types of chain extenders: pyromellitic dianhydride (PMDA) (0.1 and 0.25 wt %) and multifunctional epoxy (Joncryl ADR 4368) (0.4 wt %). Complex viscosities and extensional rheological

properties of neat and modified PET (designated as PET-P0.1, PET-P0.25, and PET-J0.4, where P and J denote modification of PET with PMDA and Joncryl, respectively, and the subsequent numerals represent the dose of the chain extender used) were examined, and the acquired results were explained based on the influences of the chain extender type on film blowability and film quality, measured in terms of characteristics including bubble stability and homogeneity of film thickness. Figure 10 shows the complex viscosity curves.

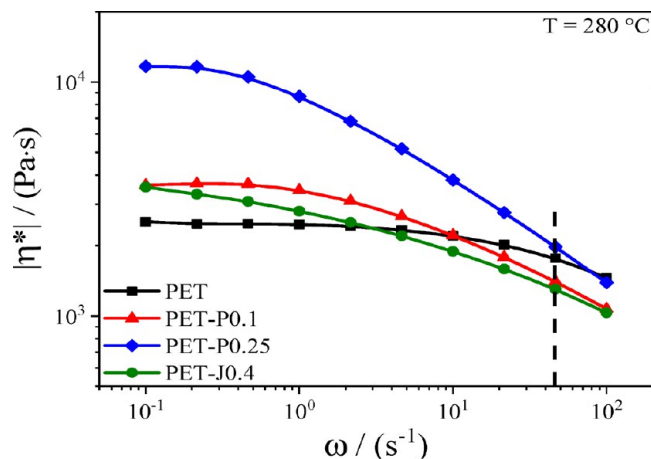


Figure 10. Magnitude of complex shear viscosity as a function of angular frequency for PET modified with PMDA or Joncryl. The vertical line represents the shear rate in the extruder during the film blowing experiments. Reproduced from ref 201. Copyright 2020 The Authors.

Modification of PET with chain extenders enhanced the viscosity of PET in the low-frequency region, and the modified PET exhibited a more notable shear thinning behavior when compared with that of neat PET. This rheological behavior was ascribed to the broadening of the MW distribution and increase in the average MW of PET because of chain extension after modification, as indicated by the results of the light scattering experiment.

Extensional viscosity curves for different elongation rates at 260 °C are depicted in Figure 11. The melt strengths of neat

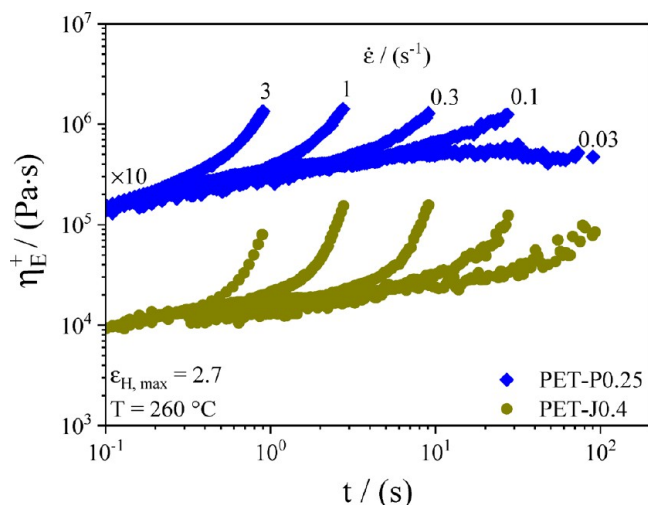


Figure 11. Time-dependent elongational viscosities at different elongational rates for PET-P0.25 and PET-J0.4. The PET0.25 curves are shifted by 10 fold as indicated in the figure. Reproduced from ref 201. Copyright 2020 The Authors.

PET and PET-P0.1 were significantly low for the measurement of extensional viscosity. PET modified with chain extenders demonstrated a distinct strain hardening behavior. Joncryl substantially increased the strain hardening of PET as compared to the case of PMDA. This was attributed to the more efficient branched structure created by Joncryl. All modified PET samples exhibited higher melt strengths than that of neat PET. However, the extensibility of the Joncryl-modified sample was lower than that of the PDMA-modified sample, which was ascribed to the higher gel content of the Joncryl-modified sample.

Bubble stability was qualitatively assessed by visual inspection. Typically, three kinds of instabilities were identified. The first instability was an axisymmetric periodic variation of the bubble diameter. The second instability was helical motion of the bubble, and the third instability was a fluctuation in the frost line. Superpositions of these instabilities were also observed. The first two types of instabilities exhibited by neat PET are shown in Figure 12(a) and (b). Modification of PET with the chain extenders resulted in a distinct enhancement of bubble stability. Figure 12(c) depicts a stable bubble formed by PET-P0.25. The samples demonstrated the following order of bubble stability:

$$\text{PET} - \text{P0.25} > \text{PET} - \text{J0.4} > \text{PET} - \text{P0.1} > \text{neat PET}$$

The bubble of PET-J0.4 periodically broke down at high TUR. This was assigned to the high gel content of the Joncryl-modified sample. Despite the differences between the bubble stabilities of neat and modified PET samples, the inhomogeneity indices of the films formed by neat PET and all the modified PET samples, except for PET-J0.4, did not exhibit any difference, thereby suggesting that film homogeneity was not related to bubble stability. The PET-J0.4 film demonstrated a lower inhomogeneity index, which was attributed to

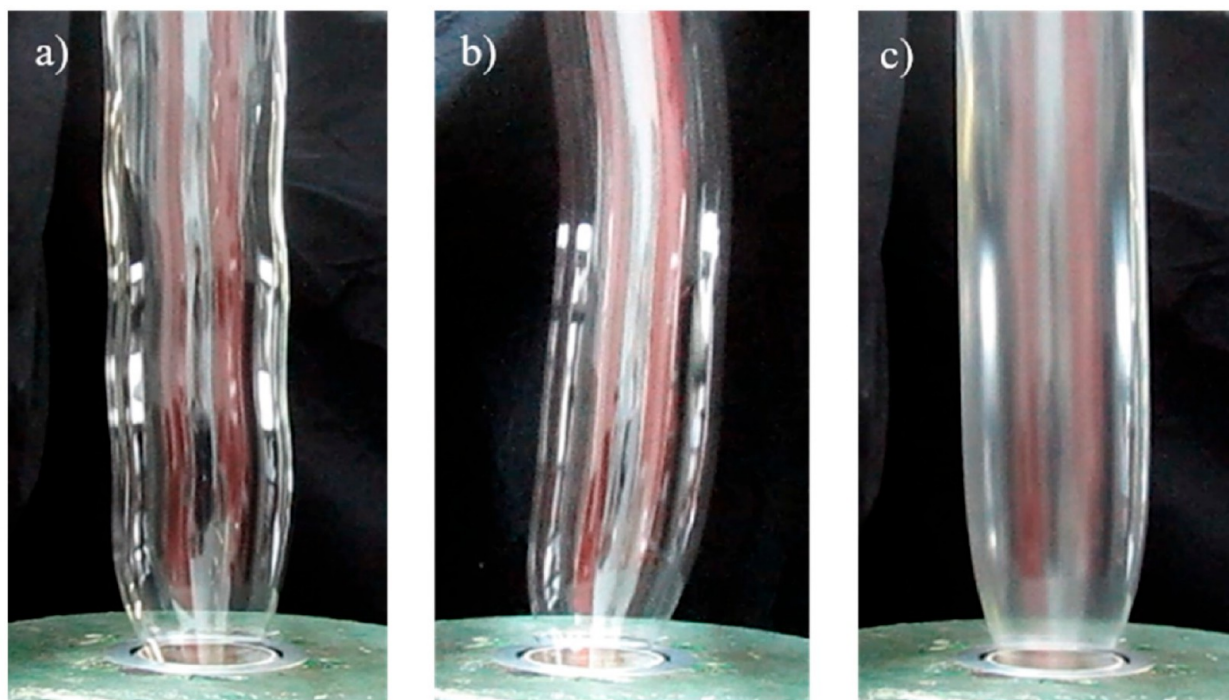


Figure 12. Images of (a) an axisymmetric periodic variation of the bubble diameter and (b) helical motion of the bubble for neat PET and (c) a stable bubble of PET-P0.25. Reproduced from ref 201. Copyright 2020 The Authors.

the notable strain hardening behavior and higher gel content of PET-J0.4. Thus, the researchers indicated that the introduction of long-chain branches into polymeric materials increases the melt strengths and strain hardening behaviors of these materials, thereby improving the film blowabilities of polymeric materials.

Importance of extensional rheology in the blown film extrusion of polymeric materials has been reported by several research groups. In their studies on the film blowabilities of LDPE, linear LDPE (LLDPE), and HDPE, Kanai and White²⁰² noticed that LDPE exhibited the highest bubble stability, evaluated in terms of the width of the operating window that produced a stable bubble, followed by those of LLDPE and HDPE. The difference between the bubble stabilities of the different grades of PE was ascribed to the difference between the strain hardening behaviors of these materials. The dependence of bubble stability on the strain hardening and melt strength of the polymeric material has been demonstrated by other researchers.^{5,203–207} Moreover, strain hardening leads to films with higher uniformities in thickness, that is, lower inhomogeneity indices.^{5,203,208}

Compared with the case of extensional rheology, fewer studies have been reported on the role of dynamic rheology in the blown film extrusion of polymeric materials. According to Ghijssels et al.,²⁰⁵ a balance of viscoelastic properties is required for bubble stability (Figure 13). Carneiro et al.²⁰⁹ have

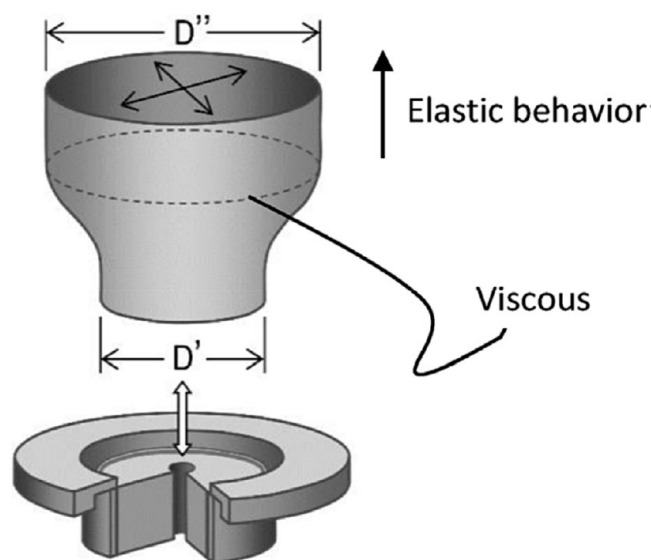


Figure 13. Schematic of a stable bubble during film blowing. Reproduced with permission ref 210. Copyright 2017 Elsevier Science Ltd.

observed that polymers with low crossover frequencies exhibit high elasticities and long relaxation times. These polymers tend to form stable bubbles during blown film extrusion. de Almeida et al.²¹⁰ utilized the results of both extensional and dynamic rheology to predict the film blowabilities of PS/high-impact PS (HIPS) blends. According to them, both high melt strength and low moduli and frequencies at the crossover point are conducive for superior film blowability. In their investigations on various grades of PE, Fang et al.²¹¹ noticed that higher elasticity (namely, higher G') resulted in higher bubble stability. Furthermore, in their studies on PLA/LLDPE blends, Singh et al.⁵ have reported the role of higher G' in the

enhancement of bubble stability. The importance of both extensional and dynamic rheologies in film blowing has been highlighted by many researchers.^{5,205,210–212}

Shear rheology is relatively less important in film blowing, and few studies have reported its role in film blowing. In their investigations on LDPE blown films, Zhu et al.²¹³ have observed that excessively high zero-shear viscosity and melt elasticity may affect surface regularities of blown films. Micic and Bhattacharya²¹⁴ have also reported that very high shear viscosity leads to bubble instability. Al-Itry et al.²¹² have attributed the high film blowability of Joncryl-modified PLA to the enhancement of both the shear and elongational properties of PLA due to its modification with Joncryl. In their studies on the blown film extrusion of bionanocomposites, Mistretta et al.²¹⁵ have stated the importance of appropriate shear viscosity in the achievement of superior film blowability. The existing studies indicate the possibility of the presence of a shear viscosity window corresponding to optimum film blowability. Nevertheless, more research is needed to reach any conclusion in this regard.

Thus, high melt strength, strain hardening behavior, and high storage modulus may result in superior processability during the blown film extrusion of polymeric materials. Additionally, a balance of viscoelastic properties possibly leads to high film blowability. However, more research is needed for a better understanding of the effects of viscoelasticity and shear rheology on film blowability.

4.2. Electrospinning. 4.2.1. Basics of Electrospinning.

Electrospinning is a technique of producing nano- or microsized continuous fibers from a solution or melt under a strong electric field. The process is simple and easy to control and can be scaled-up. Thus, it is an attractive option for the synthesis of nanofibers of polymeric materials for a broad range of applications such as in drug delivery, artificial tissues, electronics, fuel cell membranes, and biosensors.^{216–218} Figure 14(A) shows a schematic of electrospinning. The corresponding device comprises a high-voltage power supply, syringe fitted with a needle, syringe pump containing the polymer solution/melt, and grounded metal collector.^{218–220} Initially, the polymer solution/melt remains at the needle tip because of surface tension. When a high voltage (1–30 kV²¹⁶) is applied between the needle and the grounded metal collector, the hemispherical surface of the liquid at the needle tip is deformed into a cone called the Taylor cone.^{221,222} When the electric field reaches a threshold value, the surface tension is overcome by a repulsive electrostatic force, resulting in the ejection of a polymer jet from the Taylor cone tip. The ejected jet, traveling at a high speed toward the metal collector, undergoes numerous electrically impelled bending instabilities and slowly thins in air because of extension and solvent evaporation. The charged jet is ultimately obtained on the collector (Figure 14B) and forms a nonwoven web of randomly oriented nanofibers (Figure 14C).²¹⁹ Aligned nanofibers (Figure 14E) can be developed either using a slightly altered stationary collector or various dynamic collectors,²²³ for instance, using a rotating drum collector at very high speeds (Figure 14D). The diameters of the formed fibers are influenced by several factors, such as rheological characteristics of the solution/melt, surface tension, conductivity, applied voltage, distance between the syringe and the collector, temperature, air flow, and humidity.^{216,218}

4.2.2. Rheology in Electrospinning. Rheology is of significant importance in electrospinning. During the electro-

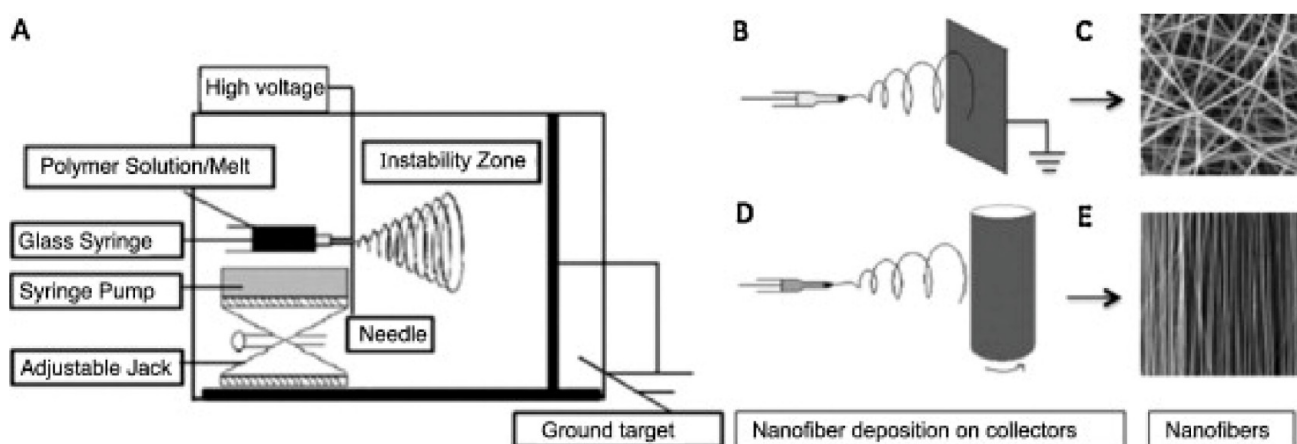


Figure 14. (A) Schematic of electrospinning. (B) A stationary metal collector. (C) Randomly oriented nanofibers acquired on the stationary collector. (D) A rotating drum collector. (E) Uniaxially aligned nanofibers obtained on the rotating drum collector. Reproduced with permission from ref 217. Copyright 2015 Elsevier Science Ltd.

spinning of a polymer solution, the solution concentration should be sufficient to create adequate chain entanglements for the construction of fibers. At concentrations lower than the entanglement concentration c_e , the entanglement density is inadequate for jet stabilization, resulting in beads instead of fibers due to Rayleigh instability.^{224,225} The critical overlap concentration c^* and c_e are two critical parameters of polymer solutions. Below c^* , the polymer molecules are in a dilute regime, functioning as independent coils. At c^* (presented by eq 46), the polymer chains begin to interact and overlap without entangling. Thus, c^* signifies the end of the dilute regime and onset of the semidilute unentangled regime.^{218,226}

$$c^* \sim \frac{1}{[\eta]} \quad (46)$$

where $[\eta]$ is the intrinsic viscosity of the solution.

When the solution concentration is further increased to c_e , the chains form entanglements. Therefore, c_e denotes the end of the semidilute unentangled regime and the onset of the semidilute entangled regime. c_e can be obtained from the log–log plot of specific viscosity (η_{sp}) (eq 47) versus solution concentration.²²⁶ c_e is the concentration above which η_{sp} increases with respect to the concentration c in accordance with $c^{3.7}$ or $c^{4.7}$ depending on the polymer/solvent pair.²²⁷

$$\eta_{sp} = \frac{\eta - \eta_0}{\eta_0} \quad (47)$$

where η and η_0 are the viscosities of the solution and solvent, respectively.

For concentrations above c_e , an increase in solution viscosity increases the diameters of the electrospun fibers.²¹⁷ Furthermore, a certain minimum concentration is necessary for obtaining bead-free fibers.²²⁷ This concentration may be as low as c_e ²²⁸ or as high as $2-2.5c_e$.²²⁹

In their studies on the electrospinning of nylon 66 solutions in formic acid, Abbasi et al.²³⁰ reported a c_e of 15 wt %. They also stated a power-law relationship between $[\eta]$ and c with the exponent values of 2.0 and 3.3 for semidilute unentangled ($c < c_e$) and semidilute entangled ($c > c_e$) regimes, respectively. Fiber radius and uniformity were governed by viscosity. Moreover, the average fiber diameter was related to zero-shear-rate viscosity and normalized concentration (c/c_e) in a power-law relationship with the exponent values of 0.298 and 0.816,

respectively. The minimum concentration necessary for the production of uniform bead-free fibers was c_e . Thus, the researchers established the dependence of the electrospinnabilities of polymer solutions, fiber diameter, and fiber quality on solution viscosity. Electrospinning was not possible outside this concentration window. Below the lower limit of the concentration window, fibers were not formed because of the lack of sufficient chain entanglements. The upper limit of the concentration window was influenced by the extensional viscosity of the solution.

Importance of viscosity in the electrospinning of polymer melts and its effect on fiber diameter have also been reported.^{231–234} As polymer melts are highly viscous and electrospinnability is lower at very high viscosities, melt electrospinning is more difficult than solution electrospinning.²³⁵ Researchers have tried to overcome this challenge by lowering the viscosities of polymer melts. In their studies on the electrospinning of PP melt, Nayak et al.²³¹ noticed that a reduction in melt viscosity achieved by varying the amounts of additives, including polyethylene glycol (PEG) and poly-(dimethyl siloxane), decreased the fiber diameter. Larrondo and St John Manley²³³ stated a reduction in fiber diameter upon the lowering of melt viscosity by an increase in temperature. Nazari and Garmabi²³⁶ observed that although neat PLA was not melt-spinnable at 200 °C, lowering the melt viscosity by blending PLA with PEG considerably enhanced the melt spinnability of PLA. The researchers synthesized fibers of 3–6 μm diameters using PLA/PEG blends containing 30 wt % PEG under the same conditions under which neat PLA was not melt-spinnable.

The role of viscoelasticity in electrospinning has also been discussed by researchers. According to Reneker et al.,²³⁷ during the electrospinning of polymer solutions, the viscoelastic force along the jet tends to stabilize the charged jet. Additionally, the function of viscoelasticity in jet stabilization has been reported by Regev et al.²³⁸ Theron et al.²³⁹ employed both the previously reported linear Maxwell model^{237,240} and the nonlinear upper-convected Maxwell model for analyzing the viscoelasticities of polymer solutions during electrospinning. Comparison of the simulation and experimental results revealed that both models provided close descriptions of the actual behaviors of polymer solution jets during electrospinning.

Yu et al.²⁴¹ conducted theoretical and experimental investigations on the influence of elasticity on electrospinning. They used Boger fluids for experimental studies. They noticed that high elasticity lowered the Rayleigh instability, thus arresting the breakup of the jet into droplets and sometimes completely suppressing the Rayleigh instability. A critical value of elastic stress indicates the complete suppression of Rayleigh instability and transformation of the beaded fiber morphology to a uniform fiber morphology.

Thompson et al.²⁴² employed an electrospinning theoretical model to examine the effect of relaxation time on the diameters of the fibers acquired during the electrospinning of polymer solutions. The model predicted an increase in the final diameters of the fibers with an increase in the relaxation time. The predicted trend matched the experimental results reported in the literature.²⁴¹

In their investigations on the melt electrospinnabilities of PLA/PEG blends, Nazari and Garmabi²⁴³ observed that under the conditions utilized for electrospinning (spinning temperature: 180 °C, flow rate: 0.5 cc/h, applied voltage: 40 kV, and nozzle-to-collector distance: 10 cm), neat PLA and the blend containing 5 wt % PEG were not electrospinnable due to their high viscosities. The blends comprising 10–30 wt % PEG were readily electrospun because of the lowering of the viscosity of PLA at higher PEG contents. Among the various investigated compositions, the blend containing 20 wt % PEG produced fibers with the lowest diameters ($4.8 \pm 0.8 \mu\text{m}$). The blends consisting of more than 30 wt % PEG were not electrospinnable because of their low elasticities caused by their higher PEG contents.

Carroll and Joo²⁴⁴ performed experimental and theoretical studies on the electrospinning of Newtonian and viscoelastic fluids. Viscoelastic models, such as Oldroyd-B and FENE-P, for polymer solutions were used for theoretical studies. Experiments were conducted on the Newtonian solutions of glycerol comprising trace amounts of lithium chloride and viscoelastic polyisobutylene (PIB)/polybutene (PB) Boger fluid. The experimentally acquired jet profiles were compared with the theoretical predictions for the conditions employed during the experiment. The simulation results were in accordance with the experimental results. The researchers noticed that an increase in viscoelasticity led to a faster initial jet thinning. Nevertheless, with an increase in the distance of the collector from the spinneret, the viscoelastic jets became thicker than the Newtonian jets due to their higher extensional viscosities.

Researchers have also demonstrated the importance of extensional rheology in electrospinning. Feng²⁴⁵ analyzed the influences of extension thinning and thickening and strain hardening on electrospinning by applying non-Newtonian rheology to a theoretical model. For a purely extension-thinning fluid, the behavior of a slightly stretched jet was different from that of a highly stretched jet. The thinning viscosity promoted the stretching of the slightly stretched jet and impeded the stretching of the highly stretched jet. For a fluid that exhibited extension thickening at lower strain rates and thinning at higher strain rates, stretching was inhibited by higher extensional viscosity for both slightly and highly stretched jets. Strain hardening increased the stretching upstream and lowered it downstream, eventually generating thicker fibers. Therefore, the researchers clearly demonstrated the influences of extensional viscosity and strain hardening on fiber diameter.

In their studies on the electrospinning of PVA solutions, Rwei and Huang²⁴⁶ observed that for PVA with a MW of 88,000, the concentration range corresponding to electrospinnable solutions was 6–14 wt %. The upper limit of this concentration range was regulated by the elongational viscosity of the solution. Each time the power-law index obtained during the extension test exceeded one, spinning was not possible regardless of the power-law index during shearing. On the basis of this observation, the researchers have concluded that elongational viscosity is a suitable indicator of electrospinnability.

In their investigations on the electrospinning of polyacrylonitrile (PAN) fibers, Liu et al.²⁴⁷ established the impact of strain hardening on the fiber diameter. Strain-hardening PAN electrospinning solutions were produced by incorporating ultrahigh-MW PAN (UHMWPAN) into medium-MW PAN (MMWPAN) solutions. The solutions containing UHMWPAN exhibited strain-hardening behaviors in capillary breakup extensional rheometer extensional rheological tests (Figure 15). Contrary to the solutions without UHMWPAN,

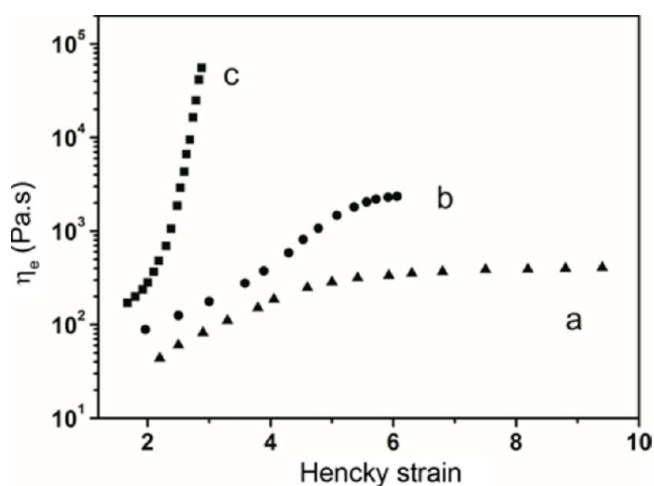


Figure 15. Extensional viscosity as a function of Hencky strain for PAN solutions (a) without UHMWPAN, (b) with 0.15 wt % UHMWPAN, and (c) with 1 wt % UHMWPAN. Reproduced with permission from ref 247. Copyright 2014 Springer.

the strain-hardening solutions were stably electrospun at high voltages and a constant source-target distance, generating uniform PAN fibers with smaller diameters (270 nm as compared to 496 nm for the nanofibers produced using solutions without the strain hardening effect) without beads (Figure 16). Thus, the researchers have demonstrated that strain hardening behavior can facilitate the development of superior quality nanofibers via electrospinning. The importance of extensional viscosity and strain hardening in electrospinning has been discussed by several researchers.^{248–252}

Therefore, knowledge of ϵ_c is crucial for the production of nanofibers by the electrospinning of polymer solutions. Electrospinnability, jet trajectory, and fiber diameter are affected by the viscosity, elasticity, and strain hardening behavior of the polymer solution, and a window corresponding to the range of rheological characteristics that generate fibers of acceptable qualities can be determined. By tailoring the rheological characteristics of the solution/melt within this

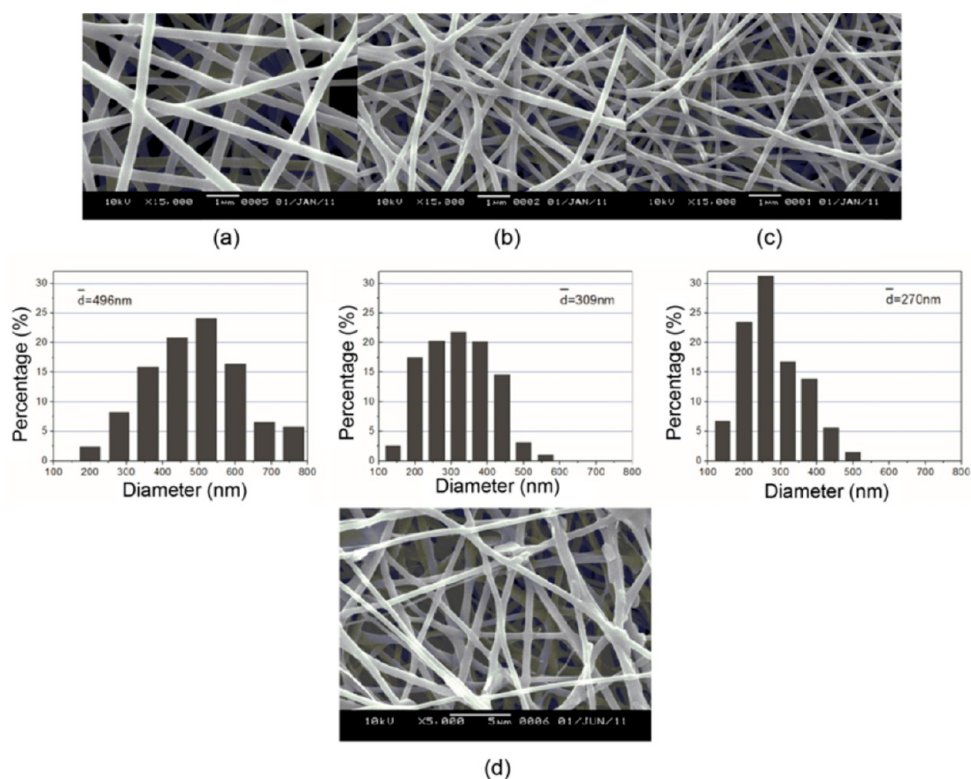


Figure 16. SEM images and fiber diameter distributions of the PAN nanofibers electrospun from the spinning solution (a) without UHMWPAN, (b) with 0.15 wt % UHMWPAN, and (c) with 1 wt % UHMWPAN, and (d) representative SEM image of the beaded PAN nanofibers. Reproduced with permission from ref 247. Copyright 2014 Springer.

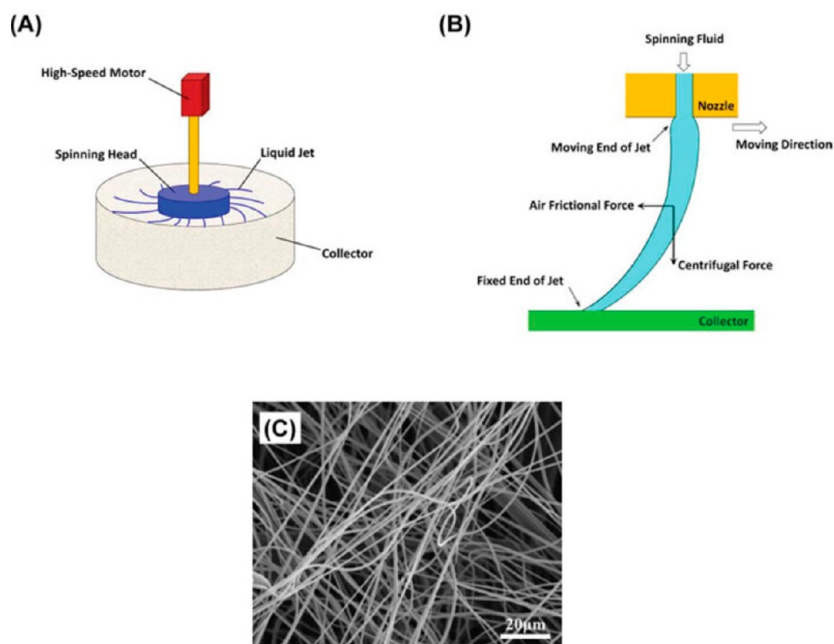


Figure 17. (A) Schematic of a basic benchtop centrifugal spinning setup, (B) the path of a liquid jet ejected from the nozzle tip during centrifugal spinning, and (C) SEM image of the PAN nanofibers prepared via centrifugal spinning. Reproduced with permission from ref 254. Copyright 2014 Taylor and Francis.

window, bead-free fibers with the required diameters may be produced.

4.3. Centrifugal Jet Spinning. **4.3.1. Fundamentals of Centrifugal Jet Spinning.** Centrifugal jet spinning is a cost-effective technique for preparing nanofibers at high speeds (up to 0.5 g/min²⁵³). The process is more economical and safer

than electrospinning. Moreover, it has a higher production rate.²³³ Centrifugal jet spinning is accomplished using a spinning head containing the polymer melt or solution (Figure 17A). When the rotation speed reaches a critical value, the surface tension of the spinning liquid is overcome by the centrifugal force, resulting in the ejection of a liquid jet from

the spinning head. The critical rotation speed is directly proportional to the concentration of the solution.²⁵⁵ The centrifugal force and air frictional force stretch the jet, leading to nanofibers. The stretched jet is deposited on the collector surface (Figure 17B), producing a nonwoven mat of nanofibers (Figure 17C).²⁵⁴

4.3.2. Rheology in Centrifugal Jet Spinning. In their studies on the synthesis of polyvinylpyrrolidone (PVP)/poly(L-lactic acid) (PLLA) composite fibers via the centrifugal jet spinning of polymer solution, Ren et al.²⁵³ noticed that the product morphology was governed by the rheological characteristics of the polymer solution along with the centrifugal force acting on the solution jet. For a specific solution viscosity, continuous fibers were formed only when the centrifugal force was higher than a critical value. The viscosity of the polymer solution was selected as a measure of the extent of entanglement of the polymer chains: an increase in the extent of entanglement increased the solution viscosity. Inadequate chain entanglements lowered the flow resistance of the jet to a level lower than that required to resist the breakup of the jet below a certain rotation speed. In these cases, the Plateau–Rayleigh instability caused the jet to split into a stream of droplets to lower the surface tension. Thus, at a certain rotation speed, a critical viscosity existed above which the fibers were generated. When the extent of chain entanglement was substantially high, the flow resistance of the jet was extremely high for the jet to be stretched into fiber assemblies. This indicated the presence of a viscosity range within which fibers were produced at a specific rotation speed. Within this viscosity range, the lowering of the polymer concentration resulted in thinner fibers. Thus, the researchers demonstrated the role of viscosity in the fabrication of fibers via centrifugal jet spinning. Furthermore, in their investigations on the centrifugal jet spinning of PA6 nanofibers, Hammami et al.²⁵⁶ reported that with an increase in the fiber diameter, the viscosity of the spinning solution enhanced.

Moreover, in their studies on PAN nanofibers produced by centrifugal jet spinning, Lu et al.²⁵⁷ have demonstrated the existence of a critical viscosity corresponding to c^* and an optimal viscosity range for the development of fibers at a particular rotation speed. The researchers observed that at very low c ($c \ll c^*$, semidilute unentangled regime), practically, no chain entanglement occurred, rendering the formation of nanofibers extremely difficult. When c was lower than but close to c^* ($c < c^*$), fibers were formed; however, they were beaded because of the absence of sufficient chain entanglements. When $c > c^*$, chain entanglement was adequate for the production of uniform and continuous bead-free fibers. Furthermore, an optimal concentration range that generated continuous bead-free nanofibers existed. Beyond this optimal range, stress relaxation time of the solution increased, which impeded the evaporation of solvents and prevented jet fracturing, stretching, and thinning. This resulted in an increased fiber diameter, leading to the production of micrometer-sized fibers. The researchers determined c^* by plotting the specific viscosity (evaluated from the zero-shear viscosity) against polymer concentration for a series of PAN solutions (Figure 18). The semidilute unentangled, semidilute entangled, and concentrated regimes were determined from the changes in the slopes, and c^* , indicated by the onset of the concentrated regime, was calculated to be 10 wt %.

The presence of a critical viscosity and an optimal viscosity range for the formation of continuous bead-free fibers has also

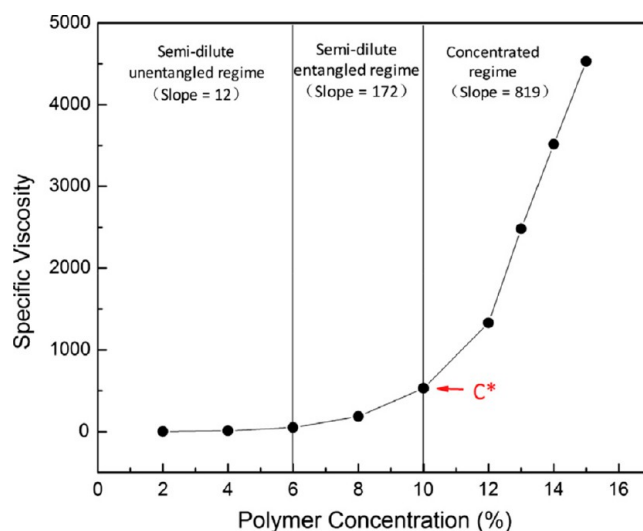


Figure 18. Specific viscosity versus polymer concentration profile for PAN solutions. Changes in the slope denoted the onset of the semidilute unentangled, semidilute entangled, and concentrated regimes. c^* was evaluated to be 10 wt %. Reproduced with permission from ref 257. Copyright 2013 Elsevier Science Ltd.

been reported by other researchers. Merchiers et al.²⁵⁸ have described the transformation of beaded fibers into continuous bead-free fibers with an increase in viscosity near c^* . With further increase in viscosity, the diameters of the bead-free fibers increased. In their investigations on the centrifugal jet spinning of both PE solution and melt, Rogalski et al.²⁵⁹ reported that excessively high viscosity caused the blockage of the die channels within the rotating spinneret. Optimal fiber production occurred in the low Newtonian viscosity range of 1–10 Pa s.

In their attempt to predict the trajectory and radius of the solution jet ejected during centrifugal jet spinning, Noroozi et al.²⁶⁰ developed a string model for a Newtonian viscous curved jet. They utilized a nonorthogonal curvilinear coordinate system and included the effects of both air drag and solvent evaporation on the trajectory and radius of the jet in their analysis. In addition to the Newtonian fluid assumption, all parameters considered in the analysis were actually involved in the curved jet flow of the process, and these parameters (such as viscosity, surface tension, mass diffusion into air, and inertial, rotational, and aerodynamic effects) were introduced as the dimensionless groups Rossby (Rb), Reynolds (Re), Weber (We), Froude (Fr), Péclet (Pe), air Reynolds (Re^*), and air Péclet (Pe^*) numbers and the collector radial position (R). Comparison of the predictions of the model with the experimental results reveals that the aerodynamic effects should indeed be considered to accurately estimate the jet trajectory and radius. A decrease in Rb resulted in a more rapid thinning of the jet. Moreover, this caused a tighter wrapping of the jet around the axis of rotation. Increases in Re, Re^* , and R resulted in a longer jet. A decrease in We led to a tighter wrapping of the jet. Nevertheless, the influence of We on solvent evaporation was minor. The effects of Pe and Pe^* on the jet trajectory were insignificant. Therefore, the researchers demonstrated the influences of various rheological parameters on the trajectory and radius of the jet during centrifugal jet spinning.

Zhmayer et al.²⁶¹ examined the influences of viscoelasticity, driving force, and rate of flow on the geometry (dimensions

and shape) and thinning of the jet during centrifugal jet spinning. They used viscoelastic PIB/PB Boger fluids with various compositions, where PB is a Newtonian fluid. Initially, high viscoelasticity resulted in a more rapid jet thinning. However, this effect was strongly related to the angular velocity. An increase in angular velocity retarded this thinning, which was ascribed to the rapid enhancement in the elongational viscosities of highly viscoelastic fluids. A decrease in the flow rate increased the rate of initial thinning. Viscoelasticity and centrifugal force considerably affected the jet contour radii. Increase in viscoelasticity and angular velocity lowered the maximum radius because of the generation of elastic hoop stress. The researchers also conducted simulation studies using the FENE-P model and compared the acquired results with those of experimental studies. They discovered that this model was suitable for predicting the thinning behavior of the jet. Thus, these studies indicated the influence of viscoelasticity on the jet during centrifugal spinning and suitability of the FENE-P model for estimating jet thinning.

The effect of viscoelasticity on the centrifugal jet spinning of polymer solutions was also investigated by Ren et al.²⁶² They identified three stages of spinning: jet initiation, jet extension, and fiber formation. Theoretical and experimental studies were performed on four different polymer solutions to understand the influences of viscoelasticity on the different stages of the process. Various dimensionless numbers including Deborah number, Weissenberg number, Ca , and the Ohnesorge number were employed for analysis. Experiments were conducted on solutions having wide ranges of relaxation times, viscosities, and solvent evaporation rates. When Ca was below 1, only beads were produced. When Ca was higher than 2, uniform fibers were obtained. Thus, fiber spinnability was controlled by Ca . Fiber radius was affected by the elasticity of the solution and rate of evaporation of the solvent. It was approximately a power-law function of an elastic processability parameter that linked filament thinning to solvent evaporation. The effects of viscoelasticity on jet thinning and trajectory and fiber radius during centrifugal jet spinning have also been reported by other researchers.^{263–265}

Very few studies have been reported on the role of extensional rheology in the centrifugal jet spinning of polymer solutions/melts. According to Mahalingam et al.,²⁶⁶ as the jet leaves the spinneret, the elongational flow becomes predominant and significantly influences molecular stretching. Even at room temperature, a higher rotation speed enhances solvent evaporation, which affects the extensional viscosity. This change in extensional viscosity substantially impacts the final fiber diameter and its distribution. Riahi²⁶⁷ developed a non-Newtonian strain hardening model for nonlinear viscoelastic polymeric fluid jet that considered the effects of different extents of strain hardening. In accordance with the model, the existence of strain hardening lowers the strain rate and decreases the rotation speed, stretching, and rate of stretching of the jet in the downstream direction away from the spinneret. This also enhances the jet radius with an increase in the distance from the spinneret. When strain hardening is significant, the stretching rate approaches zero, considerably thickening the jet. Moreover, in their investigations on discretized modeling of centrifugal jet spinning, Divvela et al.²⁶³ reported a similar finding. They stated that stretching of polymer molecules increased the extensional viscosity, which increased the jet radius in the final stage of spinning. Thus, based on the few studies that are available, it may be

summarized that extensional rheology affects the fiber diameter in centrifugal jet spinning. With an increase in elongational viscosity and strain hardening, the fiber diameter increases. Nevertheless, more research is required to develop a better understanding of the influence of elongational rheology on the spinnabilities of polymer solutions/melts by centrifugal jet spinning.

Therefore, fiber spinnability and morphology in centrifugal jet spinning are governed by the solution/melt viscosity. At a certain rotation speed, bead-free continuous fibers are produced only when the solution/melt viscosity is above a critical value and within an optimal range. Jet thinning, trajectory, and contour radii along with the final fiber radius are regulated by the viscoelasticity of the solution/melt. With an increase in elongational viscosity and strain hardening, the fiber radius increases. Thus, an insight into the rheological properties of the polymer melt or solution being spun is essential to successfully synthesize defect-free nanofibers via centrifugal jet spinning.

4.4. 3D Printing. **4.4.1. Basics of 3D Printing.** 3D printing, also known as additive manufacturing, rapid prototyping, or solid free-form fabrication, is a technique of joining materials, generally layer-by-layer, to produce objects from 3D model data.^{268,269} As accurate control of the sizes and geometries of products can be achieved via computer-aided design (CAD), 3D printing can be used to fabricate products with complex geometries without the generation of waste, which typically occurs in other manufacturing techniques. Furthermore, the process is cost-effective as it does not require molds, the design and manufacture of which can be expensive.^{270,271} This technique utilizes a meshed 3D computer model that is produced using the acquired image data or structures in a CAD software. A surface tessellation language file is usually developed. The mesh data is further sectioned into a build file of two-dimensional layers, which is inserted into the 3D printing machine.²⁷¹

There are seven methods of 3D printing: material extrusion, material jetting, binder jetting, vat polymerization, powder bed fusion (PBF), directed energy deposition, and sheet lamination.²⁷² However, some of these methods are either not cost-effective because of their equipment requirements (for example, in the cases of directed energy deposition, material and binder jetting, and PBF) or have limited accessibilities (such as in the case of sheet lamination). Polymers are 3D printed via PBF, vat polymerization, and material extrusion. Among them, vat polymerization often employs toxic chemicals and is not appropriate for the 3D printing of highly filled polymers. Additionally, the parts printed by this method typically require postprocessing, which increases the cost. The PBF mode of 3D printing has two main limitations: the equipment cost and requirement of powder feedstocks having the necessary properties. Hence, material extrusion is the most common route for the 3D printing of polymeric materials. Material extrusion has many advantages, such as ready availability, relatively inexpensive feedstocks, low energy requirements, ease of operation and maintenance, and the ability to 3D print highly filled polymeric systems, over PBF and vat polymerization.^{273,274} The scope of this section of the article is restricted to material extrusion of polymeric materials.

Material extrusion-based 3D printing comprises fused filament fabrication (FFF), also called fused deposition modeling (FDM) and 3D dispensing (3D microextrusion, plotting, and fiber deposition). FFF is a standard technique of

producing 3D polymer parts in industry. It involves the melting of a solid thermoplastic filament followed by the deposition of successive layers of the melt, which fuse to form a continuous profile (Figure 19).^{275,276}

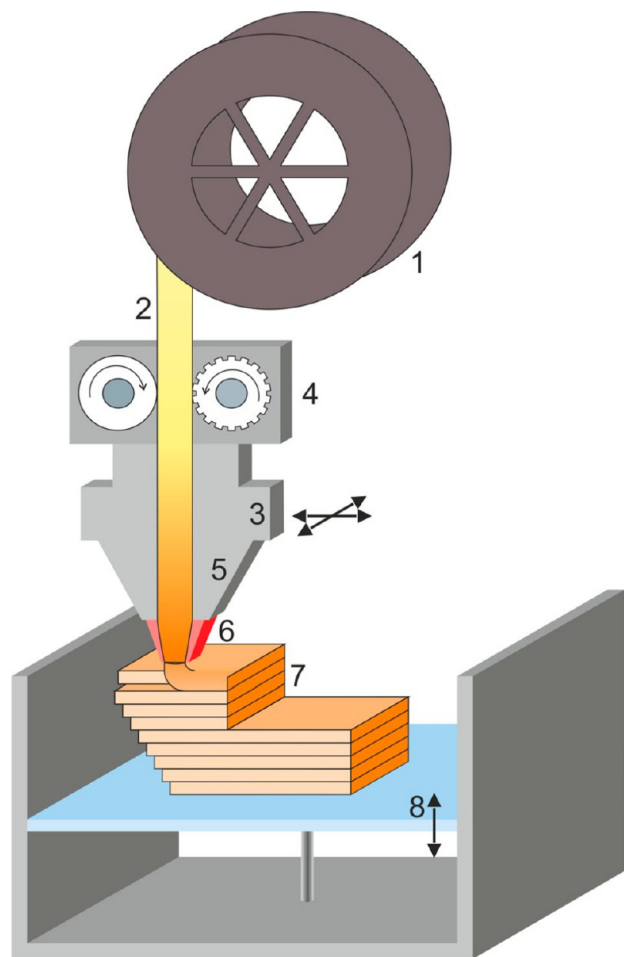


Figure 19. Schematic of material extrusion. The components are labeled as follows: (1) spooled material storage, (2) thermoplastic filament, (3) horizontally movable heated deposition unit consisting of (4) counter-rotating driving wheels, (5) a liquefier, (6) a nozzle, (7) a structural element fabricated in a layer-by-layer manner, and (8) a vertically movable build platform. Reproduced with permission from ref 275. Copyright 2020 Wiley.

Contrary to FFF, pellet-fed material extrusion-based 3D printing does not require the preprocessing step of filament preparation and hence demonstrates the advantages of lower processing time and reduced risk of thermal decomposition. This method is particularly suitable for the 3D printing of thermally unstable polymers. Furthermore, the process can be tailored to extrude multiple materials for producing printed parts with compositional gradients.²⁷⁰

4.4.2. Rheology in 3D Printing. Assessment of the 3D printabilities of materials has attracted the interest of researchers for a long time. According to Duty et al.,²⁷⁷ a 3D printable material should fulfill four criteria: (i) it must be extrudable through a nozzle, (ii) the extrudate should exhibit shape retention, (iii) the extrudate should be capable of bridging a gap of a specific length, and (iv) the extrudate should demonstrate geometric stability while being cooled to room temperature.

Zawaski et al.²⁷⁸ have reported similar criteria for “printability”. Nevertheless, they have hypothesized that any 3D printable material must be extrudable. On the basis of this assumption, they have attributed more importance to the deposition of the material, that is, maintenance of geometric accuracy, creation of small features, and bridging the gap. According to Vanzanella et al.,²⁷⁹ during FFF, the solidification kinetics must compromise between two contrary requirements. On the one hand, the material should gain a sufficient consistency to enable the product to retain its geometry. On the other hand, it should exhibit a liquidlike behavior for an adequate time period to ensure optimal bonding between two successive filament layers.

All criteria for the 3D printabilities of polymers are directly related to the rheological characteristics of polymers. Thus, regulation of the rheological characteristics of polymers as per requirements via chemical modification of the polymer molecules or their blending with other polymer(s) and/or fillers is essential for constructing 3D-printed parts with the desired geometries and properties. Moreover, a comprehensive understanding of the thermorheological properties of the materials used is necessary for optimizing the process parameters and obtaining an insight into the processing–property relationships.^{270,279}

The most important rheological property that determines the printability of a polymeric material in extrusion-based 3D printing is melt viscosity. Typically, the shear rate in the liquefier is very high.²⁸⁰ A higher extent of shear thinning is favorable as shear thinning influences not only the ability of the melt to be forced through the nozzle but also its ability to acquire the required shape and structure after deposition.²⁸¹ In their investigations on FDM of PP/talc composites, Bertolino et al.²⁸² stated the importance of a strong shear thinning effect for excellent 3D printability.

Knowledge of the ideal viscosity range can help predict the printabilities of materials. The viscosity should be adequately low for extrudability. Simultaneously, it should not be extremely low such that the melt flows like a liquid after being extruded. However, very few studies have been reported on the evaluation of the printability window for extrusion-based 3D printing. Additionally, no data is available on an acceptable viscosity range for successful 3D printing. In this regard, a simple approach is to compare the melt viscosity at the operating shear rate with that of the melt of a successfully 3D-printed standard material at the same shear rate. If the viscosities are similar, the material under consideration can be regarded as 3D printable. The apparent shear rate $\dot{\gamma}_{app}$ at the nozzle wall can be determined from the volumetric flow rate Q using eqs 48 and 49:

$$Q = \pi r^2 v \quad (48)$$

$$\dot{\gamma}_{app} = \frac{4Q}{\pi r^3} \quad (49)$$

where v is the printing speed and r is the radius of the nozzle.

Thus, viscosity at the calculated shear rate can be evaluated via rheological studies.²⁸¹

In their studies on 3D printing of β -tricalcium phosphate (TCP)-PLA composites by FFF, Elhatab et al.²⁸³ observed that the lowering of viscosity caused by an increase in nozzle temperature enhanced the melt flowability and interlayer bonding between printed layers. They highlighted the significance of the optimization of nozzle temperature for

achieving the viscosity required for successful 3D printing. According to Bertolino et al.,²⁸² during FDM, a high viscosity can result in filament buckling, rendering the material completely nonprintable.

Yield stress is another rheological characteristic of significant importance in 3D printing. In their investigations on the FDM of pure PP and PP/talc composites, Bertolino et al.²⁸² noticed that the absence of a yield stress caused drooling of the melt from the nozzle and difficulty in the achievement of the desired shape of the melt after extrusion. According to Gupta,²⁸⁴ a high yield stress along with a strong shear thinning behavior facilitates the retention of the required shape. Hu et al.²⁸⁵ have also paid attention to the importance of yield stress in the attainment of the melt with desired structural characteristics in 3D printing.

The role of viscoelasticity in 3D printing has been discussed in literature. With an increase in the storage modulus of the material, extrudability decreases and the nozzle of the 3D printer may clog even before the commencement of printing. Nevertheless, if the storage modulus is considerably low, the structure may not acquire adequate rigidity, and the printed structure may collapse because the deposited layers do not have the rigidity required to withstand the weights of the successive layers. Furthermore, the loss modulus should not be extremely low such that the material freely drains upon being extruded or fails to retain its shape. If the loss modulus is higher than the storage modulus over the entire frequency range used for rheological studies, the material usually demonstrates adequate flowability and shape retention after being printed.^{281,285,286}

In their studies on extrusion-based 3D printing of PLLA, poly(L-lactide-co-ε-caprolactone) (PCLA), poly(L-lactide-co-glycolide) (PLGA), and poly(D,L-lactide-co-glycolide) (PDLGA), Jain et al.²⁸⁷ reported that PLLA and PCLA with higher MWs were printable and exhibited lower extents of degradation before printing when compared with the cases of PLGA and PDLGA. The lower 3D printabilities of PLGA and PDLGA were ascribed to the higher complex viscosities and elasticities of their melts.

In their investigations on the FFF of polyvinyl chloride–acrylate copolymers, Peñas et al.²⁸⁸ demonstrated the significance of viscoelasticity in 3D printing. The acrylates used for copolymerization were butyl acrylate (BA), 2-ethyl hexyl acrylate (EHA), and 2-heptyl propyl acrylate (2PHA). They qualitatively assessed the adhesion performance of copolymers in 3D printing based on the Dahlquist criterion and used their findings for selecting a suitable temperature of the printing substrate. Stress–relaxation experiments were performed at various temperatures. The copolymers satisfied the Dahlquist criterion at times below 1 s at 100 °C (Figure 20). In contrast, the relaxation moduli were higher at 40 °C, indicating inadequate interlayer adhesion. On the basis of this observation, 100 °C was chosen as a more appropriate temperature for 3D printing as compared to 40 °C. Moreover, the researchers observed lowering of printability at high melt elasticities. Consequently, they established the roles of viscoelasticity in the printabilities and structural integrities of the printed products in FFF. Furthermore, they indicated the application of rheological characterization in the selection of suitable printing temperature.

In their modeling studies, Duty et al.²⁷⁷ analyzed the function of viscoelasticity in extrusion-based 3D printing. They proposed a viscoelastic model, termed as a “printability

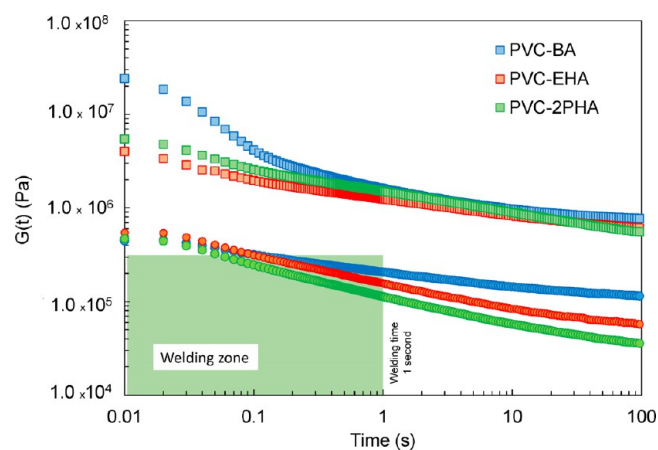


Figure 20. Stress–relaxation experiments of the synthesized copolymers at 40 °C (empty symbols) and 100 °C (filled symbols). The green area highlights the zone where the welding is expected. This zone is delimited by the Dahlquist criterion (3×10^5 Pa) and a welding time of 1 s. Reproduced from ref 288. Copyright 2020 The Authors.

model,” for evaluating the printabilities of materials in numerous extrusion-based 3D printing techniques. The model provided equations as “print criteria” for the conditions that should be fulfilled for effective 3D printing. Several materials were assessed using the printability model, and the predictions were in accordance with the experimental observations. Additionally, this model was a convenient tool for identifying suitable printing conditions (such as deposition temperature, flow rate, head speed, and limiting nozzle diameter) and suggesting compositional changes during material development.

However, very few studies have been reported on the role of extensional rheology in extrusion-based 3D printing. According to Das et al.,²⁷⁰ extensional viscosity influences die swell and hence the extrudate shape. In their studies on the FFF of carbon fiber-reinforced polymer composites, Heller et al.²⁸⁹ noticed that aligning stiff fibers along the extrudate enhanced the elongational flow in the convergence zone of the nozzle, significantly lowering the die swell during 3D printing. Additionally, the impact of extensional flow on the die swell was reported by Schuller et al.;²⁹⁰ nevertheless, they focused more on shear-induced normal stress differences. Moreover, the influences of extensional stresses on die swell in FDM were stated by De Rosa et al.;²⁹¹ however, detailed studies were not conducted. The effect of extensional rheology on 3D printability has also been reported by other researchers.^{292–294} However, a comprehensive understanding of this effect needs to be developed.

Thus, it may be summarized that melts with lower viscosities and elasticities, high yield stresses, strong shear thinning behaviors, and minimum die swells generally exhibit outstanding extrusion-based 3D printabilities. Nevertheless, extremely low viscosity and elasticity may lead to liquidlike flow of the melt after extrusion and inferior stiffnesses of the printed layers, respectively. This necessitates the identification of the windows of viscosity and elasticity for optimum 3D printability. Consequently, more research is required in this area.

5. CONCLUSIONS AND FUTURE OUTLOOK

Herein, studies on the roles of rheology in the morphological development and advanced processing of various polymeric materials are reviewed. On the basis of the findings of these studies, the following key facts are established: (a) Rheology plays a crucial role in the morphological development of polymeric materials. In the cases of blends, rheology governs not only the type of morphology (droplet/matrix, fibrillar, or cocontinuous) but also the sizes of the dispersed particles. Ca and λ are the parameters of significant importance in the evolution of blend morphology. Elongational flow facilitates the attainment of a superior quality of dispersion and also plays a crucial role in the evolution of fibrillar morphology. Flow behaviors of polymer/fiber suspensions under the influence of shear substantially affect the quality of dispersion and orientation, attrition, and flocculation of fibers, thereby influencing the development of the morphologies of discontinuous fiber-reinforced polymer composites. Elongational flow lowers the rate of attrition of fibers. In the cases of polymer nanocomposites, the quality of dispersion is controlled by shear and elongational flows. Elongational flow results in a superior quality of dispersion of nanoparticles without degrading shear-sensitive polymeric matrices. Rheology not only affects the evolution of morphology but also provides vital information on the morphological characteristics of polymer blends and nanocomposites. In fact, rheology can serve as a tool for the assessment of the morphologies of polymer blends and nanocomposites. (b) Viscoelasticity and extensional rheological properties of polymeric materials considerably influence their processabilities in film blowing. High melt strength, strain hardening behavior, and high storage modulus lead to stable bubbles and highly homogeneous film thicknesses in blown film extrusion. (c) In both electrospinning and centrifugal jet spinning, the spinnability, jet trajectory, and fiber diameter are affected by the viscosity, elasticity, and strain hardening behavior of the polymer solution/melt. For a specific electric field (electrospinning)/rotation speed (centrifugal jet spinning), a window corresponding to the range of rheological characteristics that produce fibers of acceptable qualities can be determined. By tailoring the rheological characteristics of the solution/melt within this window, bead-free fibers with the required diameters may be constructed. (d) Melts with lower viscosities and elasticities, high yield stresses, strong shear thinning behaviors, and minimum die swells typically demonstrate excellent extrusion-based 3D printabilities. However, extremely low viscosities and elasticities may result in liquidlike flow of the melt after extrusion and inferior stiffnesses of the printed layers, respectively. This necessitates the identification of the windows of viscosity and elasticity for optimum 3D printability.

Although a significant amount of research has already been performed on the role of rheology in polymer processing, there is considerable scope for research in certain areas. Knowledge on the function of rheology in the evolution of the morphologies of multiphase systems with three or more components is limited. The role of rheology in the subsequent advanced processing of these multiphase polymeric materials is yet to be understood. Further investigation is needed on how a balance of viscoelastic properties can lead to enhanced film blowabilities. Additionally, the influence of shear rheology on film blowability still needs to be understood. Moreover, a

systematic understanding of the functions of extensional rheology in centrifugal jet spinning and 3D printing is yet to be achieved.

Finally, it can be summarized that a comprehensive knowledge of the role of rheology in advanced polymer-processing operations will facilitate the enhancement of polymer processability via the tailoring of rheological characteristics via changes in the compositions of polymeric materials and process parameters. Thus, extensive rheological characterization of polymeric materials and correlation of the corresponding results with their processabilities are imperative for achieving superior product quality in advanced processing operations.

AUTHOR INFORMATION

Corresponding Author

Suprakas Sinha Ray – Department of Chemical Sciences, University of Johannesburg, Johannesburg 2028, South Africa; Centre for Nanostructures and Advanced Materials, DSI-CSIR Nanotechnology Innovation Centre, Council for Scientific and Industrial Research, Pretoria 0001, South Africa; orcid.org/0000-0002-0007-2595; Email: rsuprakas@csir.co.za, ssinharay@uj.ac.za

Author

Ritima Banerjee – Department of Chemical Engineering, Calcutta Institute of Technology, Uluberia 711316 West Bengal, India; Department of Chemical Sciences, University of Johannesburg, Johannesburg 2028, South Africa

Complete contact information is available at:

<https://pubs.acs.org/10.1021/acsomega.3c03310>

Notes

The authors declare no competing financial interest.

ACKNOWLEDGMENTS

The authors would like to acknowledge the financial support received from the Department of Science and Innovation (C6ACH77), Council for Scientific and Industrial Research, Pretoria (086ADMIN), and the University of Johannesburg (086310), South Africa.

REFERENCES

- (1) Ray, S. S.; Banerjee, R. *Foamability of Thermoplastic Polymeric Materials*; Elsevier: Amsterdam, 2021.
- (2) Banerjee, R.; Ray, S. S. Foamability and Special Applications of Microcellular Thermoplastic Polymers: A Review on Recent Advances and Future Direction. *Macromol. Mater. Eng.* **2020**, *305*, No. 2000366.
- (3) Zloczower, I. M. *Mixing and Compounding of Polymers: Theory and Practice*; Hanser: New York, 1994.
- (4) Ray, S. S.; Okamoto, M. New Poly(lactide)/Layered Silicate Nanocomposites. Part 6. Melt Rheology and Foam Processing. *Macromol. Mater. Eng.* **2003**, *288* (12), 936–944.
- (5) Singh, S.; Ghosh, A. K.; Maiti, S. N.; Gupta, R. K.; Bhattacharya, S. Rheological Aspects and Film Processability of Poly (Lactic Acid)/Linear Low-Density Polyethylene Blends. *Polym. Eng. Sci.* **2021**, *61* (1), 85–94.
- (6) Kommoji, S.; Banerjee, R.; Bhatnagar, N.; Ghosh, A. K. Studies on the Stretching Behaviour of Medium Gauge High Impact Polystyrene Sheets during Positive Thermoforming. *J. Plast. Film Sheeting* **2015**, *31*, 96–112.
- (7) Wu, H.; Lv, S.; He, Y.; Qu, J. P. The Study of the Thermomechanical Degradation and Mechanical Properties of PET

- Recycled by Industrial-Scale Elongational Processing. *Polym. Test.* **2019**, *77*, No. 105882.
- (8) Maani, A.; Naguib, H. E.; Heuzey, M.-C.; Carreau, P. J. Foaming Behaviour of Microcellular Thermoplastic Olefin Blends. *J. Cell. Plast.* **2013**, *49* (3), 223–244.
- (9) Kim, S. G.; Leung, S. N.; Park, C. B.; Sain, M. The Effect of Dispersed Elastomer Particle Size on Heterogeneous Nucleation of TPO with N₂ Foaming. *Chem. Eng. Sci.* **2011**, *66*, 3675–3686.
- (10) Dealy, J. M.; Wissbrun, K. F. *Melt Rheology and Its Role in Plastics Processing*; Van Nostrand Reinhold: New York, 1990.
- (11) Gupta, B. R. *Applied Rheology in Polymer Processing*; Asian Books Private Limited: Delhi, 2005.
- (12) Schmidt, A. X.; Marlies, C. A. *Principles of High-Polymer Theory and Practice*; McGraw-Hill Book Company, Inc.: New York, 1948.
- (13) Campbell, G. A.; Zak, M. E.; Wetzel, M. D. Newtonian, Power Law, and Infinite Shear Flow Characteristics of Concentrated Slurries Using Percolation Theory Concepts. *Rheol. Acta* **2018**, *57* (3), 197–216.
- (14) Arda, M. Torsional Vibration Analysis of Carbon Nanotubes Using Maxwell and Kelvin-Voigt Type Viscoelastic Material Models. *Eur. Mech. Sci.* **2020**, *4*, 90–95.
- (15) Ramli, H.; Zainal, N. F. A.; Hess, M.; Chan, C. H. Basic Principle and Good Practices of Rheology for Polymers for Teachers and Beginners. *Chem. Teach. Int.* **2022**, *4* (4), 307–326.
- (16) (a) Ray, S. S. *Environmentally Friendly Polymer Nanocomposites: Types, Processing and Properties*; Elsevier: Oxford, UK. (b) Ray, S. S.; Yamada, K.; Okamoto, M.; Ueda, K. New Poly(lactide)-Layered Silicate Nanocomposites. 2. Concurrent Improvements of Material Properties, Biodegradability and Melt Rheology. *Polymer* **2003**, *44* (3), 857–866.
- (17) Ray, S. S.; Okamoto, K.; Okamoto, M. Structure-Property Relationship in Biodegradable Poly (Butylene Succinate)/Layered Silicate Nanocomposites. *Macromolecules* **2003**, *36* (7), 2355–2367.
- (18) Dealy, J. M. Extensional Flow of Non-Newtonian Fluids—A Review. *Polym. Eng. Sci.* **1971**, *11* (6), 433–445.
- (19) Baird, D. G. The Role of Extensional Rheology in Polymer Processing. *Korea-Australia Rheol. J.* **1999**, *11*, 305–311.
- (20) Meissner, J. Basic Parameters, Melt Rheology, Processing and End-Use Properties of Three Similar Low Density Polyethylene Samples. *Pure Appl. Chem.* **1975**, *42* (4), 551–612.
- (21) Ruinaard, H. Elongational Viscosity as a Tool to Predict the Foamability of Polyolefins. *J. Cell. Plast.* **2006**, *42* (3), 207–220.
- (22) Meißner, J. Dehnungsverhalten von Polyäthylen-Schmelzen. *Rheol. Acta* **1971**, *10* (2), 230–242.
- (23) Macosko, C. W. Morphology Development and Control in Immiscible Polymer Blends. *Macromol. Symp.* **2000**, *149* (1), 171–184.
- (24) Scott, C. E.; Macosko, C. W. Model Experiments Concerning Morphology Development during the Initial Stages of Polymer Blending. *Polym. Bull.* **1991**, *26* (3), 341–348.
- (25) Scott, C. E.; Macosko, C. W. Morphology Development during the Initial Stages of Polymer-Polymer Blending. *Polymer (Guildf.)* **1995**, *36* (3), 461–470.
- (26) Lindt, J. T.; Ghosh, A. K. Fluid Mechanics of the Formation of Polymer Blends. Part I: Formation of Lamellar Structures. *Polym. Eng. Sci.* **1992**, *32* (24), 1802–1813.
- (27) Sundararaj, U.; Macosko, C. W. Drop Breakup and Coalescence in Polymer Blends: The Effects of Concentration and Compatibilization. *Macromolecules* **1995**, *28* (8), 2647–2657.
- (28) Sundararaj, U.; Dori, Y.; Macosko, C. W. Visualization of Morphology Development in Polymer Blends. In *Proceedings of the 52nd Annual Technical Conference ANTEC 94*; Society of Plastics Engineers: San Francisco, 1994; pp 2448–2449.
- (29) Sundararaj, U.; Dori, Y.; Macosko, C. W. Sheet Formation in Immiscible Polymer Blends: Model Experiments on Initial Blend Morphology. *Polymer* **1995**, *36* (10), 1957–1968.
- (30) Ray, S. S.; Banerjee, R. *Sustainable Poly(lactide)-Based Blends*; Elsevier: Amsterdam, 2022.
- (31) Grace, H. P. Dispersion Phenomena in High Viscosity Immiscible Fluid Systems and Application of Static Mixers as Dispersion Devices in Such Systems. *Chem. Eng. Commun.* **1982**, *14* (3–6), 225–277.
- (32) Elmendrop, J. J. A Study on Polymer Blending Microrheologie. Ph.D. Dissertation, Delft University of Technology, 1986.
- (33) Janssen, J. M. H. Dynamics of Liquid–Liquid Mixing. Ph.D. Dissertation, Eindhoven University of Technology, 1993.
- (34) Willemsse, R. C.; Ramaker, E. J. J.; Van Dam, J.; Posthuma De Boer, A. Morphology Development in Immiscible Polymer Blends: Initial Blend Morphology and Phase Dimensions. *Polymer (Guildf.)* **1999**, *40* (24), 6651–6659.
- (35) Elemans, P. H. M. Modelling of the Processing of Incompatible Polymer Blends. Ph.D. Dissertation, Eindhoven University of Technology, 1989.
- (36) Kuhn, W. Spontane Aufteilung von Flüssigkeitszylindern in Kleine Kugeln. *Kolloid-Z.* **1953**, *132* (2–3), 84–99.
- (37) Mikami, T.; Cox, R. G.; Mason, S. G. Breakup of Extending Liquid Threads. *Int. J. Multiph. Flow* **1975**, *2* (2), 113–138.
- (38) Tomotika, S. On the Instability of a Cylindrical Thread of a Viscous Liquid Surrounded by Another Viscous Fluid. *Proc. R. Soc. London. Ser. A - Math. Phys. Sci.* **1935**, *150* (870), 322–337.
- (39) Plochocki, A. P.; Dagli, S. S.; Andrews, R. D. The Interface in Binary Mixtures of Polymers Containing a Corresponding Block Copolymer: Effects of Industrial Mixing Processes and of Coalescence. *Polym. Eng. Sci.* **1990**, *30* (12), 741–752.
- (40) Shih, C.-K. Mixing and Morphological Transformations in the Compounding Process for Polymer Blends: The Phase Inversion Mechanism. *Polym. Eng. Sci.* **1995**, *35* (21), 1688–1694.
- (41) Sundararaj, U.; Macosko, C. W.; Rolando, R. J.; Chan, H. T. Morphology Development in Polymer Blends. *Polym. Eng. Sci.* **1992**, *32* (24), 1814–1823.
- (42) Baird, D. G.; Collias, D. I. *Polymer Processing*; Butterworth-Heinemann: Boston, 1995.
- (43) Schrenk, W. J.; Bradley, N. L.; Alfrey, T.; Maack, H. Interfacial Flow Instability in Multilayer Coextrusion. *Polym. Eng. Sci.* **1978**, *18* (8), 620–623.
- (44) Miles, I. S.; Zurek, A. Preparation, Structure, and Properties of Two-Phase Co-Continuous Polymer Blends. *Polym. Eng. Sci.* **1988**, *28* (12), 796–805.
- (45) Jordhamo, G. M.; Manson, J. A.; Sperling, L. H. Phase Continuity and Inversion in Polymer Blends and Simultaneous Interpenetrating Networks. *Polym. Eng. Sci.* **1986**, *26* (8), 517–524.
- (46) Utracki, L. *Polymer Alloys and Blends: Thermodynamics and Rheology*; Hanser Gardner Publications: Munich, 1989.
- (47) Utracki, L. A. On the Viscosity-concentration Dependence of Immiscible Polymer Blends. *J. Rheol.* **1991**, *35* (8), 1615–1637.
- (48) Han, C. D. *Multiphase Flow in Polymer Processing*; Academic Press: New York, 1981.
- (49) Avgeropoulos, G. N.; Weissert, F. C.; Biddison, P. H.; Boehm, G. G. A. HETEROGENEOUS BLENDS OF POLYMERS. RHEOLOGY AND MORPHOLOGY. *Rubber Chem. Technol.* **1976**, *49* (1), 93–104.
- (50) Nelson, C. J.; Avgeropoulos, G. N.; Weissert, F. C.; Böhm, G. G. A. The Relationship between Rheology, Morphology and Physical Properties in Heterogeneous Blends. *Angew. Makromol. Chem.* **1977**, *60* (1), 49–86.
- (51) Mekhilef, N.; Verhoogt, H. Phase Inversion and Dual-Phase Continuity in Polymer Blends: Theoretical Predictions and Experimental Results. *Polymer* **1996**, *37* (18), 4069–4077.
- (52) Hietaoja, P. T.; Holsti-Miettinen, R. M.; Seppälä, J. V.; Ikkala, O. T. The Effect of Viscosity Ratio on the Phase Inversion of Polyamide 66/Polypropylene Blends. *J. Appl. Polym. Sci.* **1994**, *54* (11), 1613–1623.
- (53) Andradi, L. N.; Hellmann, G. P. Morphologies of Mechanically Mixed Amorphous Blends before and after Annealing. *Polym. Eng. Sci.* **1995**, *35* (8), 693–702.
- (54) Willis, J. M.; Caldas, V.; Favis, B. D. Processing-Morphology Relationships of Compatibilized Polyolefin/Polyamide Blends - Part II The Emulsifying Effect of an Ionomer Compatibilizer as a Function

- of Blend Composition and Viscosity Ratio. *J. Mater. Sci.* **1991**, *26* (17), 4742–4750.
- (55) Favis, B. D.; Chalifoux, J. P. Influence of Composition on the Morphology of Polypropylene/Polycarbonate Blends. *Polymer* **1988**, *29* (10), 1761–1767.
- (56) Steinmann, S.; Gronski, W.; Friedrich, C. Cocontinuous Polymer Blends: Influence of Viscosity and Elasticity Ratios of the Constituent Polymers on Phase Inversion. *Polymer (Guildf)*. **2001**, *42* (15), 6619–6629.
- (57) Ho, R. M.; Wu, C. H.; Su, A. C. Morphology of Plastic/Rubber Blends. *Polym. Eng. Sci.* **1990**, *30* (9), 511–518.
- (58) Kitayama, N.; Keskkula, H.; Paul, D. R. Reactive Compatibilization of Nylon 6/Styrene-Acrylonitrile Copolymer Blends: Part 1. Phase Inversion Behavior. *Polymer (Guildf)*. **2000**, *41* (22), 8041–8052.
- (59) Everaert, V.; Aerts, L.; Groeninckx, G. Phase Morphology Development in Immiscible PP/(PS/PPE) Blends Influence of the Melt-Viscosity Ratio and Blend Composition. *Polymer (Guildf)*. **1999**, *40* (24), 6627–6644.
- (60) Pandey, V.; Maia, J. M. Extension-Dominated Improved Dispersive Mixing in Single-Screw Extrusion. Part 1: Computational and Experimental Validation. *J. Appl. Polym. Sci.* **2021**, *138* (4), 49716.
- (61) Rauwendaal, C.; Osswald, T.; Gramann, P.; Davis, B. Design of Dispersive Mixing Devices. *Int. Polym. Process.* **1999**, *14* (1), 28–34.
- (62) Yuan, Z.; Chen, X.; Yu, D. Recent Advances in Elongational Flow Dominated Polymer Processing Technologies. *Polymer* **2021**, *13*, 1792.
- (63) Scott, C. E.; Macosko, C. W. Morphology Development during the Initial Stages of Polymer-Polymer Blending. *Polymer (Guildf)*. **1995**, *36* (3), 461–470.
- (64) Kang, J.; Smith, T. G.; Bigio, D. I. Study of Breakup Mechanisms in Cavity Flow. *AIChE J.* **1996**, *42* (3), 649–659.
- (65) Rondin, J.; Bouquey, M.; Muller, R.; Serra, C. A.; Martin, G.; Sonntag, P. Dispersive Mixing Efficiency of an Elongational Flow Mixer on PP/EPDM Blends: Morphological Analysis and Correlation with Viscoelastic Properties. *Polym. Eng. Sci.* **2014**, *54* (6), 1444–1457.
- (66) Meller, M.; Luciani, A.; Marnson, J.-A. E. Flow through a Convergence. Part 2: Mixing of High Viscosity Ratio Polymer Blends. *Polym. Eng. Sci.* **2002**, *42* (3), 634–653.
- (67) Luciani, A.; Utracki, L. A. The Extensional Flow Mixer, EFM. *Int. Polym. Process.* **1996**, *11* (4), 299–309.
- (68) Pandey, V.; Chen, H.; Ma, J.; Maia, J. M. Extension-Dominated Improved Dispersive Mixing in Single-Screw Extrusion. Part 2: Comparative Analysis with Twin-Screw Extruder. *J. Appl. Polym. Sci.* **2021**, *138* (5), 49765.
- (69) Chen, H.; Maia, J. M. Improving Dispersive Mixing in Compatibilized Polystyrene/Polyamide-6 Blends via Extension-dominated Reactive Single-Screw Extrusion. *J. Polym. Eng.* **2021**, *41* (5), 397–403.
- (70) Chen, H.; Pandey, V.; Carson, S.; Maia, J. M. Enhanced Dispersive Mixing in Twin-Screw Extrusion via Extension-Dominated Static Mixing Elements of Varying Contraction Ratios. *Int. Polym. Process.* **2020**, *35* (1), 37–49.
- (71) Chen, H.; Guo, M.; Schiraldi, D.; Maia, J. M. Morphology Optimization of Poly(Ethylene Terephthalate)/Polyamide Blends Compatibilized via Extension-Dominated Twin-Screw Extrusion. *J. Polym. Eng.* **2021**, *41* (3), 218–225.
- (72) Qu, J.-P.; Zhang, G.-Z.; Chen, H.-Z.; Yin, X.-C.; He, H.-Z. Solid Conveying in Vane Extruder for Polymer Processing: Effects on Pressure Establishment. *Polym. Eng. Sci.* **2012**, *52*, 2147–2156.
- (73) Xiaochun, Y.; Zhongwei, Y.; Zengwenbing; Guangjian, H.; Zhitao, Y.; Baiping, X. The Design and Performance of a Vane Mixer Based on Extensional Flow for Polymer Blends. *J. Appl. Polym. Sci.* **2015**, *132* (9), 41551.
- (74) Wu, T.; Tong, Y.; Qiu, F.; Yuan, D.; Zhang, G.; Qu, J. Morphology, Rheology Property, and Crystallization Behavior of PLLA/OMMT Nanocomposites Prepared by an Innovative Eccentric Rotor Extruder. *Polym. Adv. Technol.* **2018**, *29* (1), 41–51.
- (75) Wu, T.; Yuan, D.; Qu, J. P. Preparation of Poly(L-Lactide)/Poly(Ethylene Glycol)/Organo-Modified Montmorillonite Nanocomposites via Melt Intercalation under Continuous Elongation Flow. *J. Polym. Eng.* **2018**, *38* (5), 449–460.
- (76) Yang, K.; Xin, C.; Huang, Y.; Jiang, L.; He, Y. Effects of Extensional Flow on Properties of Polyamide-66/Poly(2,6-Dimethyl-1,4-Phenylene Oxide) Blends: A Study of Morphology, Mechanical Properties, and Rheology. *Polym. Eng. Sci.* **2017**, *57* (10), 1090–1098.
- (77) Carson, S. O.; Covas, J. A.; Maia, J. M. A New Extensional Mixing Element for Improved Dispersive Mixing in Twin-Screw Extrusion, Part 1: Design and Computational Validation. *Adv. Polym. Technol.* **2017**, *36* (4), 455–465.
- (78) Carson, S. O.; Maia, J. M.; Covas, J. A. A New Extensional Mixing Element for Improved Dispersive Mixing in Twin-Screw Extrusion, Part 2: Experimental Validation for Immiscible Polymer Blends. *Adv. Polym. Technol.* **2018**, *37* (1), 167–175.
- (79) Blizard, K. G.; Baird, D. G. The Morphology and Rheology of Polymer Blends Containing a Liquid Crystalline Copolyester. *Polym. Eng. Sci.* **1987**, *27* (9), 653–662.
- (80) He, Y.; Yang, Z.-t.; Qu, J.-p. Super-Toughened Poly(Lactic Acid)/Thermoplastic Poly(Ether)Urethane Nanofiber Composites with in-Situ Formation of Aligned Nanofibers Prepared by an Innovative Eccentric Rotor Extruder. *Compos. Sci. Technol.* **2019**, *169*, 135–141.
- (81) Chapleau, N.; Favis, B. D. Droplet/Fibre Transitions in Immiscible Polymer Blends Generated during Melt Processing. *J. Mater. Sci.* **1995**, *30* (1), 142–150.
- (82) Arrigo, R.; Malucelli, G.; Mantia, F. P. La Effect of the Elongational Flow on the Morphology and Properties of Polymer Systems: A Brief Review. *Polymers* **2021**, *13*, 3529.
- (83) Mistretta, M. C.; Morreale, M.; Botta, L.; Ceraulo, M.; Fontana, P.; La Mantia, F. P. “Compatibilization” through Elongational Flow Processing of LDPE/PA6 Blends. *Mater.* **2018**, *Vol. 11*, Page 2375 **2018**, *11* (12), 2375.
- (84) Hedegaard, A. T.; Gu, L.; Macosko, C. W. Effect of Extensional Viscosity on Cocontinuity of Immiscible Polymer Blends. *J. Rheol. (N. Y. N. Y.)*. **2015**, *59* (6), 1397.
- (85) Advani, S. G.; Sozer, E. M. *Process Modeling in Composites Manufacturing*; Marcel Dekker, Inc: New York, 2003.
- (86) Sharuddin, S.; Salit, M. S.; Zainudin, E. S. A Review of the Effect of Moulding Parameters on the Performance of Polymeric Composite Injection Moulding. *Turkish J. Eng. Env. Sci.* **2006**, *30*, 23–24.
- (87) Lee, S. C.; Yang, D. Y.; Ko, J.; Youn, J. R. Effect of Compressibility on Flow Field and Fiber Orientation during the Filling Stage of Injection Moulding. *J. Mater. Process. Technol.* **1997**, *70*, 83–92.
- (88) Vu-Khanh, T.; Denault, J.; Habib, P.; Low, A. The Effects of Injection Moulding on the Mechanical Behavior of Long-Fiber Reinforced PBT/ PET Blends. *Compos. Sci. Technol.* **1991**, *40*, 423–435.
- (89) Gupta, V. B.; Mittal, R. K.; Sharma, P. K.; Mennig, G.; Wolters, J. Some Studies on Glass Fiber-Reinforced Polypropylene. Part I: Reduction in Fiber Length during Processing. *Polym. Compos* **1989**, *10*, 8–15.
- (90) von Turkovich, R.; Erwin, L. Fiber Fracture in Reinforced Thermoplastic Processing. *Polym. Eng. Sci.* **1983**, *23*, 743–749.
- (91) Mathews, F. L.; Rawlings, R. D. *Composite Materials: Engineering and Science*; Chapman & Hall: London, 1994.
- (92) Zhang, G.; Thompson, M. R. Reduced Fibre Breakage in a Glass-Fibre Reinforced Thermoplastic through Foaming. *Compos. Sci. Technol.* **2005**, *65*, 2240–2249.
- (93) Thomason, J. L. The Influence of Fibre Length and Concentration on the Properties of Glass Fibre Reinforced Polypropylene: 5. Injection Moulded Long and Short Fibre PP. *Compos A* **2002**, *33*, 1641–1652.

- (94) Hassan, A.; Yahya, R.; Yahaya, A. H.; Tahir, A. R. M.; Hornsby, P. R. Tensile, Impact and Fiber Length Properties of Injection-Molded Short and Long Glass Fiber-Reinforced Polyamide 6,6 Composites. *J. Reinf. Plast. Compos.* **2004**, *23*, 969–986.
- (95) Milewski, J. V. A Study of the Packing of Milled Fiberglass and Glass Beads. *Polym. - Plast Technol. Eng.* **1974**, *3* (1), 101–120.
- (96) Collins, S. H. Screw and Barrel Wear. Part I: The Causes. *Plast. Compd.* **1982**, *5* (3), 113–124.
- (97) Forgacs, O. L.; Mason, S. G. Particle Motion in Sheared Suspension: X. Orbits of Flexible Threadlike Particles. *J. Colloid Sci.* **1959**, *14*, 457–472.
- (98) Ross, R. F.; Klingenberg, D. J. Dynamic Simulation of Flexible Fibers Composed of Linked Rigid Bodies. *J. Chem. Phys.* **1997**, *106* (7), 2949–2960.
- (99) Hernandez, J.P.; Raush, T.; Rios, A.; Strauss, S.; Osswald, T.A. Analysis of Fiber Damage Mechanisms during Processing of Reinforced Polymer Melts. *Eng. Anal Bound Elem.* **2002**, *26*, 621–628.
- (100) Salinas, A.; Pittman, J. F. T. Bending and Breaking Fibers in Sheared Suspensions. *Polym. Eng. Sci.* **1981**, *21*, 23–31.
- (101) Hine, P. J.; Tsui, S.-W.; Coates, P. D.; Ward, I. M.; Duckett, R. A. Measuring the Development of Fibre Orientation during the Melt Extrusion of Short Glass Fibre Reinforced Polypropylene. *Compos. Part A* **1997**, *28A*, 949–958.
- (102) Bigg, D. M. Effect of Compounding on the Properties of Short Fibre Reinforced Injection Moldable Thermoplastic Composites. *Polym. Compos.* **1985**, *6* (1), 20–28.
- (103) Lunt, J. M.; Shortall, J. B. The Effect of Extrusion Compounding on Fibre Degradation and Strength Properties in Short Glass-Fibre Reinforced Nylon 6,6 Blends. *Plast. Rubber Process* **1979**, *4* (3), 108–114.
- (104) Lunt, J. M.; Shortall, J. B. Extrusion Compounding of Short Glass Fibre Filled Nylon 6,6 Blends. *Plast. Rubber Process* **1980**, *5* (2), 37–42.
- (105) Franzen, B.; Klason, C.; Kubat, J.; Kitano, T. Fibre Degradation during Processing of Short Fibre Reinforced Thermoplastics. *Composites* **1989**, *20* (1), 65–76.
- (106) Ray, S. S.; Banerjee, R. *Sustainable Polylactide-Based Composites*; Elsevier: Amsterdam, 2023.
- (107) Vaia, R. A.; Jandt, K. D.; Kramer, E. J.; Giannelis, E. P. Microstructural Evolution of Melt Intercalated Polymer-Organically Modified Layered Silicates Nanocomposites. *Chem. Mater.* **1996**, *8* (11), 2628–2635.
- (108) Vaia, R. A.; Giannelis, E. P. Polymer Melt Intercalation in Organically-Modified Layered Silicates: Model Predictions and Experiment. *Macromolecules* **1997**, *30* (25), 8000–8009.
- (109) Banerjee, R.; Ray, S. S. An Overview of the Recent Advances in Polylactide-based Sustainable Nanocomposites. *Polym. Eng. Sci.* **2021**, *61*, 617.
- (110) Hunter, D. L.; Kamena, K. W.; Paul, D. R. Processing and Properties of Polymers Modified by Clays. *MRS Bull.* **2007**, *32* (4), 323–327.
- (111) Dennis, H.; Hunter, D. L.; Chang, D.; Kim, S.; White, J. L.; Cho, J. W.; Paul, D. R. Effect of Melt Processing Conditions on the Extent of Exfoliation in Organoclay-Based Nanocomposites. *Polymer* **2001**, *42* (23), 9513–9522.
- (112) Vaia, R. A.; Giannelis, E. P. Lattice Model of Polymer Melt Intercalation in Organically-Modified Layered Silicates. *Macromolecules* **1997**, *30* (25), 7990–7999.
- (113) Borse, N. K.; Kamal, M. R. Estimation of Stresses Required for Exfoliation of Clay Particles in Polymer Nanocomposites. *Polym. Eng. Sci.* **2009**, *49* (4), 641–650.
- (114) Bandyopadhyay, J.; Ray, S. S.; Scriba, M.; Wesley-Smith, J. A Combined Experimental and Theoretical Approach to Establish the Relationship between Shear Force and Clay Platelet Delamination in Melt-Processed Polypropylene Nanocomposites. *Polymer* **2014**, *55* (9), 2233–2245.
- (115) Treece, M. A.; Zhang, W.; Moffitt, R. D.; Oberhauser, J. P. Twin-Screw Extrusion of Polypropylene-Clay Nanocomposites: Influence of Masterbatch Processing, Screw Rotation Mode, and Sequence. *Polym. Eng. Sci.* **2007**, *47* (6), 898–911.
- (116) Treece, M. A.; Oberhauser, J. P. Processing of Polypropylene-Clay Nanocomposites: Single-Screw Extrusion with in-Line Supercritical Carbon Dioxide Feed versus Twin-Screw Extrusion. *J. Appl. Polym. Sci.* **2007**, *103* (2), 884–892.
- (117) Zhu, L.; Xanthos, M. Effects of Process Conditions and Mixing Protocols on Structure of Extruded Polypropylene Nanocomposites. *J. Appl. Polym. Sci.* **2004**, *93* (4), 1891–1899.
- (118) Barbosa, S. E.; Ercoli, D. R.; Bibbó, M. A.; Kenny, J. M. Rheology of Short-Fiber Composites: A Systematic Approach. *Compos. Struct.* **1994**, *27* (1–2), 83–91.
- (119) Eberle, A. P. R.; Baird, D. G.; Wapperom, P.; Vélez-García, G. M. Using Transient Shear Rheology to Determine Material Parameters in Fiber Suspension Theory. *J. Rheol. (N. Y. N. Y.)* **2009**, *53* (3), 685.
- (120) Switzer, L. H.; Klingenberg, D. J. Rheology of Sheared Flexible Fiber Suspensions via Fiber-Level Simulations. *J. Rheol. (N. Y. N. Y.)* **2003**, *47* (3), 759.
- (121) Goto, S.; Nagazono, H.; Kato, H. The Flow Behavior of Fiber Suspensions in Newtonian Fluids and Polymer Solutions. II. Capillary Flow. *Rheol. Acta* **1986**, *25*, 246–256.
- (122) Kitano, T.; Kataoka, T. The Rheology of Suspensions of Nylon Fibers in Polymer Liquids. I. Suspensions in Silicone Oil. *Rheol. Acta* **1981**, *20*, 390–402.
- (123) Stary, Z.; Kruckel, J.; Weck, C.; Schubert, D. W. Rheology and Conductivity of Carbon Fibre Composites with Defined Fibre Lengths. *Compos. Sci. Technol.* **2013**, *85*, 58.
- (124) Petrie, C. J. S. The Rheology of Fibre Suspensions. *J. Non-Newtonian Fluid Mech.* **1999**, *87* (2–3), 369–402.
- (125) Ganani, E.; Powell, R.L. Suspensions of Rodlike Particles: Literature Review and Data Correlations. *J. Compos. Mater.* **1985**, *19*, 194–215.
- (126) Eberle, A. P. R.; Baird, D. G.; Wapperom, P. Rheology of Non-Newtonian Fluids Containing Glass Fibers: A Review of Experimental Literature. *Ind. Eng. Chem. Res.* **2008**, *47*, 3470–3488.
- (127) Chan, Y.; White, J. L.; Oyanagi, Y. A Fundamental Study of the Rheological Properties of Glass-Fiber-Reinforced Polyethylene and Polystyrene Melts. *J. Rheol.* **1978**, *22* (5), 507–524.
- (128) Kitano, T.; Kataoka, T.; Nagatsuka, Y. Dynamic Properties of Nylon Fibre and Glass Fibre Reinforced Polyethylene Melts. *Rheol. Acta* **1984**, *23*, 408–416.
- (129) Guo, R.; Azaiez, J.; Bellehumeur, C. Rheology of Fiber Filled Polymer Melts: Role of Fiber-Fiber Interactions and Polymer-Fiber Coupling. *Polym. Eng. Sci.* **2005**, *45*, 385–399.
- (130) Mobuchon, C.; Carreau, P. J.; Heuzey, M.-C.; Sepehr, M.; Ausias, G. Shear and Extensional Properties of Short Glass Fiber Reinforced Polypropylene. *Polym. Compos.* **2005**, *26*, 247–264.
- (131) Huq, M. A.; Azaiez, J. Effects of Length Distribution on the Steady Shear Viscosity of Semi-Concentrated Polymer-Fiber Suspensions. *Polym. Eng. Sci.* **2005**, *45*, 1357–1368.
- (132) Greene, J. P.; Wilkes, J. O. Steady-State and Dynamic Properties of Concentrated Fiber-Filled Thermoplastics. *Polym. Eng. Sci.* **1995**, *35* (21), 1670–1681.
- (133) Kim, J. K.; Song, J. H. Rheological Properties and Fiber Orientation of Short Fiber Reinforced Dplastics. *J. Rheol.* **1997**, *41* (5), 1061–1085.
- (134) Thomasset, J.; Carreau, P.J.; Sanschagrín, B.; Ausias, G. Rheological Properties of Long Glass Fiber Filled Polypropylene. *J. Non-Newtonian Fluid Mech.* **2005**, *125* (1), 25–34.
- (135) Sepehr, M.; Carreau, P. J.; Moan, M.; Ausias, G. Rheological Properties of Short Fiber Model Suspensions. *J. Rheol.* **2004**, *48* (5), 1023–1048.
- (136) Rezak, S. *Analysis of Flexible Fiber Suspensions Using the Lattice Boltzmann Method*; ProQuest: Ann Arbor, 2008.
- (137) Kerekes, R.; Schell, C. Characterization of Fiber Flocculation Regimes by a Crowding Factor. *J. Pulp Pap. Sci.* **1992**, *18* (1), 32–38.

- (138) Kerekes, R. J. Perspectives on Fibre Flocculation in Paper Making. In *Proceedings of the International Paper Physics Conference*, Sept 11–14, 1995; pp 23–31.
- (139) Jeffery, G. B. The Motion of Ellipsoidal Particles Immersed in a Viscous Fluid. *Proc. R. Soc. London Ser. A* **1922**, *102* (715), 161–179.
- (140) Eberle, A. P. R.; Velez-Garcia, G. M.; Baird, D. G.; Wapperom, P. Fiber Orientation Kinetics of a Concentrated Short Glass Fiber Suspension in Startup of Simple Shear Flow. *J. Nonnewton. Fluid Mech.* **2010**, *165*, 110–119.
- (141) Forgacs, O. L.; Mason, S. G. Particle Motion in Sheared Suspension: XI. Spin and Deformation of Threadlike Particles. *J. Colloid Sci.* **1959**, *14*, 473–491.
- (142) Petrich, M. P.; Koch, D. L. Interactions between Contacting Fibers. *Phys. Fluids* **1998**, *10*, 2111–2113.
- (143) Sundararajakumar, R. R.; Koch, D. L. Structure and Properties of Sheared Fiber Suspensions with Mechanical Contacts. *J. Non-Newt. Fluid Mech.* **1997**, *73*, 205–239.
- (144) Folgar, F. P.; Tucker, C. L. Orientation Behavior of Fibers in Concentrated Suspensions. *J. Rein. Plast. Comp* **1984**, *3*, 98–119.
- (145) Huynh, H. M. Improved Fiber Orientation Predictions for Injection-Molded Composites. Ph.D. Dissertation, University of Illinois at Urbana-Champaign, 2001.
- (146) Kamal, M. R.; Mutel, A. T. The Prediction of Flow and Orientation Behavior of Short Fiber Reinforced Melts in Simple Flow Systems. *Polym. Compos.* **1989**, *10* (5), 337–343.
- (147) Wang, J.; O'Gara, J. F.; Tucker, C. L. An Objective Model for Slow Orientation Kinetics in Concentrated Fiber Suspensions: Theory and Rheological Evidence. *J. Rheol.* **2008**, *52* (5), 1179.
- (148) Phelps, J. H.; Tucker, C. L. An Anisotropic Rotary Diffusion Model for Fiber Orientation in Short- and Long-Fiber Thermoplastics. *J. Nonnewton. Fluid Mech.* **2009**, *156* (3), 165–176.
- (149) Tseng, H.-C.; Chang, R.-Y.; Hsu, C.-H. Phenomenological Improvements to Predictive Models of Fiber Orientation in Concentrated Suspensions. *J. Rheol.* **2013**, *57* (6), 1597.
- (150) Tseng, H.-C.; Chang, R.-Y.; Hsu, C.-H. An Objective Tensor to Predict Anisotropic Fiber Orientation in Concentrated Suspensions. *J. Rheol.* **2016**, *60* (2), 215.
- (151) Tseng, H. C.; Chang, R. Y.; Hsu, C. H. Numerical Prediction of Fiber Orientation and Mechanical Performance for Short/Long Glass and Carbon Fiber-Reinforced Composites. *Compos. Sci. Technol.* **2017**, *144*, 51–56.
- (152) Yamamoto, S.; Matsuoka, T. A Method for Dynamic Simulation of Rigid and Flexible Fibres in a Flow Field. *J. Chem. Phys.* **1993**, *98*, 644–650.
- (153) Schmid, C. F.; Switzer, L. H.; Klingenberg, D. J. Simulations of Fiber Flocculations: Effects of Fiber Properties and Interfiber Friction. *J. Rheol.* **2000**, *44* (4), 781–809.
- (154) Lindstrom, S. B.; Uesaka, T. Simulation of Semi-Dilute Suspensions of Non-Brownian Fibers in Shear Flow. *J. Chem. Phys.* **2008**, *128*, 024901–024914.
- (155) Lindstrom, S. B.; Uesaka, T. Particle-Level Simulation of Forming of The Fiber Network in Papermaking. *Int. J. Eng. Sci.* **2008**, *46*, 858.
- (156) Lindstrom, S. B.; Uesaka, T. Simulation of the Motion of Flexible Fibers in Viscous Flow. *Phys. Fluids* **2007**, *19*, 113307–113316.
- (157) Burger, J. M. *On the Motion of Small Particles Elongated Form Suspended in a Viscous Liquid: 2nd Report on Viscosity and Plasticity*; North Holland Publ.: Amsterdam, 1938.
- (158) Nawab, M. A.; Mason, S. G. The Viscosity of Dilute Suspensions of Thread-like Particles. *J. Phys. Chem.* **1958**, *62*, 1248–1253.
- (159) Kitano, T.; Kataoka, T.; Shirota, T. An Empirical Equation of the Relative Viscosity of Polymer Melts with Various Inorganic Fillers. *Rheol. Acta* **1981**, *20*, 207.
- (160) Goto, S.; Nagazono, H.; Kato, H. The Flow Behaviour of Fiber Suspensions in Newtonian Fluids and Polymer Solutions. I. Mechanical Properties. *Rheol. Acta* **1986**, *25*, 119–129.
- (161) Kerkes, R. J.; Soszynsky, R. M.; Tam Doo, P. A. Papermaking Raw Materials. In *Transactions of Eighth Fundamental Research Symposium*; Mechanical Engineering Publications Limited: Oxford, 1985; pp 265–310.
- (162) Mason, S. G. The Flocculation of Pulp Suspension and the Formation of Paper. *Tappi* **1950**, *33*, 440–444.
- (163) Kalra, V.; Escobedo, F.; Joo, Y. L. Effect of Shear on Nanoparticle Dispersion in Polymer Melts: A Coarse-Grained Molecular Dynamics Study. *J. Chem. Phys.* **2010**, *132* (2), No. 024901.
- (164) Yuan, Z.; Chen, X.; Yu, D. Recent Advances in Elongational Flow Dominated Polymer Processing Technologies. *Polym.* **2021**, *Vol. 13*, Page 1792 **2021**, *13* (11), 1792.
- (165) Kugler, S. K.; Dey, A. P.; Saad, S.; Cruz, C.; Kech, A.; Osswald, T. A Flow-Dependent Fiber Orientation Model. *J. Compos. Sci.* **2020**, *Vol. 4*, Page 96 **2020**, *4* (3), 96.
- (166) Guo, K.; Wang, D.; Zhang, G.; Song, J.; Wu, T.; Qu, J. Effect of Series Explosion Effects on the Fiber Length, Fiber Dispersion and Structure Properties in Glass Fiber Reinforced Polyamide 66. *Polym. Adv. Technol.* **2021**, *32* (2), 505–513.
- (167) Wu, T.; Huang, Z.-x.; Wang, D.-z.; Qu, J.-p. Effect of Continuous Elongational Flow on Structure and Properties of Short Glass Fiber Reinforced Polyamide 6 Composites. *Adv. Ind. Eng. Polym. Res.* **2019**, *2* (3), 93–101.
- (168) Guo, M.; Li, X.; Maia, J. M. Fiber Length Distribution in Twin-Screw Extrusion of Fiber-Reinforced Polymer Composites: A Comparison between Shear and Extensional Mixing. *Int. Polym. Process.* **2021**, *36* (4), 350–357.
- (169) Wu, H.; Lu, X.; He, Y.; Qu, J. P. Continuous Mixing Process and Properties of NR/CB Nanocomposites Based on Elongational Rheology. *Compos. Part B Eng.* **2022**, *234*, No. 109705.
- (170) Goes, M. A.; Woicichowski, L. A.; Rosa, R. V. V.; Santos, J. P. F.; Carvalho, B. d. M. Improving the Dispersion of MWCNT and MMT in PVDF Melts Employing Controlled Extensional Flows. *J. Appl. Polym. Sci.* **2021**, *138* (17), 50274.
- (171) Tokihisa, M.; Yakemoto, K.; Sakai, T.; Utracki, L. A.; Sepehr, M.; Li, J.; Simard, Y. Extensional Flow Mixer for Polymer Nanocomposites. *Polym. Eng. Sci.* **2006**, *46* (8), 1040–1050.
- (172) Lin, W.; Hou, A.; Feng, Y. H.; Yang, Z. T.; Qu, J. P. UHMWPE/Organoclay Nanocomposites Fabricated by Melt Intercalation under Continuous Elongational Flow: Dispersion, Thermal Behaviors and Mechanical Properties. *Polym. Eng. Sci.* **2019**, *59* (3), 547–554.
- (173) Wu, T.; Tong, Y.; Qiu, F.; Yuan, D.; Zhang, G.; Qu, J. Morphology, Rheology Property, and Crystallization Behavior of PLLA/OMMT Nanocomposites Prepared by an Innovative Eccentric Rotor Extruder. *Polym. Adv. Technol.* **2018**, *29* (1), 41–51.
- (174) Duc, B. N.; Son, Y. Enhanced Dispersion of Multi Walled Carbon Nanotubes by an Extensional Batch Mixer in Polymer/MWCNT Nanocomposites. *Compos. Commun.* **2020**, *21*, No. 100420.
- (175) Feng, J.; Chan, C. M.; Li, J. X. A Method to Control the Dispersion of Carbon Black in an Immiscible Polymer Blend. *Polym. Eng. Sci.* **2003**, *43* (5), 1058–1063.
- (176) Yuan, J. K.; Yao, S. H.; Sylvestre, A.; Bai, J. Biphasic Polymer Blends Containing Carbon Nanotubes: Heterogeneous Nanotube Distribution and Its Influence on the Dielectric Properties. *J. Phys. Chem. C* **2012**, *116* (2), 2051–2058.
- (177) Rafeie, O.; Razavi Aghjeh, M. K.; Tavakoli, A.; Salami Kalajahi, M.; Jameie Oskooie, A. Conductive Poly(Vinylidene Fluoride)/Polyethylene/Graphene Blend-Nanocomposites: Relationship between Rheology, Morphology, and Electrical Conductivity. *J. Appl. Polym. Sci.* **2018**, *135* (23), 46333.
- (178) Jameie Oskooie, A.; Razavi Aghjeh, M. K.; Rafeie, O.; Tavakoli, A. Composition and Compatibilization Induced Morphology Alteration in PVDF/LLDPE Blends: Correlation between Rheology and Morphology. *J. Polym. Res.* **2017**, *24* (2), 1–11.
- (179) Cho, S.; Hong, J. S.; Lee, S. J.; Ahn, K. H.; Covas, J. A.; Maia, J. M. Morphology and Rheology of Polypropylene/Polystyrene/Clay Nanocomposites in Batch and Continuous Melt Mixing Processes. *Macromol. Mater. Eng.* **2011**, *296* (3–4), 341–348.

- (180) Gahleitner, M.; Kretzschmar, B.; Vliet, G. V.; Devaux, J.; Pospiech, D.; Bernreitner, K.; Ingolic, E. Rheology/Morphology Interactions in Polypropylene/Polyamide-6 Nanocomposites. *Rheol. Acta* **2005**, *45* (4), 322–330.
- (181) Aghjeh, M. R.; Asadi, V.; Mehdijabbar, P.; Khonakdar, H. A.; Jafari, S. H. Application of Linear Rheology in Determination of Nanoclay Localization in PLA/EVA/Clay Nanocomposites: Correlation with Microstructure and Thermal Properties. *Compos. Part B Eng.* **2016**, *86*, 273–284.
- (182) Chen, J.; Rong, C.; Lin, T.; Chen, Y.; Wu, J.; You, J.; Wang, H.; Li, Y. Stable Co-Continuous PLA/PBAT Blends Compatibilized by Interfacial Stereocomplex Crystallites: Toward Full Biodegradable Polymer Blends with Simultaneously Enhanced Mechanical Properties and Crystallization Rates. *Macromolecules* **2021**, *54* (6), 2852–2861.
- (183) Wang, H.; Chen, J.; Li, Y. Arrested Elongated Interface with Small Curvature by the Simultaneous Reactive Compatibilization and Stereocomplexation. *Macromolecules* **2020**, *53* (23), 10664–10674.
- (184) Wang, Z.; Zhang, K.; Wang, H.; Wu, X.; Wang, H.; Weng, C.; Li, Y.; Liu, S.; Yang, J. Strengthening Interfacial Adhesion and Foamability of Immiscible Polymer Blends via Rationally Designed Reactive Macromolecular Compatibilizers. *ACS Appl. Mater. Interfaces* **2022**, *14* (40), 45832–45843.
- (185) Banerjee, R.; Ray, S. S.; Ghosh, A. K. Investigations on Blending and Foaming Behavior of Styrene-Ethylene-Butylene-Styrene/Polystyrene Blends. *Int. Polym. Process.* **2017**, *32* (4), 434–445.
- (186) Banerjee, R.; Ray, S. S.; Ghosh, A. K. Dynamic Rheology and Foaming Behaviour of Styrene–Ethylene–Butylene–Styrene/ Polystyrene Blends. *J. Cell. Plast.* **2017**, *53* (4), 389–406.
- (187) Banerjee, R.; Ray, S. S.; Ghosh, A. K. Microstructure Development and Its Influence on the Properties of Styrene-Ethylene-Butylene-Styrene/Polystyrene Blends. *Polymers* **2018**, *10* (4), 400.
- (188) Souza, A. M. C.; Demarquette, N. R. Influence of Coalescence and Interfacial Tension on the Morphology of PP/HDPE Compatibilized Blends. *Polymer* **2002**, *43* (14), 3959–3967.
- (189) Gramespacher, H.; Meissner, J. J. Interfacial Tension between Polymer Melts Measured by Shear Oscillations of Their Blends. *J. Rheol.* **1992**, *36* (6), 1127–1141.
- (190) Vinckier, I.; Moldenaers, P.; Mewis, J. Relationship between Rheology and Morphology of Model Blends in Steady Shear Flow. *J. Rheol.* **1996**, *40* (4), 613–631.
- (191) Bhattacharya, S.; Gupta, R.; Jollands, M.; Bhattacharya, S. N. Foaming Behaviour of High Melt-Strength Polypropylene/ Clay Nanocomposites. *Polym. Eng. Sci.* **2009**, *49* (10), 2070–2084.
- (192) Yu, R.; Yu, W.; Zhou, C.; Feng, J. J. Rheology and Relaxation Processes in a Melting Thermotropic Liquid–Crystalline Polymer. *J. Appl. Polym. Sci.* **2007**, *104* (6), 3780–3787.
- (193) Banerjee, R.; Ray, S. S.; Ghosh, A. K. Rheology and Foaming Behaviour of Styrene–Ethylene–Butylene–Styrene Nanocomposites. *Colloid Polym. Sci.* **2021**, *299* (3), 481–496.
- (194) Bindu, P.; Thomas, S. Viscoelastic Behavior and Reinforcement Mechanism in Rubber Nanocomposites in the Vicinity of Spherical Nanoparticles. *J. Phys. Chem. B* **2013**, *117* (41), 12632–12648.
- (195) Afshari, M.; Kotek, R.; Haghghat Kish, M.; Nazock Dast, H.; Gupta, B. S. Effect of Blend Ratio on Bulk Properties and Matrix–Fibril Morphology of Polypropylene/Nylon 6 Polyblend Fibers. *Polymer* **2002**, *43* (4), 1331–1341.
- (196) Vankan, R.; Degee, P.; Jerome, R.; Teyssie, P. Design of Polymer Blend Rheology III. Effect of Maleic Anhydride Containing Copolymers on the Melt Viscosity of Polyamides. *Polym. Bull.* **1994**, *33*, 221–228.
- (197) Berger, W.; Kammer, H. W.; Kummerlöwe, C. Melt Rheology and Morphology of Polymer Blends. *Die Makromol. Chemie* **1984**, *8*, 101–108.
- (198) Park, S. J.; Kim, B. K.; Jeong, H. M. Morphological, Thermal and Rheological Properties of the Blends Polypropylene/Nylon-6, Polypropylene/Nylon-6/(Maleic Anhydride-g-Polypropylene) and (Maleic Anhydride-g-Polypropylene)/Nylon-6. *Eur. Polym. J.* **1990**, *26* (2), 131–136.
- (199) Zhai, W.; Wang, J.; Chen, N.; Naguib, H.; Park, C. B. The Orientation of Carbon Nanotubes in Poly(Ethylene-Co-Octene) Microcellular Foaming and Its Suppression on Cell Coalescence. *Polym. Eng. Sci.* **2012**, *52* (10), 2078–2089.
- (200) Lim, L. T.; Auras, R.; Rubino, M. Processing Technologies for Poly(Lactic Acid). *Prog. Polym. Sci.* **2008**, *33* (8), 820–852.
- (201) Härth, M.; Dörnhöfer, A. Film Blowing of Linear and Long-Chain Branched Poly(Ethylene Terephthalate). *Polymers* **2020**, *12*, 1605.
- (202) Kanai, T.; White, J. L. Kinematics, Dynamics and Stability of the Tubular Film Extrusion of Various Polyethylenes. *Polym. Eng. Sci.* **1984**, *24* (15), 1185–1201.
- (203) Münstedt, H.; Steffl, T.; Malmberg, A. Correlation between Rheological Behaviour in Uniaxial Elongation and Film Blowing Properties of Various Polyethylenes. *Rheol. Acta* **2005**, *45* (1), 14–22.
- (204) Field, G. J.; Micic, P.; Bhattacharya, S. N. Melt Strength and Film Bubble Instability of LLDPE/LDPE Blends. *Polym. Int.* **1999**, *48*, 461–466.
- (205) Ghijssels, A.; Ente, J. J. S. M.; Raadsen, J. Melt Strength Behavior of PE and Its Relation to Bubble Stability in Film Blowing. *Int. Polym. Process.* **1990**, *5* (4), 284–286.
- (206) Mekhilef, N.; Hedhli, L.; Moyses, S. Effect of Rheological Strain Hardening on Extrusion Blown Film of Polyvinylidene Fluoride. *J. Plast. Films Sheeting* **2007**, *23* (3), 203–219.
- (207) Kolarik, R.; Zatloukal, M.; Martyn, M. The Effect of Polyolefin Extensional Rheology on Non-Isothermal Film Blowing Process Stability. *Int. J. Heat Mass Transfer* **2013**, *56* (1–2), 694–708.
- (208) Münstedt, H. Extensional Rheology and Processing of Polymeric Materials. *Int. Polym. Process.* **2018**, *33* (5), 594–618.
- (209) Carneiro, O. S.; Covas, J. A.; Domingues, C. Biaxially Oriented Blown Film Technology Searching for Suitable Polymers and Processing Conditions. *Int. Polym. Process.* **2012**, *27* (3), 348–356.
- (210) de Almeida, K. M.; de Sousa, A. M. F.; de Souza Junior, F. G.; Bertolino, L. C.; Rocha, M. C. G.; Peres, A. C. C.; Ossig, A.; da Silva, A. L. N. Melt Rheology and Morphology of Binary and Ternary PS/HIPS Blends for Blown Film Extrusion Applications. *Polym. Test.* **2017**, *64*, 277–286.
- (211) Fang, Y.; Carreau, P. J.; Lafleur, P. G. Rheological Effects of Polyethylenes in Film Blowing. *Polym. Eng. Sci.* **2003**, *43* (7), 1391–1406.
- (212) Al-Itry, R.; Lamnawar, K.; Maazouz, A. Biopolymer Blends Based on Poly (Lactic Acid): Shear and Elongation Rheology/ Structure/Blowing Process Relationships. *Polymers* **2015**, *7* (5), 939–962.
- (213) Zhu, H.; Wang, Y.; Zhang, X.; Su, Y.; Dong, X.; Chen, Q.; Zhao, Y.; Geng, C.; Zhu, S.; Han, C. C.; Wang, D. Influence of Molecular Architecture and Melt Rheological Characteristic on the Optical Properties of LDPE Blown Films. *Polymer* **2007**, *48* (17), 5098–5106.
- (214) Micic, P.; Bhattacharya, S. N. Rheology of LLDPE, LDPE and LLDPE/LDPE Blends and Its Relevance to the Film Blowing Process. *Polym. Int.* **2000**, *49*, 1580–1589.
- (215) Mistretta, M. C.; Botta, L.; Arrigo, R.; Leto, F.; Malucelli, G.; La Mantia, F. P. Bionanocomposite Blown Films: Insights on the Rheological and Mechanical Behavior. *Polym.* **2021**, *Vol. 13*, Page 1167
- (216) Hu, X.; Liu, S.; Zhou, G.; Huang, Y.; Xie, Z.; Jing, X. Electrospinning of Polymeric Nanofibers for Drug Delivery Applications. *J. Controlled Release* **2014**, *185* (1), 12–21.
- (217) Jiang, T.; Carbone, E. J.; Lo, K. W. H.; Laurencin, C. T. Electrospinning of Polymer Nanofibers for Tissue Regeneration. *Prog. Polym. Sci.* **2015**, *46*, 1–24.
- (218) Akkoyun, S.; Öktem, N. Effect of Viscoelasticity in Polymer Nanofiber Electrospinning: Simulation Using FENE-CR Model. *Eng. Sci. Technol. Int. J.* **2021**, *24* (3), 620–630.

- (219) Rutledge, G. C.; Fridrikh, S. V. Formation of Fibers by Electrospinning. *Adv. Drug Delivery Rev.* **2007**, *59* (14), 1384–1391.
- (220) Reneker, D. H.; Yarin, A. L.; Fong, H.; Koombhongse, S. Bending Instability of Electrically Charged Liquid Jets of Polymer Solutions in Electrospinning. *J. Appl. Phys.* **2000**, *87*, 4531–4547.
- (221) Taylor, G. I. The Formation of Emulsions in Definable Fields of Flow. *Proc. R. Soc. London. Ser. A, Contain. Pap. a Math. Phys. Character.* **1934**, *146* (858), 501–523.
- (222) Yarin, A. L.; Koombhongse, S.; Reneker, D. H. Taylor Cone and Jetting from Liquid Droplets in Electrospinning of Nanofibers. *J. Appl. Phys.* **2001**, *90* (9), 4836.
- (223) Ramesh Kumar, P.; Khan, N.; Vivekanandhan, S.; Satyanarayana, N.; Mohanty, A. K.; Misra, M. Nanofibers: Effective Generation by Electrospinning and Their Applications. *J. Nanosci. Nanotechnol.* **2012**, *12* (1), 1–25.
- (224) Luo, C. J.; Nangrejo, M.; Edirisinghe, M. A Novel Method of Selecting Solvents for Polymer Electrospinning. *Polymer* **2010**, *51* (7), 1654–1662.
- (225) Lasprilla-Botero, J.; Álvarez-Láinez, M.; Lagaron, J. M. The Influence of Electrospinning Parameters and Solvent Selection on the Morphology and Diameter of Polyimide Nanofibers. *Mater. Today Commun.* **2018**, *14*, 1–9.
- (226) Nayak, P.; Ghosh, A. K.; Bhatnagar, N. Investigation of Solution Rheology in Electrospinning of Ultra High Molecular Weight Polyethylene. *Fibers Polym.* **2022**, *23* (1), 48–57.
- (227) Wang, C.; Wang, Y.; Hashimoto, T. Impact of Entanglement Density on Solution Electrospinning: A Phenomenological Model for Fiber Diameter. *Macromolecules* **2016**, *49* (20), 7985–7996.
- (228) Wang, C.; Cheng, Y. W.; Hsu, C. H.; Chien, H. S.; Tsou, S. Y. How to Manipulate the Electrospinning Jet with Controlled Properties to Obtain Uniform Fibers with the Smallest Diameter?—A Brief Discussion of Solution Electrospinning Process. *J. Polym. Res.* **2011**, *18* (1), 111–123.
- (229) McKee, M. G.; Wilkes, G. L.; Colby, R. H.; Long, T. E. Correlations of Solution Rheology with Electrospun Fiber Formation of Linear and Branched Polyesters. *Macromolecules* **2004**, *37* (5), 1760–1767.
- (230) Abbasi, A.; Nasef, M. M.; Takeshi, M.; Faridi-Majidi, R. Electrospinning of Nylon-6,6 Solutions into Nanofibers: Rheology and Morphology Relationships. *Chin. J. Polym. Sci.* **2014**, *32* (6), 793–804.
- (231) Nayak, R.; Padhye, R.; Kyratzis, I. L.; Truong, Y. B.; Arnold, L. Effect of Viscosity and Electrical Conductivity on the Morphology and Fiber Diameter in Melt Electrospinning of Polypropylene. *J. Plast. Films Sheeting* **2013**, *83* (6), 606–617.
- (232) Joseph, E. G.; Budhavaram, N.; DePolo, W.; Das, A. Nanoribbons Fabricated by Melt Electrospinning. *Polym. J.* **2020**, *53* (3), 493–503.
- (233) Larrondo, L.; St John Manley, R. Electrostatic Fiber Spinning from Polymer Melts. I. Experimental Observations on Fiber Formation and Properties. *J. Polym. Sci. Polym. Phys. Ed.* **1981**, *19* (6), 909–920.
- (234) Lyons, J.; Ko, F. Melt Electrospinning of Polymers: A Review. *Polym. News* **2005**, *30* (6), 170–178.
- (235) Zhou, H.; Green, T. B.; Joo, Y. L. The Thermal Effects on Electrospinning of Polylactic Acid Melts. *Polymer* **2006**, *47* (21), 7497–7505.
- (236) Nazari, T.; Garmabi, H. Polylactic Acid/Polyethylene Glycol Blend Fibres Prepared via Melt Electrospinning: Effect of Polyethylene Glycol Content. *Micro Nano Lett.* **2014**, *9* (10), 686–690.
- (237) Reneker, D. H.; Yarin, A. L.; Fong, H.; Koombhongse, S. Bending Instability of Electrically Charged Liquid Jets of Polymer Solutions in Electrospinning. *J. Appl. Phys.* **2000**, *87* (9), 4531.
- (238) Regev, O.; Vandebriel, S.; Zussman, E.; Clasen, C. The Role of Interfacial Viscoelasticity in the Stabilization of an Electrospun Jet. *Polymer (Guildf)* **2010**, *51* (12), 2611–2620.
- (239) Theron, S. A.; Yarin, A. L.; Zussman, E.; Kroll, E. Multiple Jets in Electrospinning: Experiment and Modeling. *Polymer (Guildf)* **2005**, *46* (9), 2889–2899.
- (240) Yarin, A. L.; Koombhongse, S.; Reneker, D. H. Bending Instability in Electrospinning of Nanofibers. *J. Appl. Phys.* **2001**, *89* (5), 3018.
- (241) Yu, J. H.; Fridrikh, S. V.; Rutledge, G. C. The Role of Elasticity in the Formation of Electrospun Fibers. *Polymer* **2006**, *47* (13), 4789–4797.
- (242) Thompson, C. J.; Chase, G. G.; Yarin, A. L.; Reneker, D. H. Effects of Parameters on Nanofiber Diameter Determined from Electrospinning Model. *Polymer* **2007**, *48* (23), 6913–6922.
- (243) Nazari, T.; Garmabi, H. Thermo-Rheological and Interfacial Properties of Polylactic Acid/Polyethylene Glycol Blends toward the Melt Electrospinning Ability. *J. Appl. Polym. Sci.* **2016**, *133* (44), 44120.
- (244) Carroll, C. P.; Joo, Y. L. Electrospinning of Viscoelastic Boger Fluids: Modeling and Experiments. *Phys. Fluids* **2006**, *18* (5), No. 053102.
- (245) Feng, J. J. The Stretching of an Electrified Non-Newtonian Jet: A Model for Electrospinning. *Phys. Fluids* **2002**, *14* (11), 3912.
- (246) Rwei, S. P.; Huang, C. C. Electrospinning PVA Solution-Rheology and Morphology Analyses. *Fibers Polym.* **2012**, *13* (1), 44–50.
- (247) Liu, S.; Fu, J.; Ge, M.; Tan, L.; Du, W. Electrospinning of Polyacrylonitrile Nanofibers Using Strain-Hardening Spinning Solutions. *Fibers Polym.* **2014**, *15* (11), 2441–2445.
- (248) Helgeson, M. E.; Wagner, N. J. A Correlation for the Diameter of Electrospun Polymer Nanofibers. *AIChE J.* **2007**, *53* (1), 51–55.
- (249) Wang, M.; Hsieh, A. J.; Rutledge, G. C. Electrospinning of Poly(MMA-Co-MAA) Copolymers and Their Layered Silicate Nanocomposites for Improved Thermal Properties. *Polymer (Guildf)* **2005**, *46* (10), 3407–3418.
- (250) Dallmeyer, I.; Ko, F.; Kadla, J. F. Correlation of Elongational Fluid Properties to Fiber Diameter in Electrospinning of Softwood Kraft Lignin Solutions. *Ind. Eng. Chem. Res.* **2014**, *53* (7), 2697–2705.
- (251) Stepanyan, R.; Subbotin, A. V.; Cuperus, L.; Boonen, P.; Dorschu, M.; Oosterlinck, F.; Bulters, M. J. H. Nanofiber Diameter in Electrospinning of Polymer Solutions: Model and Experiment. *Polymer (Guildf)* **2016**, *97*, 428–439.
- (252) Feng, J. J. Stretching of a Straight Electrically Charged Viscoelastic Jet. *J. Nonnewton. Fluid Mech.* **2003**, *116* (1), 55–70.
- (253) Ren, L.; Pandit, V.; Elkin, J.; Denman, T.; Cooper, J. A.; Kotha, S. P. Large-Scale and Highly Efficient Synthesis of Micro- and Nano-Fibers with Controlled Fiber Morphology by Centrifugal Jet Spinning for Tissue Regeneration. *Nanoscale* **2013**, *5* (6), 2337–2345.
- (254) Zhang, X.; Lu, Y. Centrifugal Spinning: An Alternative Approach to Fabricate Nanofibers at High Speed and Low Cost. *J. Plast. Films Sheeting* **2014**, *54* (4), 677–701.
- (255) Zhiming, Z.; Boya, C.; Zilong, L.; Jiawei, W.; Yaoshuai, D. Spinning Solution Flow Model in the Nozzle and Experimental Study of Nanofibers Fabrication via High Speed Centrifugal Spinning. *Polymer* **2020**, *205*, No. 122794.
- (256) Hammami, M. A.; Krifa, M.; Harzallah, O. Centrifugal Force Spinning of PA6 Nanofibers – Processability and Morphology of Solution-Spun Fibers. *J. Text. Inst.* **2014**, *105* (6), 637–647.
- (257) Lu, Y.; Li, Y.; Zhang, S.; Xu, G.; Fu, K.; Lee, H.; Zhang, X. Parameter Study and Characterization for Polyacrylonitrile Nanofibers Fabricated via Centrifugal Spinning Process. *Eur. Polym. J.* **2013**, *49* (12), 3834–3845.
- (258) Merchiers, J.; Meurs, W.; Deferme, W.; Peeters, R.; Buntinx, M.; Reddy, N. K. Influence of Polymer Concentration and Nozzle Material on Centrifugal Fiber Spinning. *Polym. 2020, Vol. 12, Page 575* **2020**, *12* (3), 575.
- (259) Rogalski, J. J.; Botto, L.; Bastiaansen, C. W. M.; Peijs, T. A Study of Rheological Limitations in Rotary Jet Spinning of Polymer Nanofibers through Modeling and Experimentation. *J. Appl. Polym. Sci.* **2020**, *137* (33), 48963.
- (260) Noroozi, S.; Arne, W.; Larson, R. G.; Taghavi, S. M. A Comprehensive Mathematical Model for Nanofiber Formation in Centrifugal Spinning Methods. *J. Fluid Mech.* **2020**, *892*, A26.

- (261) Zhmayev, Y.; Divvela, M. J.; Ruo, A. C.; Huang, T.; Joo, Y. L. The Jetting Behavior of Viscoelastic Boger Fluids during Centrifugal Spinning. *Phys. Fluids* **2015**, *27* (12), No. 123101.
- (262) Ren, L.; Ozisik, R.; Kotha, S. P.; Underhill, P. T. Highly Efficient Fabrication of Polymer Nanofiber Assembly by Centrifugal Jet Spinning: Process and Characterization. *Macromolecules* **2015**, *48* (8), 2593–2602.
- (263) Divvela, M. J.; Ruo, A. C.; Zhmayev, Y.; Joo, Y. L. Discretized Modeling for Centrifugal Spinning of Viscoelastic Liquids. *J. Nonnewton. Fluid Mech.* **2017**, *247*, 62–77.
- (264) Noroozi, S.; Arne, W.; Larson, R. G.; Taghavi, S. M. Centrifugal Spinning of Viscoelastic Nanofibres. *J. Fluid Mech.* **2022**, *934*, A9.
- (265) Liu, Q.; Parker, K. K. A Viscoelastic Beam Theory of Polymer Jets with Application to Rotary Jet Spinning. *Extrem. Mech. Lett.* **2018**, *25*, 37–44.
- (266) Mahalingam, S.; Edirisinghe, M. Forming of Polymer Nanofibers by a Pressurised Gyration Process. *Macromol. Rapid Commun.* **2013**, *34* (14), 1134–1139.
- (267) Riahi, D. N. On Strain Hardening of Nonlinear Polymeric Jets During Forcespinning. *Int. J. Appl. Comput. Math.* **2018**, *4* (1), 1–8.
- (268) Standard Terminology for Additive Manufacturing Technologies. <https://www.astm.org/f2792-12.html> (accessed Feb 4, 2023).
- (269) Hull, C. W. Apparatus for Production of Three-Dimensional Objects by Stereolithography. US Patent US4575330A, 1984.
- (270) Das, A.; Gilmer, E. L.; Biria, S.; Bortner, M. J. Importance of Polymer Rheology on Material Extrusion Additive Manufacturing: Correlating Process Physics to Print Properties. *ACS Appl. Polym. Mater.* **2021**, *3* (3), 1218–1249.
- (271) Wang, X.; Jiang, M.; Zhou, Z.; Gou, J.; Hui, D. 3D Printing of Polymer Matrix Composites: A Review and Prospective. *Compos. Part B Eng.* **2017**, *110*, 442–458.
- (272) Gao, W.; Zhang, Y.; Ramanujan, D.; Ramani, K.; Chen, Y.; Williams, C. B.; Wang, C. C. L.; Shin, Y. C.; Zhang, S.; Zavattieri, P. D. The Status, Challenges, and Future of Additive Manufacturing in Engineering. *Comput. Des.* **2015**, *69*, 65–89.
- (273) Gomez-Gras, G.; Jerez-Mesa, R.; Travieso-Rodriguez, J. A.; Lluma-Fuentes, J. Fatigue Performance of Fused Filament Fabrication PLA Specimens. *Mater. Des.* **2018**, *140*, 278–285.
- (274) Ambrosi, A.; Pumera, M. 3D-Printing Technologies for Electrochemical Applications. *Chem. Soc. Rev.* **2016**, *45* (10), 2740–2755.
- (275) Spoerk, M.; Holzer, C.; Gonzalez-Gutierrez, J. Material Extrusion-Based Additive Manufacturing of Polypropylene: A Review on How to Improve Dimensional Inaccuracy and Warpage. *J. Appl. Polym. Sci.* **2020**, *137* (12), 48545.
- (276) Turner, B. N.; Strong, R.; Gold, S. A. A Review of Melt Extrusion Additive Manufacturing Processes: I. Process Design and Modeling. *Rapid Prototyp. J.* **2014**, *20* (3), 192–204.
- (277) Duty, C.; Ajinjeru, C.; Kishore, V.; Compton, B.; Hmeidad, N.; Chen, X.; Liu, P.; Hassen, A. A.; Lindahl, J.; Kunc, V. What Makes a Material Printable? A Viscoelastic Model for Extrusion-Based 3D Printing of Polymers. *J. Manuf. Process.* **2018**, *35*, 526–537.
- (278) Zawaski, C. E.; Wilts, E. M.; Chatham, C. A.; Stevenson, A. T.; Pekkanen, A. M.; Li, C.; Tian, Z.; Whittington, A. R.; Long, T. E.; Williams, C. B. Tuning the Material Properties of a Water-Soluble Ionic Polymer Using Different Counterions for Material Extrusion Additive Manufacturing. *Polymer* **2019**, *176*, 283–292.
- (279) Vanzanella, V.; Scatto, M.; Zant, E.; Sisani, M.; Bastianini, M.; Grizzuti, N. The Rheology of PEOT/PBT Block Copolymers in the Melt State and in the Thermally-Induced Sol/Gel Transition Implications on the 3D-Printing Bio-Scaffold Process. *Mater.* **2019**, *Vol. 12*, Page 226 **2019**, *12* (2), 226.
- (280) Boetker, J.; Water, J. J.; Aho, J.; Arnfast, L.; Bohr, A.; Rantanen, J. Modifying Release Characteristics from 3D Printed Drug-Eluting Products. *Eur. J. Pharm. Sci.* **2016**, *90*, 47–52.
- (281) Azad, M. A.; Olawuni, D.; Kimbell, G.; Badruddoza, A. Z. M.; Hossain, M. S.; Sultana, T. Polymers for Extrusion-Based 3D Printing of Pharmaceuticals: A Holistic Materials–Process Perspective. *Pharm.* **2020**, *Vol. 12*, Page 124 **2020**, *12* (2), 124.
- (282) Bertolino, M.; Bateggazzore, D.; Arrigo, R.; Frache, A. Designing 3D Printable Polypropylene: Material and Process Optimisation through Rheology. *Addit. Manuf.* **2021**, *40*, No. 101944.
- (283) Elhattab, K.; Bhaduri, S. B.; Sikder, P. Influence of Fused Deposition Modelling Nozzle Temperature on the Rheology and Mechanical Properties of 3D Printed β -Tricalcium Phosphate (TCP)/Polylactic Acid (PLA) Composite. *Polymers* **2022**, *14* (6), 1222.
- (284) Gupta, R. K. *Polymer and Composite Rheology*; CRC Press: Boca Raton, FL, 2000.
- (285) Hu, Y.; Wang, J.; Li, X.; Hu, X.; Zhou, W.; Dong, X.; Wang, C.; Yang, Z.; Binks, B. P. Facile Preparation of Bioactive Nanoparticle/Poly(ϵ -Caprolactone) Hierarchical Porous Scaffolds via 3D Printing of High Internal Phase Pickering Emulsions. *J. Colloid Interface Sci.* **2019**, *545*, 104–115.
- (286) Polamaply, P.; Cheng, Y.; Shi, X.; Manikandan, K.; Kremer, G. E.; Qin, H. 3D Printing and Characterization of Hydroxypropyl Methylcellulose and Methylcellulose for Biodegradable Support Structures. *Procedia Manuf.* **2019**, *34*, 552–559.
- (287) Jain, S.; Fuoco, T.; Yassin, M. A.; Mustafa, K.; Finne-Wistrand, A. Printability and Critical Insight into Polymer Properties during Direct-Extrusion Based 3D Printing of Medical Grade Polylactide and Copolyesters. *Biomacromolecules* **2020**, *21* (2), 388–396.
- (288) Peñas, M. I.; Calafel, M. I.; Aguirresarobe, R. H.; Tierno, M.; Conde, J. I.; Pascual, B.; Santamaría, A. How Is Rheology Involved in 3D Printing of Phase-Separated PVC-Acrylate Copolymers Obtained by Free Radical Polymerization. *Polymers* **2020**, *12* (9), 2070.
- (289) Heller, B. P.; Smith, D. E.; Jack, D. A. Effects of Extrudate Swell and Nozzle Geometry on Fiber Orientation in Fused Filament Fabrication Nozzle Flow. *Addit. Manuf.* **2016**, *12*, 252–264.
- (290) Schuller, T.; Fanzio, P.; Galindo-Rosales, F. J. Analysis of the Importance of Shear-Induced Elastic Stresses in Material Extrusion. *Addit. Manuf.* **2022**, *57*, No. 102952.
- (291) De Rosa, S.; Tammara, D.; D’Avino, G. Experimental and Numerical Investigation of the Die Swell in 3D Printing Processes. *Micromachines* **2023**, *Vol. 14*, Page 329 **2023**, *14* (2), 329.
- (292) Tagliaferri, S.; Panagiotopoulos, A.; Mattevi, C. Direct Ink Writing of Energy Materials. *Mater. Adv.* **2021**, *2* (2), 540–563.
- (293) Outrequin, T. C. R.; Gamonpilas, C.; Siritwatwechakul, W.; Sreearunothai, P. Extrusion-Based 3D Printing of Food Biopolymers: A Highlight on the Important Rheological Parameters to Reach Printability. *J. Food Eng.* **2023**, *342*, No. 111371.
- (294) Wilms, P.; Daffner, K.; Kern, C.; Gras, S. L.; Schutyser, M. A. I.; Kohlus, R. Formulation Engineering of Food Systems for 3D-Printing Applications – A Review. *Food Res. Int.* **2021**, *148*, No. 110585.